TECHNISCHE UNIVERSITÄT MÜNCHEN

Max-Planck-Institut für Plasmaphysik

Kinetic Investigation of Magnetic Islands in Tokamaks

Mattia SICCINIO

Vollständiger Abdruck der von der Fakultät für Physik der Technischen Universität München zur Erlangung des akademischen Grades eines

Doktors der Naturwissenschaften

genehmigten Dissertation.

Vorsitzender: Univ.-Prof. Dr. R. Krücken

Prüfer der Dissertation:

1. Hon.-Prof. Dr. S. Günter
2. Univ.-Prof. Dr. A. G. Peeters, Universität Bayreuth

Die Dissertation wurde am 11.01.2010 bei der Technischen Universität München eingereicht und durch die Fakultät für Physik am 29.03.2010 angenommen.

Contents

Alle persone che mi sono state vicine negli ultimi 27 anni.

Grazie di cuore.

M.

Acknowledgements

I am indebted to a great number of people for help and advice throughout my time as a PhD. Of course, my first and absolutely necessary thanks go to my family, which always supported me and my choices all my life long. All my gratefulness goes indeed to my wife Eva, who was so crazy not only to marry me, but also to follow me in this long trip to Germany...

I gratefully acknowledge the friendly attitude of all my colleagues at the IPP, referring especially to the large Italian community (Clemente Angioni, Vittoria Belmondo, Nicola Bertelli (a.k.a. Bertelli the Netherlands), Alessandro Biancalani, Roberto Bilato, Emiliano Fable, Tobias Hein (Italian citizen *honoris causa*), Andrea Scarabosio, Giuliana Sias, Giovanni Tardini). In particular, I am strongly indebted with Dr. Omar Maj (my favourite mathematical handbook) and Dr. Alberto Bottino (my favourite computer problem solver), which conjugate their immense knowledge to an uncommon kindness.

I had the opportunity during the last year to start a very interesting and promising collaboration with the Plasma Physics Group to the University of Warwick, Coventry, United Kingdom. For this reason, I would like to thank Prof. Arthur G. Peeters and Dr. William A. Hornsby, not only for their scientific value but also for their hospitality during the weeks I spent in Warwickshire.

Finally, last but indeed not least, my most grateful thanks go to my IPP

supervisor, Dr. Emanuele Poli. He is a person of undoubted competence, able to transmit all his passion, and endowed at the same time with an indescribable patience (I can be extreeeemely boring sometimes).

Thanks a lot to you all!!
Mattia

Es dürfte uns gut tun, uns manchmal daran zu erinnern, dass wir zwar in dem Wenigen, das wir wissen, sehr verschieden sein mögen, dass wir aber in unserer grenzenlosen Unwissenheit alle gleich sind.

Karl Popper

Chapter 1

Nuclear Fusion and Tokamaks

1.1 Nuclear Fusion

Nuclear fusion represents an alternative energy source which offers several advantages compared to both fossil fuels and the conventional nuclear fission. A future fusion power plant will not produce any carbon-dioxyde, as no combustion takes place, and also any long-lived radioactive wastes during its operation (apart from those originating from the decommissioning of the power plant, and they would mainly consist in intermediate level waste). Moreover, deuterium and tritium, the fuels needed by a fusion reactor, are available in relatively large amounts all over the world (deuterium is present in water, while tritium can be produced through the "breeding" of lithium, which is in turn relatively abundant).

The nuclear reaction envisaged for a fusion power plant is

$$ {}^{2}_{1}\mathrm{D} + {}^{3}_{1}\mathrm{T} \rightarrow {}^{4}_{2}\mathrm{He}(3.5\ \mathrm{MeV}) + {}^{1}_{0}\mathrm{n}(14\ \mathrm{MeV}). \tag{1.1} $$

In order for such reactions to take place, the nuclei must have a sufficient kinetic energy to get close enough to each other, so as to overcome the electrostatic barrier due to their electric charge. If this energy is supplied as thermal energy, a temperature exceeding some hundred millions of degrees is necessary to ensure a sufficient rate of fusion reactions. At these tempera-

tures, electrons have sufficient energy to escape from the lower atomic levels, and actually are free to move. The gas becomes an ionized medium, although electrically quasi-neutral, known with the name of *plasma*. The goal of a fusion reactor is to confine the plasma for a time sufficiently long in order to achieve a relevant number of fusion events. Neutrons arising from the nuclear reactions, which cannot be caught by magnetic confinement, are supposed to provide the heat for the thermodynamic cycle of the plant (Fig.1.1), while α-particles are useful to sustain the reaction, converting their energy into heating through collisions with the background plasma, so as to compensate energy losses. As this reaction is not a chain reaction, it cannot diverge and lead to catastrophic events, as for conventional fission reactors. Fusion reactors own for this reason remarkable advantages also from the safety point of view.

Since no materials can survive at such high temperatures, no mechanical confinement of the plasma is efficient in the frame of the construction of a reactor. A way that is actively investigated is the *magnetic confinement*. So far, the most widely studied and promising machine designed for such purpose is the *tokamak* [1, 2], (acronym from Russian тороидальная камера в магнитных катушках, to be read "toroidal'naya kamera v magnitnykh katushkakh", toroidal chamber with magnetic coils). A short description of the main features of this machine is illustrated in the following section.

1.2 The Tokamak

1.2.1 Properties of the Plasma

The plasma is defined as an ionized gas, electrically quasi-neutral, although media that do not correspond to this definition are sometimes also referred to as plasmas (e.g. non neutral gases, partially ionized gases *et cetera*).

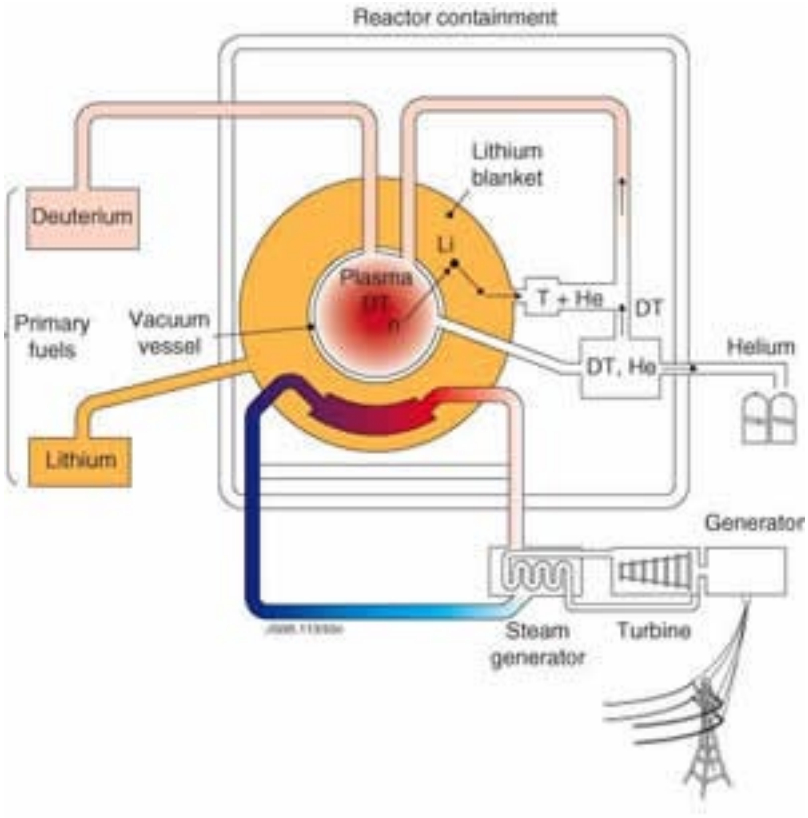

Figure 1.1: Schematic draw of a fusion power plant. The heat generated by nuclear reactions in the plasma chamber is converted in electric power through a conventional thermodynamic cycle (Source: European Commission for Energy, http://ec.europa.eu).

However, tokamak plasmas fulfil the definition given above.

The expression "quasi-neutral" refers to the fact that, on sufficiently large space- and timescales, a volume of plasma can be considered globally neutral. This is because the electrostatic potential associated to a single charge is efficiently shielded, and any charge separation is rapidly compensated, as the charged particles are free to move very quickly. The space- and timescale above which quasineutrality holds (called *Debye length* and *inverse plasma frequency*, respectively, see for example [3]) are typically shorter than most

of the characteristic scales of interest in a tokamak plasma discharge. By consequence, quasineutrality represents a valid assumption for most aspects of fusion reactor physics, and indeed its importance in the investigation of tokamak plasmas is crucial.

From a mathematical point of view, quasineutrality implies that the (local) charge density ρ_q remains small, and therefore its time derivative can be neglected. Thus, via the charge continuity equation

$$\frac{\partial \rho_q}{\partial t} + \nabla \cdot \mathbf{J} = 0, \tag{1.2}$$

the expression for quasineutrality becomes simply

$$\nabla \cdot \mathbf{J} = 0. \tag{1.3}$$

$\mathbf{J}$ being the current density. The peculiarity of plasmas, which characterises them by contrast with neutral gases is represented by the *collective phenomena*. In a neutral gas, in fact, molecules can interact only through collision (which are basically binary events), and thus any information can travel through the medium only because of molecule-to-molecule phenomena. This is no longer true in a plasma. Although collisions still take place, charge separations between ions and electrons give rise to electric fields, while charged-particle flows give rise to currents and magnetic fields. Therefore, if in a neutral gas the dynamics of a single molecule is affected by surrounding molecules only if collisions occur, the dynamics of a particle in a plasma depends, in general, on the dynamics of *all* particles in the plasma volume. This "collective" behaviour, opposed to the "binary" behaviour of neutral gases, has noteworthy repercussions even on the macroscopic level.

1.2.2 Principles of a Tokamak

As previously stated, the tokamak is a machine designed to confine the plasma by means of magnetic fields in order to allow nuclear fusion events

to take place. It is known from elementary electrodynamics that a charged particle is free to move along a magnetic field line, while its motion is constrained in the plane perpendicular to it. To confine the particle also in the parallel direction, a plausible solution is to adopt a magnetic configuration with closed field lines, e.g. bending a system of coils to a torus. The tokamak has for this reason such a shape. It turns out, however, that a purely *toroidal* magnetic field is not sufficient to yield a proper confinement (see section 2.2). An additional field pointing in the *poloidal* direction (i.e. in the direction locally perpendicular both to the minor radius and to the toroidal direction) must be added. As a result, the magnetic field lines have the form of helics that ergodically describe nested toroidal surfaces, called *magnetic surfaces* or *flux surfaces* (Fig.1.2).

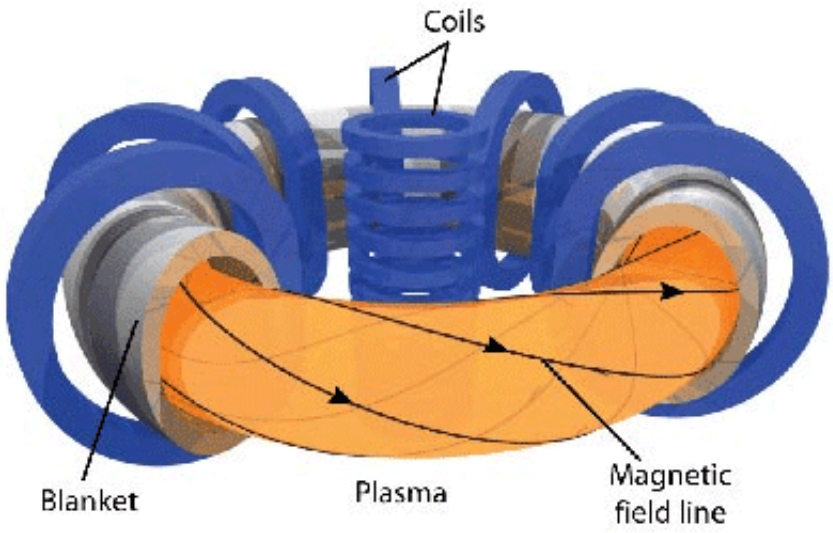

Figure 1.2: Representation of a tokamak. The central solenoid and the magnetic surfaces, ergodically covered by helical magnetic field lines, are clearly visible (Source: http://fusionforenergy.europa.eu).

The main feature of a tokamak machine is that the toroidal component of the confining magnetic field is imposed by external coils, while the poloidal

one is generated by the plasma itself by internal currents. This is achieved by means of a *central solenoid* (Fig.1.2), which induces a toroidal current in the plasma chamber, letting the plasma behaving like a secondary circuit of a transformer. This current is known as *plasma current*, and it represents actually the most important distinctiveness of the tokamak. In other devices, such as *stellarators* (Fig.1.3), the whole confining magnetic field is determined by means of external coils, but this implies a by far more complex geometry of the machine, which leads to difficulties in the development, building and assembling phases. On the other hand, since in a tokamak the plasma current is induced through a transformator, it is not suitable for a steady-state reactor, as it depends on the time-derivative of the magnetic flux in the central solenoid, which cannot indefinitely increase (or decrease). Although the plasma current can be generated by other mechanisms, this aspect represents still a major challenge in view of the construction of an operating fusion reactor.

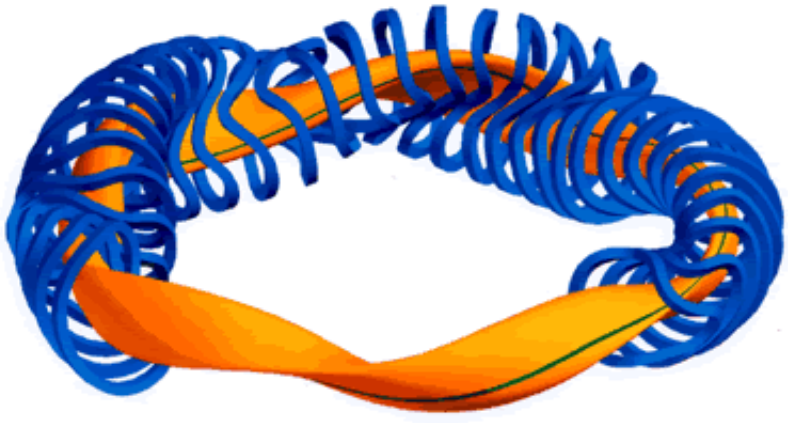

Figure 1.3: Sketch of a stellarator. The shape of the plasma and of the coils is complicated in comparison to a tokamak.

In a magnetic confinement device, the basic equation describing the bal-

ance between the confining magnetic (Lorentz) force and the expansion of the plasma is

$$\mathbf{J} \times \mathbf{B} = \nabla p, \tag{1.4}$$

where $\mathbf{J}$ is again the current density, $\mathbf{B}$ the magnetic field and p the plasma pressure. The pressure gradient results from the fact that the pressure must increase from a low value at the edge, where the plasma is close to the material walls, to a sufficiently high value in the centre, where most of the fusion reactions are supposed to take place. Two important remarks emerge from from Eq.(1.4):

- Taking the cross product of Eq.(1.4) with $\mathbf{B}$ shows that a current, called *diamagnetic current* and being proportional to $(\mathbf{B} \times \nabla p)/B^2$, appears in a tokamak equilibrium. It flows on the magnetic surfaces, and it is everywhere perpendicular to magnetic field lines.

- The pressure gradient is always perpendicular to magnetic surfaces, as can be seen performing the scalar product of Eq.(1.4) times $\mathbf{B}$. Equivalently, pressure is constant on magnetic surfaces.

A quantity $\mathcal{Q}$ for which, as for pressure,

$$\mathbf{B} \cdot \nabla \mathcal{Q} = 0 \tag{1.5}$$

is therefore called *flux-surface quantities*.

1.3 Tokamak Geometry

1.3.1 Magnetic Coordinates

As can be inuitively inferred from Eq.(1.4), the dynamics of a plasma has very different features *across* the magnetic surfaces and *along* it. For this reason, to properly describe a tokamak configuration, a coordinate system which easily allows to identify magnetic surfaces is highly desirable.

The simple choice r, θ and ζ (where r is the geometrical minor radius, θ is the poloidal angle and ζ is the toroidal angle) as a coordinate system turns out to be unfit, because magnetic surfaces do not correspond to constant-r surfaces (unless the poloidal section of the tokamak is circular, which is in general not the case, see Fig.1.4). For this reason, the poloidal flux χ is introduced.

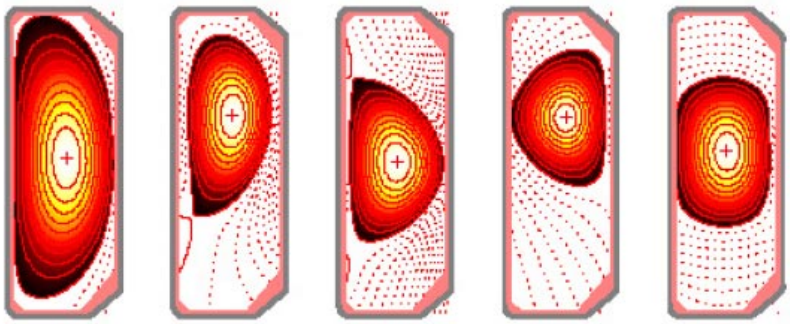

Figure 1.4: Curves of constant magnetic flux (magnetic surfaces) in different configurations of the TCV tokamak, showing that magnetic surfaces can strongly deviate from a circular cross section of the poloidal magnetic field.

This quantity represents the flux across a ribbon-like surface stretched between the magnetic axis (the degenerate magnetic surface where the pressure attains its maximum) and a fixed magnetic surface, for convenience divided by a factor 2π. It is clear that such a quantity is constant on every magnetic surface, i.e.

$$\mathbf{B} \cdot \nabla \chi = 0, \tag{1.6}$$

and thus χ is a flux-surface quantity. The poloidal and toroidal angular coordinate can be then re-defined in such a way that the contravariant component of the magnetic field is for both of them a flux-surface quantity:

$$\mathbf{B} \cdot \nabla \theta = B^{\theta}(\chi), \tag{1.7}$$

$$\mathbf{B} \cdot \nabla\zeta = B^{\zeta}(\chi), \tag{1.8}$$

This means that the $\nabla\theta$ and $\nabla\zeta$ directions are defined to be *on* the magnetic surface. The choice of θ and ζ such to satisfy Eq.(1.7) and Eq.(1.8) is not unique, and for this reasons many different coordinate system are available, each one with different properties (e.g. Hamada coordinates [4] and Boozer Coordinates [5]). Such systems are sometimes called *straight field-line coordinates*, because in these systems magnetic field-lines look like straight lines in a (θ, ζ)-plane. The pitch of these lines is defined by means of

$$q \doteq \frac{B^{\zeta}}{B^{\theta}} = q(\chi). \tag{1.9}$$

This parameter, named *safety factor*, plays a crucial role in the fusion reactor physics. It physically corresponds to the number of toroidal turns that have to be performed along a field line in order to complete a poloidal turn, and in a tokamak it typically increases monotonically with χ. For stability reasons, on the magnetic axis the value of q should be kept above 1 (although it is not always the case), while on the edge it seldom drops below the value of 3. The parameter

$$\hat{s} = \frac{\chi}{q}\frac{\mathrm{d}q}{\mathrm{d}\chi} \tag{1.10}$$

plays also a relevant role, and it is typically referred to as *magnetic shear*.

1.3.2 Large Aspect-Ratio Approximation

A common approximation in tokamak theory is the so called *large aspect-ratio approximation*. The aspect ratio is defined as the ratio between the major radius of the tokamak, R, and the minor radius r. Thus, the inverse aspect ratio, defined as

$$\epsilon \doteq \frac{r}{R} \ll 1 \tag{1.11}$$

is a small parameter, and can thus be used for series expansions. In the present work, a tokamak with circular cross-sections is considered, as the shaping of the flux surfaces discussed above is not supposed to influence significantly (at least qualitatively) the physical processes investigated in this thesis. The major radius in a circular cross-section tokamak can be written as

$$R = R_0 \left(1 + \epsilon \cos\theta\right) \tag{1.12}$$

where R_0 represents its value on the magnetic axis, while θ is supposed to be zero on the outer midplane (Fig.1.5). Because of the geometry of the tokamak, it can be shown by integrating Ampère's law along a toroidal turn inside the plasma chamber that the magnitude of the magnetic field, which is generated by the current of the external coils, in vacuum must scale as

$$BR = B_0 R_0 = const. \tag{1.13}$$

Here, B_0 denotes the value of the magnetic field on the magnetic axis. Hence

$$B = \frac{B_0}{1 + \epsilon \cos\theta} \approx B_0 \left(1 - \epsilon \cos\theta\right). \tag{1.14}$$

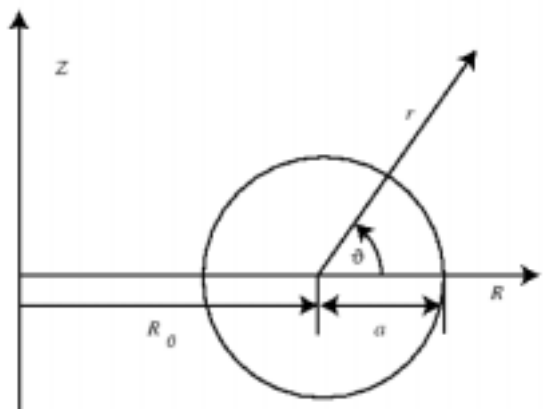

Figure 1.5: Geometric coordinates in a circular large aspect-ratio tokamak.

Adopting the large aspect-ratio approximation, the tokamak can be modelled as a cylinder with a magnetic field which is inhomogeneous on the poloidal cross section following Eq.(1.14). Such inhomogeneity also accounts for the curvature effects, which enters at $\mathcal{O}(\epsilon)$. In such geometry, the contravariant components of the magnetic field are obtained through

$$B^{\zeta} = \mathbf{B} \cdot \nabla\zeta \approx \frac{B_t}{R} \tag{1.15}$$

and

$$B^{\theta} = \mathbf{B} \cdot \nabla\theta \approx \frac{B_p}{r}. \tag{1.16}$$

In the previous formulae, B_t (toroidal) and B_p (poloidal) are the components of the magnetic field in a local unit vector basis,

$$\mathbf{B} = B_t \hat{\mathbf{e}}_{\zeta} + B_p \hat{\mathbf{e}}_{\theta}, \tag{1.17}$$

where $\hat{\mathbf{e}}$-s denote unit vectors. The subscripts t and p should avoid any confusion with the covariant components B_ζ and B_θ, respectively.

In view of Eq.(1.15) and (1.16), the safety factor in the large aspect-ratio approximation possesses thus the expression (see Eq.(1.9))

$$q = \frac{B^{\zeta}}{B^{\theta}} \approx \frac{rB_t}{RB_p}. \tag{1.18}$$

As in a tokamak q is typically of the order of unity, it follows that

$$B_p = \frac{\epsilon}{q} B_t \ll B_t. \tag{1.19}$$

Hence

$$B = |\mathbf{B}| = \sqrt{B_t^2 + B_p^2} = B_t + \mathcal{O}\left(\epsilon^2\right). \tag{1.20}$$

This approximation is largely used in the present thesis.

According to the definition exposed above, the poloidal flux χ in a large aspect-ratio machine can be expressed as

$$\chi = rRB_p. \tag{1.21}$$

A convenient way to write the magnetic field in a large aspect-ratio tokamak follows from this result. Introducing

$$I = RB_t \tag{1.22}$$

the magnetic field takes the form (which is actually valid also for general tokamak configurations)

$$\mathbf{B} = I\nabla\zeta + \nabla\zeta \times \nabla\chi. \tag{1.23}$$

Unless specified, this thesis refers to a large aspect-ratio circular tokamak, where the equilibrium magnetic field is represented by the mixed co- and contravariant formulation used in Eq.(1.23)

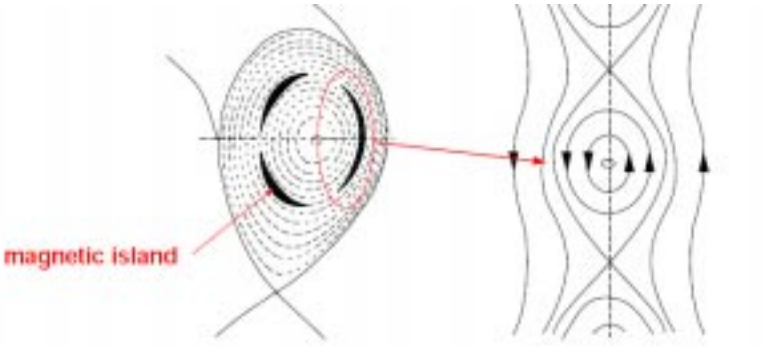

Figure 1.6: Poloidal cross-section of a tokamak in presence of a magnetic island chain. Islands have a radial extent and follow the field lines generating helically winding structures along the torus.

1.3.3 Perturbed Equilibria

In this introductory chapter, the main features related to the tokamak equilibrium have been outlined. One of the crucial points which have been intensely investigated by fusion scientists concerns the *stability* of such equilibrium. A confined plasma represents a driven system, forced away from

its natural thermodynamic equilibrium state, and also for this reason it is rarely completely stable. Observed equilibria display in fact a large variety of unstable excitations. In the present work, a particular kind of instability, the *neoclassical tearing mode*, will be analyzed. This mode has a growth rate which is relatively slow, compared to other instabilities, but for reasons that will be discussed in detail afterwards, they have highly undesirable consequences on the performance of a tokamak.

Tearing modes modify the topology of the magnetic surfaces by means of a perturbed radial component of the magnetic field, which in turn "reconnects" different magnetic surfaces. The subsequent magnetic field configuration, displayed in Fig.1.6, exhibits helical structures which are named, because of their shape, *magnetic islands*. It can be intuitively inferred that such magnetic perturbations is related to a perturbed current in the plasma, according to Ampère's law. The goal of the present work is to study the currents which are generated by a rotating magnetic island, and their influence on the stability of the island itself.

Chapter 2

Particle Motion in an Inhomogeneous Magnetic Field

In this chapter, some generalities about the motion of a charged particle in an electromagnetic field are recalled. First, the simple case of constant electric and magnetic fields is considered. Then, this assumption is relaxed, in order to provide the basis to understand the dynamics of a single particle in a tokamak.

2.1 The Small Larmor-Radius Expansion

2.1.1 Motion with Constant Fields

If the electric and magnetic fields ($\mathbf{E}$ and $\mathbf{B}$, respectively) are uniform and time-independent, the solution of the equation of motion Eq.(2.2) is straightforward. Writing the velocity vector as

$$\mathbf{v} = \mathbf{b}v_{\parallel} + \mathbf{v}_{\perp}, \tag{2.1}$$

$\mathbf{b}$ being $\mathbf{B}/B$ (i.e. the unit vector parallel to the magnetic field), $\mathbf{v}_{\perp} = \mathbf{b} \times (\mathbf{v} \times \mathbf{b})$ and the subscript $\parallel$ referring to the magnetic field, the equation of motion (called sometimes Lorentz equation)

$$m_p \frac{\mathrm{d}\mathbf{v}}{\mathrm{d}t} = q_p \left(\mathbf{E} + \frac{1}{c} \mathbf{v} \times \mathbf{B} \right), \tag{2.2}$$

where m_p is the particle mass and q_p the particle charge, has the solution

$$v_{\parallel}(t) = v_{\parallel}(t=0) + \frac{q_p}{m_p} E_{\parallel} t \tag{2.3}$$

$$\mathbf{v}_{\perp}(t) = v_{\perp} \left[\mathbf{e}_2 \cos(\omega_c t) - \mathbf{e}_3 \sin(\omega_c t) \right] + c \frac{\mathbf{E} \times \mathbf{B}}{B^2}, \tag{2.4}$$

where the unit vectors $\mathbf{e}_2$ and $\mathbf{e}_3$ form an orthonormal triplet with $\mathbf{b}$ (i.e. $\mathbf{b} \cdot \mathbf{e}_2 \times \mathbf{e}_3 = 1$). These unit vectors can always be chosen in such a way that $\mathbf{v}_{\perp}$ is parallel to $\mathbf{e}_2$ at $t = 0$. In Eq.(2.4), the so called *cyclotron frequency* ω_c

$$\omega_c = \frac{q_p B}{m_p c} \tag{2.5}$$

is introduced. This frequency characterises the gyration motion (or gyromotion) of the particle around the magnetic field line, as well-known from classical electrodynamics. The term in Eq.(2.4) which contains the electric field is referred to as $\mathbf{E} \times \mathbf{B}$-*drift*. It is a constant term, perpendicular to both the electric and the magnetic field, which exhibits the remarkable feature of being charge- and mass-independent. As a consequence, no charge separation phenomena are associated to such drift. From a physical point of view, an electric field perpendicular to $\mathbf{B}$ locally modifies the radius of the gyration of a particle, accelerating or decelerating it. The result is the helical trajectory depicted in Fig.2.1.

A typical procedure in the physics of magnetized plasma consists in separating the part of the velocity associated to the gyromotion from the other contributions. The motion of a particle is written as the superposition of the gyration plus the motion of the centre of the rotation (called *guiding centre*),

$$\mathbf{x}(t) = \mathbf{X}(t) + \mathbf{r}(t), \tag{2.6}$$

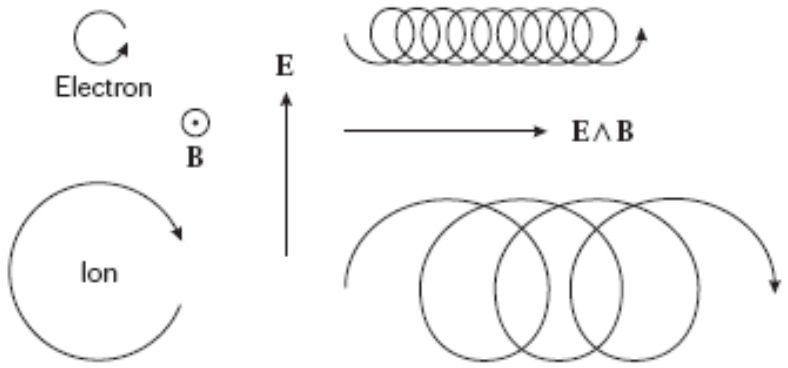

Figure 2.1: Effect of a uniform perpendicular electric field on the motion of a gyrating ion and of a gyrating electron. The resulting drift is constant and perpendicular to both electric and magnetic field.

where

$$\mathbf{X}(t) = c\frac{\mathbf{E}\times\mathbf{B}}{B^2}t + \mathbf{b}v_{\parallel}t + \mathbf{X}(t=0) \tag{2.7}$$

$$\mathbf{r}(t) = \rho_L\left[\mathbf{e}_2\sin(\omega_c t) + \mathbf{e}_3\cos(\omega_c t)\right] \tag{2.8}$$

$\mathbf{X}(t)$ being the position of the guiding centre and $\mathbf{r}(t)$ the gyrating term. The quantity $\rho_L \doteq v_\perp/\omega_c$ in Eq.(2.8) is known as the *Larmor radius*, and it represents the radius of the gyroorbit. The *gyroaverage* of $\mathbf{r}$, defined as

$$\langle\mathbf{r}\rangle_\gamma = \frac{1}{2\pi}\int_0^{2\pi} \mathrm{d}\gamma\mathbf{r}(\gamma,t) \tag{2.9}$$

is identically zero (here, γ represents the phase of the gyromotion), so that the position of the guiding centre is defined by the relation

$$\mathbf{X} = \langle\mathbf{x}\rangle_\gamma . \tag{2.10}$$

The possibility of identifying a guiding centre becomes crucial for the treatment of non-uniform electric and magnetic field, as discussed in the next section.

2.1.2 Motion with Space- and Time-Varying Fields

There is no general solution for the Lorentz equation when fields are allowed to have space- and time-dependence. However, if the gyromotion occurs on faster timescales compared to the guiding centre motion, a perturbative approach to the problem is possible. Such approach can be formally obtained by replacing the ratio m_p/q_p with $\delta m_p/q_p$, where δ is the small parameter of the perturbative analysis, which can be introduced as

$$\delta = \frac{\rho_L}{L_B}, \tag{2.11}$$

where L_B is the characteristic length of variation of the magnetic field. In other words, a perturbative approach is appropriate if the variation of the fields is small on the gyration time- and space-scale, or equivalently if the fields do not vary strongly in the region explored by a particle during a single gyration. The Lorentz equation takes the form

$$\frac{\mathrm{d}^2\mathbf{x}}{\mathrm{d}t^2} = \frac{q_p}{\delta m_p}\mathbf{E}\left(\mathbf{x},t\right) + \frac{q_p}{\delta m_p c}\frac{\mathrm{d}\mathbf{x}}{\mathrm{d}t} \times \mathbf{B}\left(\mathbf{x},t\right). \tag{2.12}$$

The coordinate $\mathbf{x}$ is expanded as

$$\mathbf{x}\left(t\right) = \mathbf{X}\left(t\right) + \delta\mathbf{r}_1\left(\gamma\left(t\right),t\right) + \delta^2\mathbf{r}_2\left(\gamma\left(t\right),t\right) + \ldots \tag{2.13}$$

The vectors $\mathbf{r}$ are supposed to rapidly rotate with the phase $\gamma\left(t\right)$. Concerning the time derivatives, the guiding centre velocity is written as

$$\dot{\mathbf{X}}\left(t\right) = \mathbf{v}_0 + \delta\mathbf{v}_1 + \ldots \tag{2.14}$$

and

$$\dot{\gamma}\left(t\right) = \frac{1}{\delta}\omega_0\left(t\right) + \omega_1 + \ldots \tag{2.15}$$

The factor $1/\delta$ originates from the fact that the result $\omega_0 = \omega_c$ is expected, but noting that $m_p/q_p \to \delta m_p/q_p$, it follows that $\omega_c \to \omega_c/\delta$. The expression for the particle velocity takes the form

$$\frac{\mathrm{d}\mathbf{x}}{\mathrm{d}t} = \mathbf{v}_0 + \delta\mathbf{v}_1 + \ldots + \frac{\partial \mathbf{r}_1}{\partial \gamma}\left(\omega_0 + \delta\omega_1 + \ldots\right) + \delta\frac{\partial \mathbf{r}_1}{\partial t} + \ldots \tag{2.16}$$

and a similar but more complicated expression can be found for the acceleration. The fields are expanded as

$$\mathbf{B} = \mathbf{B}\left(\mathbf{X}, t\right) + \delta\left(\mathbf{r}_1 \cdot \nabla\right)\mathbf{B}\left(\mathbf{X}, t\right) + \ldots \tag{2.17}$$

and similarly for the electric field. In order to avoid runaway particles, it is necessary to suppose that the lowest-order term of the electric field has no parallel component, because there is no term which can balance it. All these results can be substituted in Eq.(2.12), which can now be solved order by order. A complete calculation can be found for example in Ref.[6]. In this chapter, the details of the solution will not be reported, but the most relevant results are summarized, highlighting the most noteworthy physical aspects.

From the lowest-order equation for $\mathbf{r}$, one obtains

$$\mathbf{r}_1\left(\gamma, t\right) = \rho_L\left[\mathbf{e}_2\left(t\right)\sin\gamma + \mathbf{e}_3\left(t\right)\cos\gamma\right] \tag{2.18}$$

and

$$\omega_0\left(t\right) = \frac{q_p}{m_p c}B\left(\mathbf{X}\right) = \omega_c\left(\mathbf{X}, t\right). \tag{2.19}$$

This means that the lowest order frequency is the gyrofrequency *calculated at the guiding centre position*. In most of the relevant cases, no higher order corrections to the gyrating part of the particle motion are retained.

On the other hand, considering the guiding centre motion, the calculation yields

$$\mathbf{v}_0 = v_{0\|}\mathbf{b} + c\frac{\mathbf{E}\left(\mathbf{X}\right) \times \mathbf{B}\left(\mathbf{X}\right)}{B^2\left(\mathbf{X}\right)}. \tag{2.20}$$

Thus, to the lowest order the guiding centre motion is the same as for the case of uniform fields. This reflects the fact that, during a gyration period, the

guiding centre moves on a space scale that is supposed to be small compared to L_B, and thus no lowest-order variations of the magnetic and electric field can be experienced by the particle (this is the meaning of the scale separation, recall Eq.(2.11)).

Significant contributions to the perpendicular velocity arise from $\mathcal{O}(\delta)$ terms. In particular, the explicit expression for $\mathbf{v}_1$ is

$$\mathbf{v}_{1\perp} = \frac{1}{\omega_c B}\mathbf{B} \times \frac{\mathrm{d}\mathbf{v}_0}{\mathrm{d}t} + \frac{\omega_c \rho_L^2}{2B^2}\mathbf{B} \times \nabla B. \tag{2.21}$$

The second term on the right-hand side is easier to be treated. It is known as the *grad-B drift*, $\mathbf{v}_{\nabla B}$. In fact, a space-dependent magnetic field, in complete analogy with the $\mathbf{E}\times\mathbf{B}$-drift (see Fig.2.1), causes a local variation of the particle gyroradius during gyromotion, which gyroaverages to a net displacement of the guiding centre.

To properly analyze the first term on the right-hand side of Eq.(2.21), (recall $\mathbf{v}_0 = v_{0\parallel}\mathbf{b} + \mathbf{v}_{0\perp}$), it is first noted that

$$\frac{\mathrm{d}\mathbf{b}}{\mathrm{d}t} = \frac{\partial \mathbf{b}}{\partial t} + v_\parallel \mathbf{b}\cdot\nabla\mathbf{b} + \mathbf{v}_{0\perp}\cdot\nabla\mathbf{b} \tag{2.22}$$

$$\frac{\mathrm{d}\mathbf{v}_{0\perp}}{\mathrm{d}t} = c\left(\frac{\partial}{\partial t} + \mathbf{v}_0\cdot\nabla\right)\frac{\mathbf{E}\times\mathbf{B}}{B^2} \tag{2.23}$$

$$\frac{\mathrm{d}v_{0\parallel}}{\mathrm{d}t} = \frac{q_p}{m_p}E_\parallel - \frac{q_p\rho_L^2\omega_c}{2m_p c}\mathbf{b}\cdot\nabla B. \tag{2.24}$$

Eq.(2.24) comes from the expression for the accelerations. Note that the parallel electric field which enters Eq.(2.24) is in fact $\delta E_\parallel$, as no lowest-order parallel electric field has been considered. Substituting each term in Eq.(2.21), it is possible to obtain a complete expression for the first-order velocity.

For the phenomena of interest in the present thesis (which refers to typical tokamak discharges), the presence of a $\mathcal{O}(1)$ electric field is typically excluded. This fact is expressed mathematically by the assumption

$$E \sim \delta B. \tag{2.25}$$

As a consequence, the velocity of the guiding centre has no perpendicular component at the lowest order (i.e. the $\mathbf{E}\times\mathbf{B}$ drift moves to $\mathcal{O}(\delta)$). Moreover, as a static confining field is assumed, the partial derivative of $\mathbf{b}$ with respect to time is not relevant in such context (the perturbation associated to the magnetic island is small compared to the equilibrium magnetic field, and this introduces only higher-order corrections on $\mathbf{b}$). Eq(2.21, 2.22) and Eq.(2.24) take for this reason the form

$$\mathbf{v}_{1\perp} = v_{\mathbf{E}\times\mathbf{B}} + \frac{1}{\omega_c B}\mathbf{B}\times\frac{\mathrm{d}\mathbf{v}_0}{\mathrm{d}t} + \frac{\omega_c\rho_L^2}{2B^2}\mathbf{B}\times\nabla B \tag{2.26}$$

$$\frac{\mathrm{d}\mathbf{b}}{\mathrm{d}t} = v_\parallel \mathbf{b}\cdot\nabla\mathbf{b} \tag{2.27}$$

$$\frac{\mathrm{d}v_{0\parallel}}{\mathrm{d}t} = \frac{q_p}{m_p}E_\parallel - \frac{q_p\rho_L^2\omega_c}{2m_p c}\mathbf{b}\cdot\nabla B. \tag{2.28}$$

It is worth to discuss the physical meaning of the terms. Introducing the curvature vector $\boldsymbol{\kappa}$ as

$$\boldsymbol{\kappa} = \mathbf{b}\cdot\nabla\mathbf{b} = -\mathbf{b}\times(\nabla\times\mathbf{b}), \tag{2.29}$$

the term on the right-hand side of Eq.(2.27) leads, once substituted in the $\mathrm{d}\mathbf{v}_0/\mathrm{d}t$ term in Eq.(2.26), to the so called *curvature drift*, whose expression is

$$\mathbf{v}_c = \frac{v_\parallel^2}{\omega_c B}(\mathbf{B}\times\boldsymbol{\kappa}). \tag{2.30}$$

Again, this drift is caused by the inhomogeneity of the magnetic field which locally modifies the Larmor radius. Note that the usual definition of the curvature actually corresponds to $-\boldsymbol{\kappa}$, as a minus sign has been introduced for convenience.

The second term on the right-hand side of Eq.(2.28) represents the so called *mirror force*. As depicted in Fig.2.2, as field lines draw near (i.e the magnetic field strength increases), a parallel component of the Lorentz force $(q_p/c)\mathbf{v}\times\mathbf{B}$, pointing towards the region of "weaker" B develops. Thus,

particles with sufficiently low parallel velocity are "reflected" back, wherefore the name "mirror force".

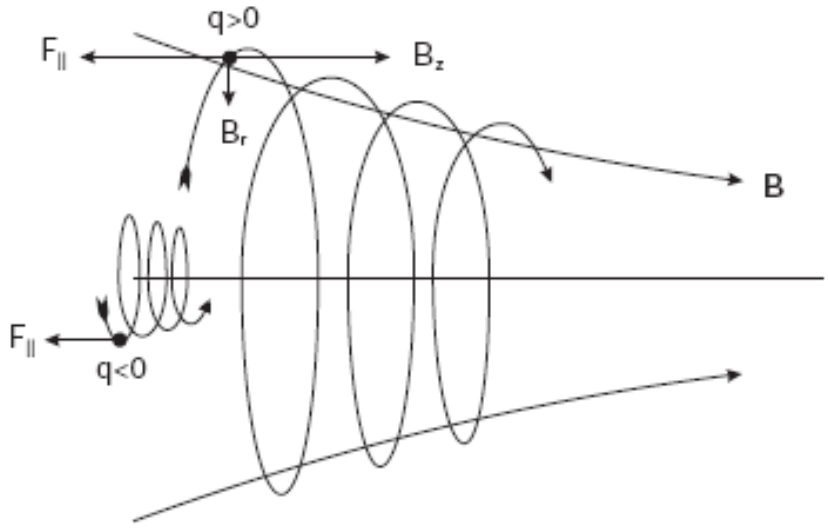

Figure 2.2: Physical interpretation of the mirror force for ions and electrons. As field lines get closer, a component of the Lorentz force is present, which opposes the motion of the guiding centre.

In view of Eq.(2.26), it is evident that drifts coming from the inhomogeneity of the magnetic field (i.e. $\mathbf{v}_c$ and $\mathbf{v}_{\nabla B}$) are mass- and charge-dependent, and thus they can cause the appearance of electrostatic potentials via charge separation. These separations must be immediately compensated in order to ensure quasi-neutrality (see Eq.(1.3)). This point will be discussed in details in the following chapters, as it represents a key mechanism for the generation of parallel currents which play a major role in the stability of a tearing mode (see chapter 3).

It is finally noted that Eq.(2.23), if $E \sim \delta B$, moves to the second order in δ, and thus it is negligible. It is related to the so called *polarization drift*, which is caused by time-varying electric fields. This term is not contained in the drift-kinetic equation, which will be discussed in chapter 4, but becomes

again important for the gyrokinetic case, when the scale of variation of the electric field starts to be comparable with the Larmor radius (see chapter 7).

Summarizing for convenience the results previously derived

$$\begin{aligned} \mathbf{v}_0 &= v_\parallel \mathbf{b} && (2.31) \\ \mathbf{v}_{1\perp} &= c\frac{\mathbf{E}\times\mathbf{B}}{B^2} + \frac{\mu}{m_p\omega_c}\mathbf{b}\times\nabla B + \frac{v_\parallel^2}{\omega_c B}(\mathbf{B}\times\boldsymbol{\kappa}) \\ &= \mathbf{v}_\mathbf{E}\times\mathbf{B} + \mathbf{v}_{\nabla B} + \mathbf{v}_c && (2.32) \\ \frac{\mathrm{d}v_{0\parallel}}{\mathrm{d}t} &= \frac{q_p}{m_p}E_\parallel - \frac{q_p\rho_L^2\omega_c}{2m_p c}\mathbf{b}\cdot\nabla B. && (2.33) \end{aligned}$$

Here, there magnetic moment

$$\mu = \frac{m_p v_\perp^2}{2B} \tag{2.34}$$

has been introduced. This quantity has a remarkable importance in tokamak physics, because it is a so called *adiabatic invariant* of the particle motion. This means that, if the magnetic field is varying on slow time- and spatial scales compared to those of the gyromotion (i.e. if a scale separation is admissible), the total time derivative of μ is negligible. This result can be rigorously obtained, adopting a Hamiltonian approach (Ref.[7] and [8]). In fact, the Hamiltonian for the guiding centre motion, as can be intuitively inferred, is independent on the phase of the gyration, whose conjugate moment is proportional to the magnetic moment.

2.2 Motion of Particles in a Tokamak

This section describes the different types of particle orbits that occur in a tokamak as a consequence of the motion along the field lines and of the various drifts discussed above.

2.2.1 Particle Orbits

As already mentioned, because of the mirror force, particles moving inward in the R-direction (where B is higher) decrease their parallel velocity. For some particles, this effect is such that, at some poloidal position $\theta_b < \pi$ their parallel velocity goes to zero. Thus, these particles cannot follow the (helical) field lines when they reach the so-called high-field side of the tokamak, but they are forced to bounce between $-\theta_b$ and θ_b. Such particles are named *trapped* particles, while those which can follow the field lines along their whole length are known as *passing*. There is a simple criterion to identify trapped and passing particles in a large aspect-ratio circular tokamak, once parallel and perpendicular velocities evaluated at the outer midplane ($\theta = 0$) are known. As both μ and the kinetic energy

$$\mathcal{E} = \frac{m_p v_\parallel^2}{2} + \mu B \tag{2.35}$$

are conserved, and as obviously $v_\parallel^2$ must be a non-negative number, the sole particles which can explore the whole poloidal section are the ones for which

$$v_\parallel^2 (\theta = 0) > \frac{2}{m_p} \mu \left(B (\theta = \pi) - B (\theta = 0) \right). \tag{2.36}$$

According to Eq.(1.14)

$$\frac{2}{m_p} \mu \left(B (\theta = \pi) - B (\theta = 0) \right) = 2\epsilon v_\perp^2 (\theta = 0). \tag{2.37}$$

Hence, a particle is passing if

$$v_\parallel (\theta = 0) > \sqrt{2\epsilon} v_\perp (\theta = 0). \tag{2.38}$$

Note that the trapping condition does not depend on the *magnitude* of the parallel velocity, but on the ratio between $v_\parallel$ and $v_\perp$, i.e. on the angle between the velocity and the field line.

As $\mathbf{B}$ is approximatively toroidal, and both $\boldsymbol{\kappa}$ and ∇B point in the $-\nabla R$ direction, curvature and grad-B drifts lead to a nearly vertical drift. Therefore, both passing and trapped particles do not lie, during their motion, on a single magnetic surface, but they are shifted. For trapped particles, this gives to the projection of the orbit on a poloidal plane the characteristic shape of a banana, and for this reason they are called *banana orbits*. Fig.2.3 shows a typical orbit both for the trapped and for the passing case.

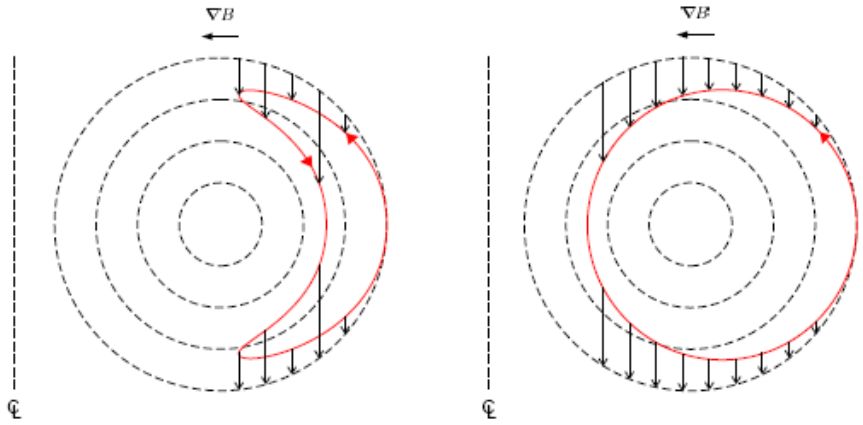

Figure 2.3: Orbits of trapped and passing particle in a tokamak. Black arrows highlight the effect of curvature and grad-B drift.

The width of the banana orbit at the outer midplane can be calculated knowing that the canonical toroidal momentum ($p_t = m_p R v_t + q_p A_t$, where A_t is the toroidal component of the equilibrium vector potential) is a conserved quantity, as ζ is an ignorable coordinate. This, in the limit of a circular tokamak with large aspect-ratio, brings to the following expression for the (half)-banana width ρ_b:

$$\rho_b = \frac{q\rho_L}{\sqrt{\epsilon}} = \sqrt{\epsilon}\rho_\theta, \tag{2.39}$$

where ρ_θ is the *poloidal Larmor radius* (i.e. the Larmor radius calculated

with the poloidal component of the magnetic field). Thus, the banana orbit is typically larger than the Larmor radius. A similar argument can be applied to passing particles. Their orbit has nearly the same shape as a magnetic surface, but it is shifted with respect to it by

$$\Delta_p = -q\frac{v_\parallel}{\omega_c} \tag{2.40}$$

in the R-direction. Here, $v_\parallel$ must be calculated at $\theta = 0$. The shift of a passing particle is thus smaller by a factor of $\epsilon^{1/2}$ than the banana width (for comparable values of $v_\parallel$). This implies that a trapped particle, while bouncing, explores a wider range of magnetic surfaces. It is important to note that Δ_p depends on the sign of the parallel velocity of the particle.

In conclusion of this paragraph, the reason for the necessity of the poloidal component of the equilibrium magnetic field mentioned in section 1.2 is briefly exposed. Curvature and grad-B drift, as stated before, lead to a nearly vertical drift, which occurs in opposite directions for the ions and the electrons. Without the smaller poloidal component of the magnetic field, this would lead to charge separation, and thus to a vertical electric field, giving rise to a strong $\mathbf{E} \times \mathbf{B}$-drift. This would lead to a very fast loss of particles, which would terminate the plasma discharge. By adding a small poloidal field, particles still primarily follow the field lines, but they now explore the entire poloidal cross section before returning close to where they started. Each species still has a vertical drift associated, but this now cancels in the upper and lower halves of the torus, with the effect that there is no net vertical drift.

2.2.2 Toroidal Precession of Trapped Particles

In this subsection, it is shown that trapped particles exhibit a precession in the toroidal direction, and the timescales for this drift around the torus are derived. Analytic expressions for the orbit drifts are obtained in the approx-

imation of a circular large aspect-ratio tokamak, and the derived expressions are accurate to the lowest order in ϵ, following Ref.[9]. More detailed calculations can be found in Ref.[10] and [11].

The first contribution to the toroidal precession is linked to the magnetic drifts. Curvature and grad-B drifts have in fact a poloidal component, which can be written as (see Eq.(2.31))

$$\dot{\theta} = \frac{v_\parallel^2 + v_\perp^2/2}{\omega_c R^2 \epsilon} \cos\theta \tag{2.41}$$

Because of the helicity of the field

$$\dot{\zeta} = q\dot{\theta} + \mathcal{O}(\epsilon). \tag{2.42}$$

Thus

$$\dot{\zeta} \doteq \omega_D = q\frac{v_\parallel^2 + v_\perp^2/2}{\omega_c R^2 \epsilon} \cos\theta. \tag{2.43}$$

For passing particles, this contribution almost cancels on a poloidal turn. This is not true for a trapped particle, which is poloidally confined in the region $-\theta_b < \theta < \theta_b$, and by consequence the θ-average of Eq.(2.43) is in general nonzero. Fig.2.4 shows the toroidal precession of a trapped particle. The same effect can be observed for any drift which has a poloidal component, for example an $\mathbf{E} \times \mathbf{B}$-drift generated by a purely radial electric field. The corresponding toroidal precession frequency in such case can be shown to be

$$\omega_E = c\frac{E_r}{RB_\theta}, \tag{2.44}$$

where E_r is the strenght of the radial electric field.

The second cause of a magnetic toroidal drift of the orbits is linked to the dependence of the safety factor q on the minor radius (the so called *magnetic shear*, Eq.(1.10)). This dependence, in combination with the excursion of the trapped particle across the magnetic surfaces, leads to a difference in toroidal distance between the bounce points for the inner and the outer

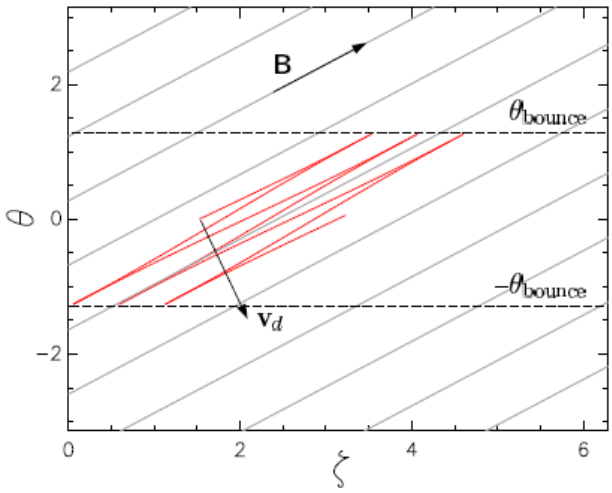

Figure 2.4: Sketch of the toroidal precession of banana orbits induced by magnetic drifts. The representation can be thought of as a side view of a tokamak, with the poloidal coordinate "unfolded".

leg of the banana orbit. This again brings to a slight shift in the toroidal direction after a bounce period. Referring to a large aspect-ratio tokamak, the displacement of the particle from the surface where the bounce points lie is of the order of banana width, i.e. (see Eq.(2.39))

$$\Delta r \approx \rho_b \approx \frac{q}{\epsilon\omega_c} v_\parallel, \tag{2.45}$$

having estimated $v_\parallel \sim \sqrt{\epsilon} v_\perp$ according to Eq.(2.38). The parallel motion in the poloidal direction is expressed as

$$\dot{\theta} = \frac{v_\parallel}{Rq}. \tag{2.46}$$

Thus, the toroidal precession due to the variation of the helicity of the magnetic field across the magnetic surface amounts to

$$\dot{\zeta} \doteq \omega_{\hat{s}} = (\Delta q)\,\dot{\theta} = \frac{\mathrm{d}q}{\mathrm{d}r}\Delta r\dot{\theta} = \frac{q\hat{s}}{R^2\epsilon^2\omega_c} v_\parallel^2 \tag{2.47}$$

where the magnetic shear $\hat{s}$ defined in Eq.(1.10) has been used in the last step. The value of the shear to be used in Eq.(2.47) is the one corresponding to the surface where $v_{\|}$ is zero.

Chapter 3

The Tearing Mode

As mentioned at the end of chapter 1, the focus of this work is on the kinetic investigation of a tokamak plasma in the presence of a magnetic perturbation due to the appearance of a so-called *tearing mode*. In this chapter, which is the last of the introductory part of the present thesis, the main aspects of the physics of the tearing mode are discussed. The following analysis is not meant to be complete, as the stability of tearing modes is both an extremely wide topic and an active area of research. Only the fundamental points necessary for the subsequent analysis are highlighted here.

3.1 Classical Stability of the Tearing Mode

The confinement efficiency of a tokamak is determined by the fact that, to lowest order, ions and electrons follow the magnetic field lines, which in turn lie on toroidal symmetric nested surfaces, as presented in the previous chapters. However, there exists a number of plasma instabilities which can modify such geometry, leading to a reduction of the machine's performances. The *tearing mode* belongs to them. The magnetic configuration in presence of such instability is characterized by the occurrence of a periodic, mainly radial magnetic perturbation, which leads to the formation of a chain of *magnetic islands*, as shown in Fig.3.1 and Fig.3.2. As the motion of the particles is very

fast along the field lines, this radial component of the magnetic field greatly enhances the transport of both particles and energy in the radial direction, causing a flattening of the radial profiles over a distance comparable with the island width (see Fig.3.1). This leads to a significant degradation of the overall confinement.

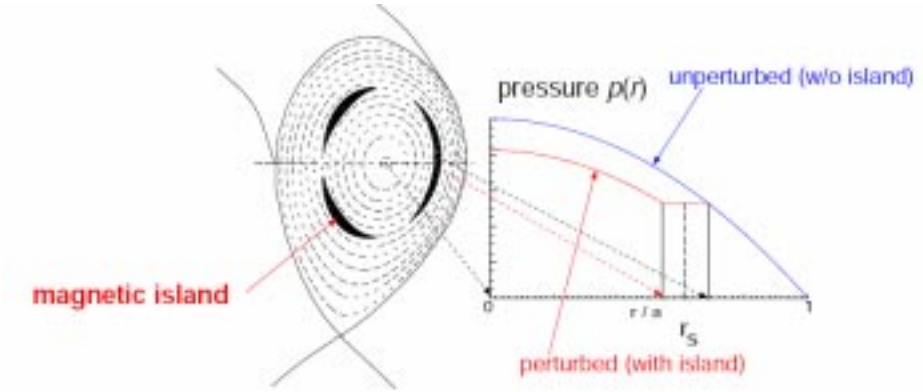

Figure 3.1: Typical pressure profile in a tokamak for an unperturbed equilibrium and in presence of a magnetic island.

For this reason, the study of the stability of tearing modes is considered a crucial issue towards the realization of a fusion reactor.

3.2 Modelling of a Magnetic Island

Every physical quantity in a tokamak plasma must be periodic with respect to both the poloidal and the toroidal angle, as it cannot obviously be multi-valued at any point of the machine. Thus, every possible perturbed physical quantity connected to an instability $P(\chi, \theta, \zeta)$ admits a Fourier representation, such as

$$P(\chi, \theta, \zeta) = \sum_{l,k} P_{l,k}(\chi) \exp(il\theta - ik\zeta), \tag{3.1}$$

where (χ, θ, ζ) are the coordinates chosen to characterise the magnetic equilibrium, cf. subsection 1.3.1. From a stability analysis (see e.g. [6]), it can be shown that the modes which are more likely to get destabilized are the ones which have (almost) the same helicity of the magnetic field line, i.e. perturbations which tend to remain (almost) constant along the field line. This is because magnetic field lines behave in fact as elastic "strings", where the modes with low $k_\parallel$ are easier to be excited in comparison with high-$k_\parallel$ ones. If the safety factor q, on a given surface, has an irrational value, magnetic field lines are non-periodic, and therefore they cover ergodically a flux surface without closing on themselves. Thus, it is impossible for any perturbation to be aligned with the magnetic field lines, as it would clearly violate the periodicity constraint. This is no longer true when the parameter q has a rational value. These particular surfaces are called *rational surfaces*, and they play a fundamental role in the plasma confinement physics. The tearing mode is an instability which develops on rational surfaces, where

$$q = \frac{m}{n}, \tag{3.2}$$

being m, n the poloidal and toroidal mode number of the mode, respectively. Fig.3.2 shows the magnetic configuration in a tokamak where a $m = 2$, $n = 1$ (short (2,1)) is present. The limiting surface of the island is called *separatrix*. Because of their shape, the two points of the separatrix where magnetic surfaces cross are known as *X-points*, while the centre of the island is called *O-point* (see Fig.3.3)

A convenient coordinate to study the magnetic island is the helical angle

$$\xi = m\theta - n\zeta \tag{3.3}$$

This coordinate labels (i.e. it is constant on) the magnetic field lines on the rational surface, and it also represents the coordinate of periodicity for the m, n-th harmonic of the mode. The unperturbed magnetic field has a helical

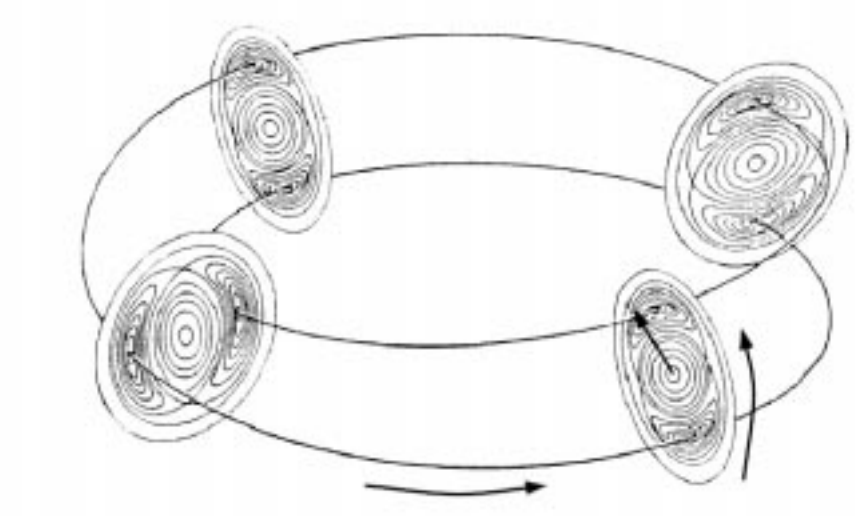

Figure 3.2: Magnetic topology of a tokamak in presence of a $m = 2$, $n = 1$ tearing mode.

component B_h (i.e. in the $\nabla\xi$-direction) expressed by

$$B_h = B_\theta \left(m - nq(\chi)\right), \tag{3.4}$$

when the large aspect-ratio approximation is adopted. The role of the tearing mode instability is to provide the (mainly) radial component of magnetic field required to generate a magnetic island. Denoting this by $\delta B = B_r \sin\xi$, a perturbed field line will follow a trajectory given by

$$\frac{\mathrm{d}\chi}{\chi_s \mathrm{d}\xi} = \frac{\delta B}{B_h}, \tag{3.5}$$

where the subscript s indicates quantities calculated on the rational surface. From Eq.(3.5) it is possible to see how the largest radial excursions are localized in the vicinity of the rational surface, where $B_h \to 0$. Taylor expanding the safety factor about the rational surface $\chi = \chi_s$, it is possible to substitute Eq.(3.4) into Eq.(3.5), and then integrate. This yields

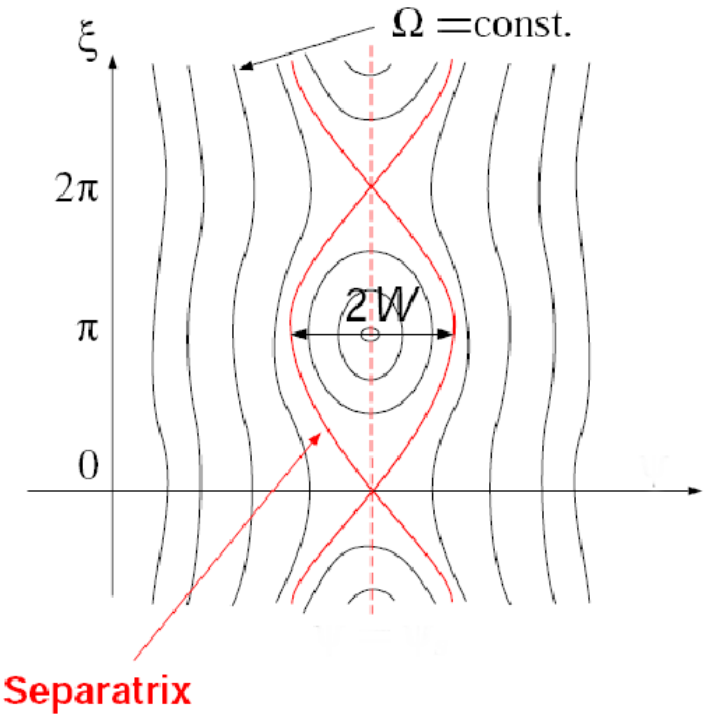

Figure 3.3: Structure and coordinates of a single magnetic island.

$$\Omega = \frac{2\left(\chi - \chi_s\right)^2}{W_\chi^2} - \cos\xi. \tag{3.6}$$

The integration constant Ω plays the role of a flux-surface label for the perturbed magnetic surfaces, in analogy with χ in the unperturbed case, see Fig.3.3. The quantity W_χ has the meaning of island half-width expressed in χ-units. Its value corresponds to

$$W_\chi = 2\left(\frac{\chi_s q B_r}{m B_\theta \mathrm{d}q/\mathrm{d}\chi}\right)^{1/2}, \tag{3.7}$$

where both q and its derivative are calculated on the resonant surface. The value $\Omega = 1$ identifies the island separatrix, while $\Omega = -1$ corresponds to the

island O-point.

The usual way of including tearing modes in the tokamak magnetic geometry, Eq.(1.23), consists in introducing a perturbation ψ on the poloidal flux

$$\mathbf{B} = I\nabla\zeta + \nabla\zeta \times \nabla\left(\chi + \psi\right), \tag{3.8}$$

being

$$\psi = \tilde{\psi}\cos\xi. \tag{3.9}$$

This perturbed flux is connected to the parallel vector potential perturbation through

$$A_{\|} = -\frac{\psi}{R} = -\frac{\tilde{\psi}}{R}\cos\xi \tag{3.10}$$

which is linked in turn to the perturbed radial magnetic field δB. The perturbed flux is moreover related to the island width W_χ through

$$W_\chi^2 = \frac{4\tilde{\psi}q_s}{q_s'}. \tag{3.11}$$

Here, $\tilde{\psi}$ is assumed to vary only slowly with radius over the island width length scale, as discussed in the next section.

For reasons that will be discussed in more detail later on, magnetic islands experience in general a rotation in the $\nabla\xi$ direction. To account for this, it is convenient to transform

$$\xi \rightarrow m\theta - n\zeta - \omega t, \tag{3.12}$$

where ω is the island rotation frequency. This transformation has clearly a unitary Jacobian, and thus all the equation derived in the present section are still valid as the island rotation is included.

3.3 Classical Tearing Modes and Rutherford Equation

The stability of the tearing mode is strictly connected to the perturbed current due to the presence of the mode itself. Early studies described the mechanism of appearance of these currents in a purely inductive way, i.e. the time-dependent perturbed magnetic field induces an electric field that, together with the finite plasma resistivity, determines the current.[1] This mechanism characterises the so called *classical* description of a tearing mode. An analysis of this phenomenon is usually given in terms of resistive fluid equations. In this introductory chapter, only the most relevant features are described in order to provide an intuitive picture.

A remarkable point of the cited fluid derivation is that the equation system is solved with the help of a *boundary layer* technique. This is because the resistive terms in the fluid equations are negligible everywhere in the plasma *but* in a small layer around the resonant surface, where the current perturbation is localized. On the other hand, in such layer, resistive effects dominate. The equations are hence solved in the two regions in the respective limits. The two solutions are then asymptotically matched together at the boundary of both layers (see for example Ref.[6]). The linear description of a classical tearing mode was first presented in Ref.[13], while the nonlinear saturation has been explained in the fundamental work of Rutherford [14].

From the analysis of the outer region (where resistivity is negligible), it is found that the perturbed poloidal flux ψ presents a discontinuous derivative

[1] A dissipative effect, such as resistivity, is mandatory to properly depict magnetic reconnection. In fact in a non resistive plasma, according to the well-known "frozen-in law" of ideal magnetohydrodynamics (see for example Ref.[12]), the magnetic flux associated to a Lagrangian plasma volume must remain constant during the time-evolution of the volume itself. This implies that two distinct field lines must remain such, and therefore no change in the magnetic topology would be admissible. Resistivity introduces a diffusive term for magnetic field lines, in turn allowing reconnection to take place.

across the resonant surface. This discontinuity is linked to the free energy available for the growth of the instability, and it is typically introduced by means of the parameter

$$\Delta' = \frac{1}{\psi}\left[\left.\frac{\mathrm{d}\psi}{\mathrm{d}r}\right|_{r\to r_s^+} - \left.\frac{\mathrm{d}\psi}{\mathrm{d}r}\right|_{r\to r_s^-}\right], \tag{3.13}$$

alternatively defined as

$$\Delta' = \int_{-\infty}^{\infty} \mathrm{d}x \frac{\mathrm{d}^2 \ln\psi}{\mathrm{d}x^2}, \tag{3.14}$$

as the perturbation ψ has a vanishing derivative if $x = r - r_s \to \pm\infty$. In the limit of small island width, tearing modes are characterized by

$$|\Delta' w| \ll 1, \tag{3.15}$$

where w is the island half-width. Within such limit, the constant-ψ approximation (see Eq.(3.9)) holds. The evolution of the island is described by the Ampère's law, namely

$$\nabla\cdot\left(R^{-2}\nabla\psi\right) = \frac{4\pi}{c} J_\parallel. \tag{3.16}$$

As only the fundamental ξ harmonic of the tearing perturbation is kept, see Eq.(3.9), Eq.(3.16) is conveniently multiplied times $\cos\xi$ and then integrated on the whole domain in x (through the coordinate Ω, see Eq.(3.6)), and over a period in ξ . For a large aspect-ratio tokamak geometry, this yields (see e.g. Ref.[15])

$$\frac{q_s'}{q_s}\frac{c\Delta'}{8\sqrt{2}R}\left|\nabla\chi\right|_s^2 w = \int_{-1}^{\infty}\mathrm{d}\Omega \oint \mathrm{d}\xi \frac{J_\parallel\cos\xi}{\sqrt{\Omega+\cos\xi}}. \tag{3.17}$$

A key point emerges from this equation: *only the components of the parallel current which are in phase with the perturbed poloidal flux* ψ (*i.e. components in* $\cos\xi$) *affect the stability of the mode*, see also Eq.(3.9). Out-of-phase currents are on the other side responsible for the rotation of the island, as they are in phase with the radial magnetic field (which is proportional to $\sin\xi$) and thus are able to generate a $\mathbf{J}\times\mathbf{B}$ torque which does not vanish after volume integration.

As previously outlined, the classical description of the tearing mode is characterised by the fact that the parallel current in Eq.(3.17) is determined only by means of the induction's law, taking into account the finite plasma resistivity. Recalling that ψ is proportional to the perturbed magnetic vector potential (see Eq.(3.10)), it is possible to write

$$J_{\parallel} = \frac{1}{\eta R c} \frac{\partial \tilde{\psi}}{\partial t} \cos \xi, \tag{3.18}$$

where η is the plasma resistivity. The component of the parallel electric field coming from the island electrostatic potential vanishes after volume integration, and has been therefore neglected. Substituting these results in Eq.(3.17), one obtains

$$\frac{\mathrm{d}w}{\mathrm{d}t} = 0.27 \frac{\eta c^2}{4\pi} \Delta', \tag{3.19}$$

where the relation between $\tilde{\psi}$ and w has been invoked (Eq.(3.11)). This fundamental result is known as *Rutherford equation*, and it represents the starting point for the study of the stability of the magnetic islands. Standard models, like those presented shortly afterwards, follow indeed the same derivation path, but consider other contributions to the perturbed parallel current. The stability criterion for a classical tearing mode is hence simply

$$\Delta' > 0 \rightarrow \textit{instability}. \tag{3.20}$$

Thus, according to this model, an equilibrium magnetic configuration which ensures $\Delta' < 0$, which is typically the case in present tokamak experiments, is sufficient to avoid the presence of magnetic islands. Unfortunately, other mechanisms are involved, driving unstable modes otherwise stable in a classical sense.

3.4 The Neoclassical Drive

In the previous section, only the inductive contribution to the perturbed current $J_{\parallel}$ was considered. However, other effects, referable to the so called

neoclassical theory [16], have been shown to play a crucial role in the dynamic of magnetic islands. Roughly speaking, the neoclassical theory deals with all those phenomena which arise from the motion of the particles in a toroidal system and their interaction through Coulomb collisions. This theory will be used quite massively in the remainder of this thesis. The influence of neoclassical effects on the stability of a magnetic island characterizes the so called *neoclassical tearing modes* (NTMs).

The first important neoclassical contribution comes from the *bootstrap current*. This current is present also in an unperturbed tokamak, and can be thought of as the analougue, in the parallel direction, of the diamagnetic current found in chapter 1. The mechanism generating such current is quite complicated. In fact, in the presence of a radial density gradient, the number of banana orbits having their outer leg lying on a given magnetic surface can be larger than the number of orbits having their inner leg on the same surface (likewise, the average velocity of the particles is larger for "inner" bananas than for "outer" bananas in presence of a temperature gradient). Thus, as the sign of the parallel velocity changes between the two legs, an unbalanced toroidal angular momentum, mainly carried by ions, develops. Such momentum is then transmitted via collisions both to passing electrons and to passing ions. The difference between the two flows is what is referred to as bootstrap current [17, 18]. Fig.3.4 depicts what discussed.

An estimate of this contribution for a large aspect-ratio tokamak brings to

$$J_{\parallel,\mathrm{bs}} \propto \frac{\sqrt{\epsilon} p'}{B_p}, \tag{3.21}$$

denoting

$$p' = \frac{\mathrm{d}p}{\mathrm{d}\chi} \tag{3.22}$$

the radial gradient of equilibrium pressure profile.

In presence of a magnetic island, pressure profiles are flattened, as already

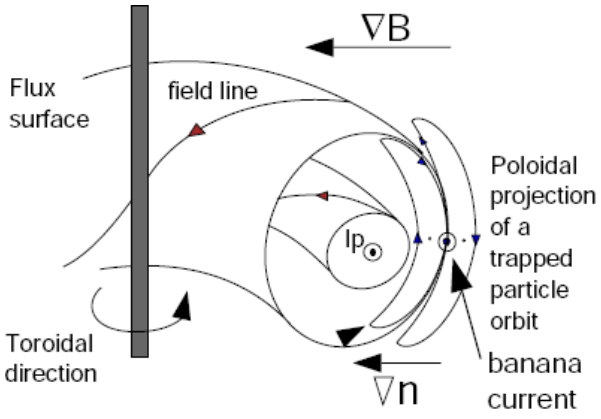

Figure 3.4: Mechanism of appearance of bootstrap current. On a given magnetic surface, the number of outer legs of banana orbit may exceed the number of inner legs, allowing an unbalanced toroidal momentum to take place. The transmission via collisions to passing electrons of such momentum generates the bootstrap current, which always points in the same direction as the plasma current.

mentioned at the beginning of this chapter. Thus, the bootstrap current is in turn weakened. Such loss can be thought of as the appearence of a "negative" parallel current (with respect to the direction of the unperturbed bootstrap current), which affects in turn the island stability through the Ampère's equation. Incidentally, such effect has strong experimental evidences, as discussed in Ref.[19, 20]. This mechanism is often named *neoclassical drive* for a magnetic island. Adding the bootstrap current drive to the parallel current in Eq.(3.17), Rutherford equation is modified in the following way [15]:

$$\frac{\mathrm{d}w}{\mathrm{d}t} = 0.27\frac{\eta c^2}{4\pi}\Delta' - 1.23\sqrt{\epsilon}\frac{\eta c^2 L_s}{B_p}\frac{r_s}{q_s}\frac{p'}{w}\left|\nabla\chi\right|_s^2 \tag{3.23}$$

where $L_s^{-1} = Rq_s/r\left|\mathrm{d}\ln q/\mathrm{d}r\right|$ is the characteristic scale lengths of variation for the magnetic shear. Two important points have to be stressed:

- The bootstrap current drive, as the pressure gradient is in general neg-

ative and the magnetic shear is positive, is a positive term and thus is *destabilizing* the mode. This means that in toroidal geometry, modes that are stable in the classical limit can be driven non-linearly unstable by the presence of the neoclassical term.

- The neoclassical drive is inversely proportional to the island width. This means that the growth rate of the island decreases as the island increases its size [2]. Thus, a small "seed" island is strongly destabilized, and its growth will continue until the neoclassical drive reaches the value of $-\Delta'$, where saturation of the mode occurs. For a given value of $L_p = (1/p\mathrm{d}p/\mathrm{d}r)^{-1}$, the bootstrap current drive is much stronger if the pressure p is high.

Fig.3.5 summarizes all these considerations. In the region I, where the island is very small, stabilizing terms dominate. The nature of such "threshold", which is often observed experimentally [19], is still under debate, as discussed in the next section. In region II, if the pressure is high enough, the neoclassical drive may overcome Δ', so that the magnetic island starts developing. However, there will always exist a critical island size for whom neoclassical effects are sufficiently reduced and therefore saturation occurs, as represented in region III. Incidentally, if the magnetic island is large enough, the non-linear dependence of Δ' on the island width (which enhances the stabilizing effect of the classical drive) might play an important role in the saturation process. Because of the nature of the drives, saturation points can be shown to correspond to stable equilibria. It is important to remark that the neoclassical drive introduces a limit for the pressure admissible in a tokamak (at given magnetic field), above which neoclassical tearing modes will occur, even in a classically stable magnetic equilibrium.

[2] The divergence of the neoclassical driving term for $w \to 0$ is cancelled as the pressure profile does not completely flatten below a given treshold, determined by transport [21] and finite orbit effects [22].

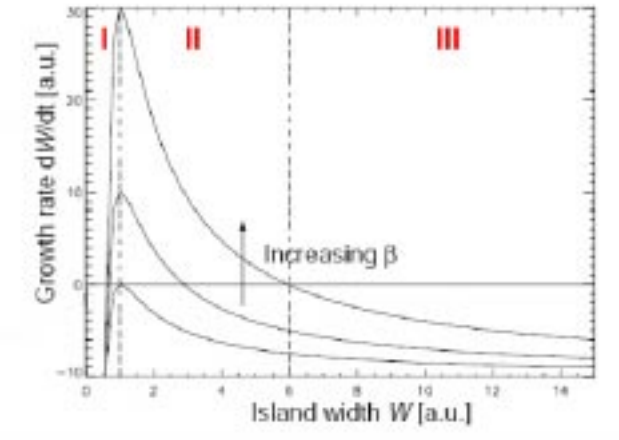

Figure 3.5: Growth rate of a tearing mode as a function of the island width. The first region accounts for threshold effects. In the second region, the neoclassical drive prevales, while in the third region saturation occurs. Here, the pressure dependence is accounted for through the parameter $\beta = 8\pi p/B^2$.

3.5 The Polarization Current

Another important neoclassical effect is linked to the so called *polarization current*, which arises because of the relative rotation of the island with respect to the surrounding plasma. A detailed calculation of the neoclassical polarization current will be provided in chapter 4. Here, a quick introductory sketch is discussed, stressing the most relevant physical features.

A rotating magnetic island, from a physical point of view, is a time-varying magnetic perturbation, and thus it generates through Faraday's law an electric field proportional to the island rotation frequency, as $\partial A_\parallel/\partial t \sim \omega A_\parallel$. This field can be shown to have a strong radial component, namely

$$E_r \approx \hat{E}_r(\chi)\cos\xi \tag{3.24}$$

As particles experience a time-dependent electric field in the radial direction, they undergo a radial drift proportional to $\mathrm{d}E_r/\mathrm{d}t$ called *polarization drift*.

Such drift averages to zero on a complete poloidal turn. However, trapped particles do not explore the whole poloidal cross section, and therefore their θ-averaged contribution does not vanish. Fig.3.6 depicts such considerations. This drift is mass-dependent and much larger for ions, so that a perpendicular current is generated. Recalling Eq.(1.2), it is clear that

$$\nabla \cdot \mathbf{J} = \nabla_{\parallel} J_{\parallel} + \nabla_{\perp} \cdot \mathbf{J}_{\perp} = 0 \tag{3.25}$$

As the perpendicular polarization current is not divergence-free, a closure

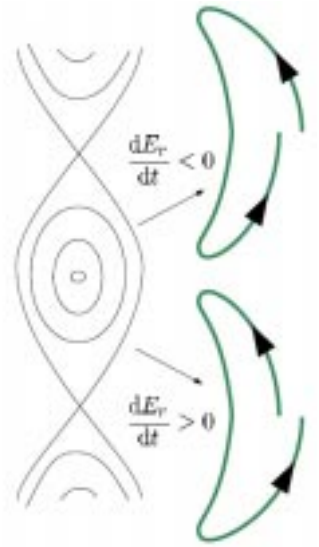

Figure 3.6: Effects of the island radial electric field on a trapped particle, leading to the polarization current.

parallel current, mostly carried by electrons, appears, and this is what ultimately affects the evolution of the magnetic island through Ampére's law (Eq.(3.16)). In the tearing mode jargon, the closure current itself is named "polarization current" as well.

A remarkable feature of the polarization current is that *its average on the island surface goes to zero.* This peculiarity distinguishes it from the

bootstrap current, and it is a useful property in order to isolate such contribution. Note also that a time-dependent radial electric field leads to a time dependence of the toroidal precession frequency of trapped particles ω_E (see Eq.(2.44)). Polarization drift can be therefore interpreted as a consequence of such toroidal acceleration together with angular momentum balance, namely (see Fig.3.7)

$$m_i \frac{\mathrm{d}\mathbf{v}_E}{\mathrm{d}t} = \mathbf{J}_{\mathrm{Pol}} \times \mathbf{B}. \tag{3.26}$$

These features will be thoroughly discussed from a mathematical point of view in the next chapter.

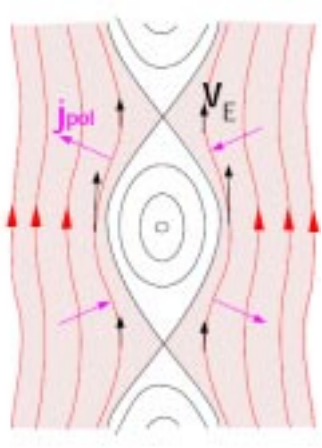

Figure 3.7: Fluid picture of the polarization current mechanism. The time-dependent toroidal precession v_E subsequent to the island radial electric field forces the particles to accelerate and decelerate along the magnetic surfaces. Because of angular momentum conservation, a perpendicular flow therefore develops.

Once determined the expression for the parallel polarization current, it is possible to go back to Eq.(3.17) to find a new term in Eq(3.23), repeating the same calculation previously outlined (see Ref.[23]). This yields

$$\frac{\mathrm{d}w}{\mathrm{d}t} = 0.27\frac{\eta c^2}{4\pi}\Delta' - 1.23\sqrt{\epsilon}\frac{\eta c^2 L_s}{B_p}\frac{r_s}{q_s}\frac{p'}{w}\left|\nabla\chi\right|_s^2 +$$

$$-C_{\rm Pol}\epsilon^{3/2}\left(\frac{\rho_\theta}{W_\chi}\right)^3\left(\frac{L_q}{L_p}\right)^2\frac{\omega\left(\omega-\omega_{*p,i}\right)}{\omega_{*,e}}\beta_\theta, \tag{3.27}$$

where $C_{\rm Pol}$ is a geometric coefficient, ρ_θ is the poloidal Larmor radius (i.e. the Larmor radius calculated on the poloidal component of the magnetic field), $L_q = (1/q\mathrm{d}q/\mathrm{d}r)^{-1}$, $\beta_\theta = 8\pi p/B_p^2$ and

$$\omega_{*,i-e} = \frac{mcT_{i-e}n_e'}{q_{i-e}qn_e} \tag{3.28}$$

is the (ion-, subscript i, or electron-, subscript e) diamagnetic frequency ($n_e = n_i$ represents the electron density, while the prime denotes derivatives with respect to χ), while

$$\omega_{*p,i-e} = \omega_{*,i-e}\left[1+\eta_{i-e}\right], \tag{3.29}$$

being η_{i-e} the ratio between the characteristic scale length of density $L_n = (1/n_e\mathrm{d}n_e/\mathrm{d}r)^{-1}$ and temperature $L_{T,i-e} = (1/T_{i-e}\mathrm{d}T_{i-e}/\mathrm{d}r)^{-1}$.

Eq.(3.27) is valid in the low-collisional limit, i.e. $\nu/\epsilon\omega \ll 1$, being ν the collision frequency. It is important to stress that

- The W_χ^{-3} dependence suggest that the polarization current *is not important for the saturation of a large island, which is thus still determined by the balance between Δ' and the bootstrap current drive, as discussed before.*

- Nevertheless, it has a crucial role for the stability of small "seed" islands. In particular, it has been invoked as an explanation for the experimentally observed "threshold" of magnetic islands mentioned above [24].

The current connected with the rotation of a magnetic island with respect to the plasma is the main subject of the present thesis. It will be shown that the polarization current is not the only contribution to the island dynamics due to the island rotation. In particular, *resonance phenomena* between island and particle motion have a noteworthy influence on the overall picture.

Chapter 4

The Drift-Kinetic Equation

4.1 Derivation of the Drift-Kinetic Equation

The drift-kinetic equation is a simplified form of the general Boltzmann kinetic equation. It describes the time evolution of the distribution of the guiding centres, i.e. gyrating particles are described as massive charged points, whose position coincides with that one of their guiding centre, and all the quantities which can affect their motion (e.g. electromagnetic fields) are evaluated at the guiding centre position. Clearly, the validity of the drift-kinetic equation is restricted to cases where a scale separation between gyration and guiding centre motion is possible, see chapter 2. Here, an intuitive derivation of the drift-kinetic equation, following Ref. [6], is presented. A more rigorous approach, using Hamiltonian techniques, can be found for example in Ref. [7, 8], but it will be not discussed here.

The starting point is the Boltzmann equation for the distribution function f_j of charged particles of species j in an electromagnetic field:

$$\frac{\partial f_j}{\partial t} + \mathbf{v} \cdot \frac{\partial f_j}{\partial \mathbf{x}} + \frac{q_j}{m_j} \left(\mathbf{E} + \frac{1}{c} \mathbf{v} \times \mathbf{B} \right) \cdot \frac{\partial f}{\partial \mathbf{v}} = C\left(f_j\right). \tag{4.1}$$

Note that the fields which appear in Eq.(4.1) are "ensemble-averaged", i.e. they do not account for the charge separation which occurs on scales shorter than the Debye length, see for example [25]. The term on the left-hand

side represents the conservation of the particle distribution along the phase space trajectories, while the right-hand side accounts for deviations from this behaviour due to interactions between particles. The details of the collision operator are not important for the purposes of the present section, and therefore they will be addressed later. Each guiding centre can be identified by its position, its magnetic moment μ and its energy U. The corresponding phase space is for this reason a five-dimensional space. This is due to the fact that the distribution of the guiding centres contains no informations about the gyrophase, i.e. the sixth coordinate has been averaged away. Hence, f evolves according to

$$\frac{\partial f_j}{\partial t} + \mathbf{v}_{gc,j} \cdot \nabla f_j + \frac{\mathrm{d}U}{\mathrm{d}t}\frac{\partial f_j}{\partial U} + \frac{\mathrm{d}\mu}{\mathrm{d}t}\frac{\partial f_j}{\partial \mu} = C\left(f_j\right), \tag{4.2}$$

where the gradient refers to guiding centre coordinates. In chapter 2, the motion of the guiding centre has been analyzed. The result for the guiding centre velocity $\mathbf{v}_{gc,j}$ is reported here for convenience

$$\mathbf{v}_{gc,j} = v_\parallel \mathbf{b} + \mathbf{v}_{\mathbf{E}\times\mathbf{B}} + \frac{1}{\omega_{cj}}\mathbf{b} \times \left(\frac{\mu}{m_j}\nabla B + v_\parallel^2 \boldsymbol{\kappa}\right) \tag{4.3}$$

The case $v_\parallel \gg v_{\mathbf{E}\times\mathbf{B}}$, see subsection 2.1.2, is considered, and for this reason Eq.(2.31, 2.32) are employed for the guiding centre velocity, retaining terms up to $\mathcal{O}\left(\delta = \rho_L/L_B\right)$. The magnetic moment, at this order, is treated as a constant of motion. It actually becomes somewhat analogous to the spin of the particle in quantum mechanics, in the sense that it represents an intrinsic property of the particle.

The total energy of the particle amounts to

$$U = \frac{m_j v_\parallel^2}{2} + q_j\phi + \mu B, \tag{4.4}$$

ϕ being the electrostatic potential. Note that the term μB, which represents the "perpendicular" kinetic energy, plays the role of a potential for the mirror

force, see Eq.(2.32). In fact, the lowest-order guiding centre kinetic energy is approximated by the "parallel" term, as

$$v_{gc,j}^2 = v_\parallel^2 + \mathcal{O}\left(\delta^2\right). \tag{4.5}$$

The total time derivative of the energy takes the form

$$\frac{\mathrm{d}U}{\mathrm{d}t} = \mathbf{v}_{gc,j} \cdot \left(q_j \mathbf{E} - \nabla\left(\mu B\right)\right) + q_j \frac{\mathrm{d}\phi}{\mathrm{d}t} + \mu \frac{\mathrm{d}B}{\mathrm{d}t}, \tag{4.6}$$

in view of Eq.(4.5) and writing the change in kinetic energy as the usual product of force and velocity. The total time derivative is defined as $\mathrm{d}/\mathrm{d}t = \partial/\partial t + \mathbf{v}_{gc,j} \cdot \nabla$. According to Faraday's law

$$\mathbf{E} = -\nabla\phi - \frac{1}{c}\frac{\partial \mathbf{A}}{\partial t}, \tag{4.7}$$

Eq.(4.6) becomes

$$\frac{\mathrm{d}U}{\mathrm{d}t} = -\frac{q_j}{c}\mathbf{v}_{gc,j} \cdot \frac{\partial \mathbf{A}}{\partial t} + q_j \frac{\partial \phi}{\partial t} + \mu \frac{\partial B}{\partial t}. \tag{4.8}$$

Since the magnetic moment is a constant of motion, and since the time-dependent part of the vector potential is in most of the problems of interest parallel to the magnetic field, in view of Eq.(4.8), the drift-kinetic equation Eq.(4.2) reads

$$\frac{\partial f_j}{\partial t} + \mathbf{v}_{gc,j} \cdot \nabla f_j + \left[q_j \frac{\partial \phi}{\partial t} + \mu \frac{\partial B}{\partial t} - \frac{q_j}{c} v_{\parallel,j} \frac{\partial A_\parallel}{\partial t}\right] \frac{\partial f_j}{\partial U} = C\left(f_j\right), \tag{4.9}$$

For the purpose of this thesis, a slightly different form of Eq.(4.9) is conveniently adopted. It utilizes, as a phase space coordinate, the total kinetic energy $\mathcal{E} = m_j\left(v_\parallel^2 + v_\perp^2\right)/2$ instead of $U = \mathcal{E} + q_j\phi$. Since

$$\left.\frac{\partial}{\partial \mathbf{X}}\right|_U = \left.\frac{\partial}{\partial \mathbf{X}}\right|_\mathcal{E} + q_j \frac{\partial \phi}{\partial \mathbf{X}} \frac{\partial}{\partial \mathcal{E}} \tag{4.10}$$

$$\left.\frac{\partial}{\partial t}\right|_U = \left.\frac{\partial}{\partial t}\right|_\mathcal{E} + q_j \frac{\partial \phi}{\partial t} \frac{\partial}{\partial \mathcal{E}}, \tag{4.11}$$

and since for the problems treated in the present work the partial time derivative of B is negligible compared to other terms in brackets in Eq.(4.9), as the neoclassical tearing mode is not such to significantly affect the strength of the total magnetic field, the drift kinetic equation becomes finally

$$\frac{\partial f_j}{\partial t} + \mathbf{v}_{gc,j} \cdot \nabla f_j + q_j \mathbf{v}_{gc,j} \cdot \mathbf{E} \frac{\partial f_j}{\partial \mathcal{E}} = C\left(f_j\right), \tag{4.12}$$

where of course spatial derivatives have to be intended at constant kinetic energy. It is appropriate to introduce the so called pitch-angle variables [6] as a coordinate system for the velocity space. In particular, the variable $\lambda = 2\mu/m_i v^2$ is defined. Such coordinate turns out to be extremely useful to account for mirror force, and at the same time to distinguish passing and trapped particles. In fact, the parallel velocity can be written as

$$v_{\|} = \sigma v \sqrt{1 - \lambda B}. \tag{4.13}$$

$\sigma = \pm 1$ being the sign. In the large aspect-ratio approximation (see chapter 2), Eq.(4.13) becomes

$$v_{\|} = \sigma v \sqrt{1 - \lambda B_0 + \lambda B_0 \epsilon \cos\theta}. \tag{4.14}$$

A trapped particle is denoted by $1/B > \lambda > 1/B_M$, where B_M is the maximum value of the magnetic field on a given flux surface. The integration operator over velocity space can be in turn shown to take the form

$$\int_{-\infty}^{\infty} \ldots \mathrm{d}^3 v = \pi B \sum_{\sigma=\pm 1} \int_0^{\infty} v^2 \mathrm{d}v \int_0^{\frac{1}{B}} \ldots \frac{\mathrm{d}\lambda}{\sqrt{1-\lambda B}}, \tag{4.15}$$

where the factor π comes from the trivial integral on the gyrophase.

4.2 The Drift-Kinetic Equation for a Perturbed Tokamak Geometry

In this section, a convenient form for the drift-kinetic equation in presence of a magnetic island is derived. For the present analysis, a large aspect-ratio

tokamak (see chapter 2), with circular cross sections and an equilibrium magnetic field (see Eq.(1.23))

$$\mathbf{B} = I\nabla\zeta + \nabla\zeta \times \nabla\chi. \tag{4.16}$$

is chosen. To account for the magnetic island, the constant-ψ approximation is adopted. The inclusion of the perturbation leads to the following expression for the total magnetic field (see Eq.(3.8))

$$\mathbf{B} = I\nabla\zeta + \nabla\zeta \times \nabla\left(\chi + \psi\right) \tag{4.17}$$

with (see Eq.(3.9))

$$\psi = \tilde{\psi}\cos\xi. \tag{4.18}$$

The main goal of the present work is to study the perturbed currents arising as a responce to a magnetic perturbation of given frequency and amplitude. Hence, the time evolution of the island width is neglected, implying

$$\frac{\mathrm{d}\tilde{\psi}}{\mathrm{d}t} = 0. \tag{4.19}$$

The island rotation frequency is denoted by ω, also supposed to be constant in time. Thus, the helical coordinate should be intended as (Eq.(3.12))

$$\xi = m\theta - n\zeta - \omega t. \tag{4.20}$$

The perturbed flux-surface function Ω, introduced in chapter 3 and re-written here for convenience

$$\Omega = 2\frac{\left(\chi - \chi_s\right)^2}{W_\chi^2} - \cos\xi \tag{4.21}$$

has a noteworthy usefulness in the derivation. However, unless where specified, the chosen coordinate system is (ξ, χ, θ).

The drift-kinetic calculation of the neoclassical polarization current generated by the rotation of the island is described in this and in the following

paragraphs, mainly following the work of Wilson *et al.* [26]. Since the focus of this thesis is on the effects connected with the rotation of the island with respect to the plasma, the important simplification is introduced, that the equilibrium density and temperature profiles are flat. Although fundamental for the complete description of the island dynamics, density and temperature gradients do not influence directly the processes connected with the island rotation described in the next two chapters (where ω is treated as a free parameter), and can therefore be disregarded. The starting point is the drift-kinetic equation in the form of Eq.(4.12).

$$\frac{\partial f_j}{\partial t} + v_{\|j}\nabla_\| f_j + \mathbf{v}_{\mathbf{E}\times\mathbf{B}}\cdot\nabla f_j + \mathbf{v}_{Dj}\cdot\nabla f_j - \frac{q_j}{m_j}\frac{\mathbf{v}_{Dj}\cdot\nabla\phi}{v}\frac{\partial f_j}{\partial v} = C_j(f_j). \quad (4.22)$$

where v_D is the magnetic drift velocity given by the last two terms of Eq.(4.3). Note that in Eq.(4.22), parallel electric fields have been neglected. This assumption will be justified below. In the presence of a magnetic island, the parallel gradient operator appearing in the second term of Eq.(4.22) can be expressed as

$$\nabla_\| = \frac{\mathbf{B}}{B}\cdot\nabla = \frac{1}{B}\left(B^h\frac{\partial}{\partial\xi} + B^\theta\frac{\partial}{\partial\theta} + B^\chi\frac{\partial}{\partial\chi}\right) \quad (4.23)$$

where B^i indicates the i-th contravariant component. According to Eq.(3.4) and Eq.(3.5), and in the limit of large aspect-ratio approximation, it is possible to write

$$B^\theta = \frac{B_p}{r} \quad (4.24)$$

$$B^h = \frac{B_p}{r}\left(m - nq\left(\chi\right)\right) \quad (4.25)$$

$$B^\chi = \left.\frac{\partial\chi}{\partial\xi}\right|_\Omega B^h. \quad (4.26)$$

Taylor expanding the safety factor around the resonant surface ($q = m/n$) and considering Eq.(3.7), one finds

$$\frac{1}{B}B^\theta \approx \frac{1}{Rq} \quad (4.27)$$

$$\frac{1}{B}B^h \approx k_\parallel \tag{4.28}$$

$$\frac{1}{B}B^\chi \approx k_\parallel \left.\frac{\partial\chi}{\partial\xi}\right|_\Omega, \tag{4.29}$$

where

$$k_\parallel = -m\frac{\chi-\chi_s}{Rq}\frac{q_s'}{q_s}, \tag{4.30}$$

the apex $'$ denoting derivatives with respect to χ and the subscript s indicating quantities calculated on the resonant surface. Hence, the parallel gradient amounts to

$$\nabla_\parallel = \frac{1}{Rq}\frac{\partial}{\partial\theta} + k_\parallel\frac{\partial}{\partial\xi} + k_\parallel \left.\frac{\partial\chi}{\partial\xi}\right|_\Omega \frac{\partial}{\partial\chi}. \tag{4.31}$$

The first term on the right-hand side of Eq.(4.31) is the "equilibrium" term (i.e not related to the magnetic perturbation), that is linked to the motion of the particle along the field line, and it represents the fastest time-scale of the particle dynamic for the present problems. The second term takes into account the relative motion of the particle with respect to the island in the $\nabla\xi$ direction, which takes place since the magnetic island and the magnetic field line on which the particle is travelling do not have in general the same helicity (unless the particle is streaming on the rational surface, where in fact $k_\parallel = 0$). The interplay between the island drift ω and this particle drift $k_\parallel v_\parallel$ will represent a central problem in the next chapter. The third term is linked to the radial component of the parallel velocity which arises because of the radial component of the magnetic field connected to the presence of the magnetic island. Indeed

$$\left.\frac{\partial\chi}{\partial\xi}\right|_\Omega = -\frac{W_\chi^2}{4\left(\chi-\chi_s\right)^2}\sin\xi \tag{4.32}$$

is zero when no island is present. It is possible to write the last two terms of Eq.(4.31) in a more compact and physically transparent form noting that

$$\frac{\partial}{\partial\xi} + \left.\frac{\partial\chi}{\partial\xi}\right|_\Omega \frac{\partial}{\partial\chi} = \left.\frac{\partial}{\partial\xi}\right|_\Omega, \tag{4.33}$$

and then

$$\nabla_{\parallel} = \frac{1}{Rq}\frac{\partial}{\partial\theta} + k_{\parallel} v_{\parallel} \left.\frac{\partial}{\partial\xi}\right|_{\Omega}. \tag{4.34}$$

This expression will be used in the present work.

In the present model, the electrostatic potential ϕ associated to the island is not self-consistently calculated solving the Poisson equation, but an approximated analytical expression is derived on the basis of simple physical arguments. As the characteristic timescales of island-related processes are typically much slower than the parallel electron dynamics, it is reasonable to suppose that every parallel electric field is immediately shortened out by electrons themselves. According to Maxwell's equation, this condition reads

$$\nabla_{\parallel}\phi + \frac{1}{c}\frac{\partial A_{\parallel}}{\partial t} = 0 \tag{4.35}$$

The potential is supposed to be independent on θ, which means that fluctuations of ϕ along the field-lines are small and thus negligible. Noting that

$$\frac{\partial}{\partial t} = -\omega\frac{\partial}{\partial\xi} \tag{4.36}$$

and according to the identity

$$k_{\parallel} \left.\frac{\partial\chi}{\partial\xi}\right|_{\Omega} = \frac{m}{q}\frac{\partial A_{\parallel}}{\partial\xi}, \tag{4.37}$$

Eq.(4.35) can be directly integrated to give

$$\phi = \frac{\omega q}{mc}\left[\chi - \chi_s - h\left(\Omega\right)\right], \tag{4.38}$$

where the function $h\left(\Omega\right)$ is an integration constant, which can be determined on the basis of the electron transport in the island region [26], with the boundary condition of vanishing ϕ at a large distance from the island (i.e. possible "equilibrium" electric fields are disregarded). In the present work, a simple expression for $h\left(\Omega\right)$, which can be found in Ref. [27], is adopted:

$$h\left(\Omega\right) = \frac{W_{\chi}}{\sqrt{2}}\left[\sqrt{\Omega} - 1\right]\Theta\left(\Omega - 1\right), \tag{4.39}$$

where W_χ is defined to have the same sign of $\chi - \chi_s$, and $\Theta(x)$ is the Heaviside step function (which is equal to 1 for $x > 0$ and 0 otherwise). A qualitative sketch of the profile of $h(\Omega)$ is represented in Fig.4.1a, while the total profile of the potential is qualitatively drawn in Fig.4.1b. The latter goes to zero far away from the island, according to the boundary conditions chosen, while inside the island, where $\Theta(\Omega - 1) = 0$, it is linear in the radial coordinate. The subsequent radial electric field arising inside the island lets the plasma

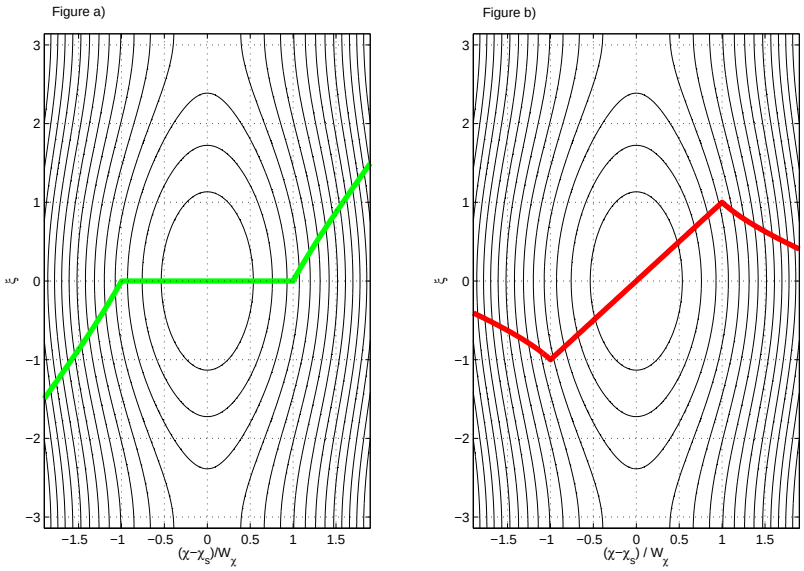

Figure 4.1: Qualitative behaviour of $h(\Omega)$(a) and of the total potential ϕ (b). The perturbed magnetic surfaces are plotted on the background.

inside the island rotate rigidly together with the island itself at a frequency ω through an $\mathbf{E} \times \mathbf{B}$-drift. As a consequence, the function $h(\Omega)$ can be interpreted as the profile of the electrostatic potential in the frame of reference where the island is at rest.

In Eq.(4.22) the sum of the grad-B and curvature drifts is indicated as

$\mathbf{v}_{Dj}$. A convenient form for such term is [28]

$$\mathbf{v}_{Dj} = -v_{\parallel}\mathbf{b} \times \nabla \left(\frac{v_{\parallel}}{\omega_{c,j}} \right). \tag{4.40}$$

which is valid in the limit of low β (ratio between thermal pressure and magnetic pressure). This form is included in the present formalism. It is noted that radial derivatives of $v_{\parallel}/\omega_c$ are associated to drifts in the poloidal directions, while poloidal derivatives of $v_{\parallel}/\omega_c$ to drifts in the radial direction.

As briefly mentioned before, electrons are only supposed to short out every parallel electric field, so as to carry the necessary parallel current to ensure quasineutrality (see Eq.(1.3)). As it will become clear later on, most of the effects governing the perpendicular dynamics are linked to finite orbit effects, which are larger for ions. Hence, only the solution of the drift-kinetic equation for ions is considered. Subscripts j can therefore be dropped from Eq.(4.22) without ambiguity. Only for ion charge (q_i) and ion mass (m_i) the subscript i is kept, in order to avoid confusions with the safety factor q and the poloidal mode number m, respectively.

According to the considerations exposed so far, the drift-kinetic equation Eq.(4.22) with the full expression for all the drifts is written in the form

$$\begin{aligned}
&-\omega\frac{\partial g}{\partial \xi} + \frac{v_{\parallel}}{Rq}\frac{\partial g}{\partial \theta} + k_{\parallel}v_{\parallel}\left.\frac{\partial g}{\partial \xi}\right|_{\Omega} + m\frac{c}{B}\frac{I}{Rq}\frac{\partial \phi}{\partial \chi}\frac{\partial g}{\partial \xi} + \\
&-m\frac{c}{B}\frac{I}{Rq}\frac{\partial \phi}{\partial \xi}\frac{\partial g}{\partial \chi} + \frac{Iv_{\parallel}}{Rq}\frac{\partial}{\partial \theta}\left(\frac{v_{\parallel}}{\omega_c}\right)\frac{\partial g}{\partial \chi} - m\frac{Iv_{\parallel}}{Rq}\frac{\partial}{\partial \chi}\left(\frac{v_{\parallel}}{\omega_c}\right)\frac{\partial g}{\partial \xi} \\
&-\frac{q_i}{m_i v}\left[\frac{Iv_{\parallel}}{Rq}\frac{\partial}{\partial \theta}\left(\frac{v_{\parallel}}{\omega_c}\right)\frac{\partial \phi}{\partial \chi} - m\frac{Iv_{\parallel}}{Rq}\frac{\partial}{\partial \chi}\left(\frac{v_{\parallel}}{\omega_c}\right)\frac{\partial \phi}{\partial \xi}\right]\frac{\partial g}{\partial v} = \\
&= -\frac{q_i F_M}{T}\left[\frac{Iv_{\parallel}}{Rq}\frac{\partial}{\partial \theta}\left(\frac{v_{\parallel}}{\omega_c}\right)\frac{\partial \phi}{\partial \chi} - m\frac{Iv_{\parallel}}{Rq}\frac{\partial}{\partial \chi}\left(\frac{v_{\parallel}}{\omega_c}\right)\frac{\partial \phi}{\partial \xi}\right] + C\left(f\right).
\end{aligned} \tag{4.41}$$

Eq.(4.41) has been written splitting the distribution function f into an analytically known part F_0, assumed to be an isotropic Maxwellian

$$F_M\left(v\right) = n_0\left(\frac{m_i}{2\pi T}\right)^{3/2} e^{m_i v^2/2T}$$

where density and temperature are assumed to be constant, as elucidated above, and a part g to be determined perturbatively. This method, often called δf method, is completely general, as no particular constraints are requested for the unknown function g. However, it turns out to be helpful only if

$$F_0 \gg g. \tag{4.42}$$

This result is expected for the problem analyzed in the present work, since the deviations from F_0 are due to drift velocities assumed to be of $\mathcal{O}(\delta)$.

4.2.1 Analytical Solution: the Double Parameter Expansion

The analytical technique chosen for the solution of the drift-kinetic equation consists in a double-parameter expansion [26] of the perturbed distribution function:

$$g = \sum_{m,n}^{\infty} g^{(m,n)} \delta^m \Delta^n, \tag{4.43}$$

where

$$\delta = \frac{\rho_b}{w} \tag{4.44}$$

and

$$\Delta = \frac{w}{a}, \tag{4.45}$$

where ρ_b is the thermal ion banana-width, w is the island width expressed in length units, and a is the tokamak minor radius. Both parameters defined in Eq.(4.44) and Eq.(4.45) are supposed to be small. The first one represents the ratio between the characteristic orbit size and the relevant gradient scale, as the most important physical quantities of interest are supposed to vary on the island scale. In this sense, it is analogous to the small parameter δ adopted for the small Larmor radius expansion, see chapter 2. The second one expresses the fact that the island is supposed to be small compared to the tokamak size. Note that the tokamak size represents also the characteristic equilibrium

scale length, if equilibrium gradients were included. Basic assumptions for the scaling are

$$\frac{q_i\phi}{T} \sim \frac{g}{F_M} \sim \Delta \qquad \rho_\theta \sim w$$

ρ_θ being the poloidal ion Larmor radius. A very specific range of magnetic island's size is therefore considered. Islands are supposed to be neither too large, so that the polarization current drive is still significant, see chapter 3, nor too small, so that finite Larmor radius effects are negligible.

As discussed before, the fastest timescale described by Eq.(4.41) is represented by the parallel streaming of particles along the field line. The term in $v_\parallel/Rq$ plays therefore the role of scaling parameter, i.e. all other terms in Eq.(4.41) are ordered with respect to $v_\parallel/Rq$. Hereafter, the ordering of the most relevant terms is discussed in detail, as the scaling of remaining terms simply follows along the same line.

First of all, some considerations on the ordering of the term proportional to the island rotation frequency ω (first term in Eq.(4.41)) are necessary. Nowadays, a reliable model for the determination of the island rotation frequency ω is not available, although several mechanisms have already been discussed in the literature [26, 29, 30, 31]. For this reason, in the present thesis, ω is treated like an external parameter not self-consistently calculated but *a priori* ordered. In this chapter, the case

$$\omega \sim \omega_{*,e}, \tag{4.46}$$

being

$$\omega_{*,e} = \frac{mcT_e n'}{q_e q n}, \tag{4.47}$$

the electron diamagnetic frequency (m is the poloidal mode number, T_e the electron temperature, q_e the electron charge, n the unperturbed density and the apex $'$ refers to derivatives with respect to χ), is considered. This estimate is the most common in the literature of NTM, as it ensues from linear fluid

calculations. The assumption $\omega \sim \omega_{*,e}$ brings to

$$\omega \frac{Rq}{v_\parallel} \sim \Delta. \tag{4.48}$$

As will be shown later,

$$k_\parallel v_\parallel \frac{Rq}{v_\parallel} \sim \Delta. \tag{4.49}$$

Thus, $\omega \sim \omega_{*,e}$ implies, according to the scaling criteria adopted

$$\omega \sim k_\parallel v_\parallel. \tag{4.50}$$

In the present thesis, equilibrium gradients have been disregarded. This implies $\omega_{*,e} = 0$. *Nevertheless, it is in any case possible to keep the assumption* $\omega \sim k_\parallel v_\parallel$, *with* ω *being a free parameter.* The meaning of this operation is retaining the same ordering for the island rotation frequency as in the standard approaches, isolating at the same time the currents caused by the island rotation. The assumption $\omega \sim \omega_{*,e}$ will be mantained also in the next chapter, while in chapter 6 such ordering will be relaxed.

The term proportional to $k_\parallel v_\parallel$ (third term in Eq.(4.41)) can be estimated (with respect to the second term in Eq.(4.41), chosen as mentioned as a scaling parameter) as

$$\frac{Rq}{v_\parallel} \left(\frac{\partial g}{\partial \theta} \right)^{-1} k_\parallel v_\parallel \left. \frac{\partial g}{\partial \xi} \right|_\Omega . \tag{4.51}$$

All angular derivatives are supposed to be $\mathcal{O}(1)$, i.e. $\partial g/\partial\theta \sim \partial g/\partial\xi \sim g$. Thus, in view of Eq.(4.30)

$$\frac{Rq}{v_\parallel} \left(\frac{\partial g}{\partial \theta} \right)^{-1} k_\parallel v_\parallel \left. \frac{\partial g}{\partial \xi} \right|_\Omega \sim \frac{q_s'}{q_s} (\chi - \chi_s) \sim \Delta, \tag{4.52}$$

assuming $L_q = (\mathrm{d} \ln (q) / \mathrm{d}r)^{-1} \sim a$ and $(\chi - \chi_s) \sim W_\chi$.

The $\mathbf{E} \times \mathbf{B}$ terms is made up of two parts, corresponding to the two components of the electric field. For the scaling of radial derivatives, the

following criterion is adopted: quantities related to the island have a radial scale of variation of the same order of the island width. Thus

$$m\frac{c}{B}\frac{I}{Rq}\frac{\partial\phi}{\partial\chi}\frac{\partial g}{\partial\xi}\sim m\frac{c}{B}\frac{I}{Rq}\frac{\partial\phi}{\partial\xi}\frac{\partial g}{\partial\chi}\sim\frac{c}{B}\frac{I}{Rq}\frac{\phi}{W_\chi}g. \tag{4.53}$$

Estimating $v_\parallel\sim v_{\rm th}\sim T/m_iv_{\rm th}$, and recalling $W_\chi=RB_pw$, the scaling of $\mathbf{E}\times\mathbf{B}$ terms yields

$$m\frac{c}{B}\frac{I}{Rq}\frac{\phi}{W_\chi}g\frac{Rq}{v_\parallel}\left(\frac{\partial g}{\partial\theta}\right)^{-1}\sim v_{\rm th}\frac{cm_i}{B_\theta}\frac{\phi}{T}\frac{1}{w}\sim\frac{\rho_\theta}{w}\frac{q_i\phi}{T}\sim\Delta, \tag{4.54}$$

The magnetic drifts also have two components. Nevertheless, there exists an important difference to the previous case. After a displacement of order a in the $-\nabla R$ direction, the variation of the parallel velocity is of the order of $\epsilon^{1/2}v_{\rm th}$ (see Eq.(2.38)). A variation of the same order is experienced by particles also after half-turn around the poloidal cross section of the tokamak. Thus

$$\frac{\partial}{\partial\theta}\left(\frac{v_\parallel}{\omega_c}\right)\sim\epsilon^{1/2}\frac{v_{\rm th}}{\omega_c} \tag{4.55}$$

$$\frac{\partial}{\partial\chi}\left(\frac{v_\parallel}{\omega_c}\right)\sim\frac{\epsilon^{1/2}}{RrB_\theta}\frac{v_{\rm th}}{\omega_c} \tag{4.56}$$

This means

$$\frac{Iv_\parallel}{Rq}\frac{\partial}{\partial\theta}\left(\frac{v_\parallel}{\omega_c}\right)\frac{\partial g}{\partial\chi}\frac{Rq}{v_\parallel}\left(\frac{\partial g}{\partial\theta}\right)^{-1}\sim\epsilon^{1/2}\rho_L\frac{B}{wB_\theta}\sim\delta, \tag{4.57}$$

as $\rho_b=\epsilon^{1/2}\rho_\theta$, and

$$m\frac{Iv_\parallel}{Rq}\frac{\partial}{\partial\chi}\left(\frac{v_\parallel}{\omega_c}\right)\frac{\partial g}{\partial\xi}\frac{Rq}{v_\parallel}\left(\frac{\partial g}{\partial\theta}\right)^{-1}\sim\epsilon^{1/2}\rho_L\frac{B}{rB_\theta}\sim\Delta\delta. \tag{4.58}$$

Thus, it is apparent that *the two terms of the magnetic drifts do not have the same order*. This fact will have a considerable importance for the present investigation. All other terms in Eq.(4.41) can be easily ordered by means

of analogous considerations. The final result that the terms in the ion drift-kinetic equation (4.41) are ordered as

$$\Delta : 1 : \Delta : \Delta : \Delta : \delta : \Delta\delta : \Delta\delta : \Delta^2\delta = \delta : \Delta\delta. \tag{4.59}$$

For the moment, collisions are excluded from the calculation. Their role will be discussed afterwards.

4.3 Numerical Solution: the HAGIS Code

In the present thesis, analytical calculations will be supported by numerical simulations. The chosen numerical tool is the HAGIS code.

The HAGIS code (HAmiltonian GuIding centre System) [32] solves the drift-kinetic equation for ions by means of a Hamiltonan approach and with the help of the δf technique. As discussed above, the effects investigated in the present work are actually due to ions. Thus, the absence of a drift-kinetic equation for electrons does not represent a limit for the purposes of the present work, although it does not allow the code to determine self-consistently the electrostatic potential. The HAGIS code calculates the evolution in time of the distribution function by means of "markers" which span the whole phase space and represent the ions. These "markers" evolve according to the Hamiltonian equations of motion, which are integrated by the code.

In the code HAGIS, the island frequency is not self-consistently simulated, but, as in the analytical approach, it represents an input parameter. This tool turns out to be extremely useful for the exploration of various frequency ranges. The perturbed vector potential and the electrostatic potential are also not calculated self-consistently, but the analytical expressions derived above (Eq.(4.18) and Eq.(4.38)) are implemented. The determination of the electrostatic potential from the ions and electrons response is discussed in chapter 7.

Collisions are described by a Monte Carlo algorithm which models pitch-angle scattering [33]. In the simulations presented in this thesis, a tokamak with circular concentric flux surfaces and major radius $R = 8$ m, aspect ratio $a/R = 0.5$, magnetic field $B_0 = 8$ T, deuterium plasma with density $n_i = 10^{20}$ m^{-3} and temperature $T = 5$ keV is considered. Equilibrium gradients are set to zero in agreement with the previous considerations. A (3,2) magnetic island with a fixed half-width $w = 6.8$ cm is included in the simulations. With these values, the ratio between the island width and the thermal ion banana width corresponds to $w/\rho_b \approx 9.6$ and the ratio between the island width and the tokamak minor radius a corresponds to $w/a \approx 0.017$. Thus, the choice is compatible with the smallness of parameters Δ and δ introduced in the previous section. In addition, as the island is located on a magnetic surface where $\epsilon \approx 0.25$, it follows that $\rho_\theta \approx \rho_b/\sqrt{\epsilon} \sim w$. The space domain is divided into "radial" cells (between two neighbouring perturbed flux surfaces) and into helical cells, in such a way that the volume between two X-points of a magnetic island consists of six helical cells (for further details see Ref. [34]). All numerical results presented below refer to the "upper" half of the magnetic island (i.e. from O-point to X-point travelling in the positive-ξ direction). In the "lower" half, results can be shown to simply change their sign, unless where specified.

4.4 The "Standard" Polarization Current

4.4.1 The Perturbed Distribution

At the end of this chapter, the calculation of the polarization current due to a rotating island is reported in some detail, following Ref.[26]. This is done with the aim of introducing the formalism of the solution of drift-kinetic equation employed also in chapter 5 and 6, and as a reference for comparison with the physics results presented in those chapters.

The polarization current can be found solving the drift-kinetic equation

order by order, see Eq.(4.43). The first equation is $\mathcal{O}(1)$

$$\frac{v_\parallel}{Rq}\frac{\partial}{\partial\theta}g^{(0,0)} = 0. \tag{4.60}$$

Hence, it is clear that $g^{(0,0)}$ is independent on θ. From here on, θ-independent functions are denoted with a bar (i.e. $g^{(0,0)} = \bar{g}^{(0,0)}$). In the paper of Wilson *et al.* [26], $\bar{g}^{(0,0)}$ is linked to the background equilibrium gradients which are neglected here. For this reason, it is possible to set

$$\bar{g}^{(0,0)} = 0. \tag{4.61}$$

The $\mathcal{O}(\delta)$ equation reads

$$\frac{v_\parallel}{Rq}\frac{\partial}{\partial\theta}g^{(1,0)} = -\frac{q_i F_M}{T}\frac{I v_\parallel}{Rq}\frac{\partial}{\partial\theta}\left(\frac{v_\parallel}{\omega_c}\right)\frac{\partial\phi}{\partial\chi}, \tag{4.62}$$

which can be directly integrated to give

$$g^{(1,0)} = -I\frac{v_\parallel}{\omega_c}\frac{\partial\phi}{\partial\chi}\frac{q_i F_M}{T} + \bar{h}_P^{(1,0)} + \bar{h}_T^{(1,0)}, \tag{4.63}$$

where $\bar{h}^{(1,0)}$-s are θ-independent functions which represent integration constants. For convenience, the integration constant has been split in two parts, representing passing and trapped region of phase space (subscript P and T, respectively). The physical meaning of the θ-dependent part is interesting. One can observe that:

$$-I\frac{v_\parallel}{\omega_c}\frac{\partial\phi}{\partial\chi}\frac{q_i F_M}{T} = -c\frac{E_r}{B_\theta}\frac{\partial F}{\partial v_\parallel}. \tag{4.64}$$

Thus, it represents the first order correction in the $v_\parallel$ coordinate of a Maxwellian, due to the electrical toroidal precession $\omega_E = cE_r/RB_\theta$ (Eq.(2.44)).

As $g^{(0,0)} = 0$, the $\mathcal{O}(\Delta)$ equation simply amounts to

$$\frac{v_\parallel}{Rq}\frac{\partial}{\partial\theta}g^{(0,1)} = 0. \tag{4.65}$$

Thus, $g^{(0,1)} = \bar{g}^{(0,1)}$ is θ-independent. No other information is needed, as will emerge in the next subsection.

Before proceeding with the calculation, it is important to introduce the bounce-average operator. This operator has different forms depending on the region of the velocity space considered. In fact, passing particles can explore the whole poloidal cross section while following a magnetic field line, and for this reason the corresponding average operator is defined starting from the θ-average operator

$$\langle \dots \rangle_\theta = \frac{1}{2\pi} \oint \dots \mathrm{d}\theta,$$

as [6]

$$\left\langle \frac{Rq}{v_\parallel} \dots \right\rangle_\theta = \frac{1}{2\pi} \oint \frac{Rq}{v_\parallel} \dots \mathrm{d}\theta. \tag{4.66}$$

On the contrary, trapped particles are not able to explore the whole poloidal cross section, and by consequence quantities averaged on the trapped region of phase space have to be computed by means of

$$\left\langle \frac{Rq}{\left|v_\parallel\right|} \dots \right\rangle_\theta^T = \sum_{\sigma=\pm 1} \frac{1}{2\theta_b} \int_{-\theta_b}^{\theta_b} \frac{Rq}{\left|v_\parallel\right|} \dots \mathrm{d}\theta, \tag{4.67}$$

where θ_b is the bounce angle, introduced in chapter 2. Here, σ represents the sign of the parallel velocity as in Eq.(4.13).

To calculate the $\bar{h}$-functions, it is necessary to turn to $\mathcal{O}(\Delta\delta)$ equation. According to the identity

$$\frac{\partial}{\partial t} + c\frac{\mathbf{B}\times\nabla\phi}{B^2}\cdot\nabla \doteq \frac{\mathrm{d}_0}{\mathrm{d}t} = \frac{\mathrm{d}h}{\mathrm{d}\Omega}\frac{\omega}{m\tilde{\psi}} Rqk_\parallel \left.\frac{\partial}{\partial\xi}\right|_\Omega + \frac{\omega}{m}\left(1 - \frac{\partial h}{\partial\chi}\right)\frac{\partial}{\partial\theta}, \tag{4.68}$$

which corresponds to the MHD-total time derivative, equation $\mathcal{O}(\Delta\delta)$ can be written as

$$\begin{aligned} &\frac{\mathrm{d}h}{\mathrm{d}\Omega}\frac{\omega}{m\tilde{\psi}} Rqk_\parallel \left.\frac{\partial g^{(1,0)}}{\partial\xi}\right|_\Omega + \frac{\omega}{m}\left(1 - \frac{\partial h}{\partial\chi}\right)\frac{\partial g^{(1,0)}}{\partial\theta} + \frac{v_\parallel}{Rq}\frac{\partial g^{(1,1)}}{\partial\theta} + \\ &+k_\parallel v_\parallel \left.\frac{\partial g^{(1,0)}}{\partial\xi}\right|_\Omega + \frac{Iv_\parallel}{Rq}\frac{\partial}{\partial\theta}\left(\frac{v_\parallel}{\omega_c}\right)\frac{\partial g^{(0,1)}}{\partial\chi} = m\frac{Iv_\parallel}{Rq}\frac{\partial}{\partial\chi}\left(\frac{v_\parallel}{\omega_c}\right)\frac{\partial\phi}{\partial\xi}\frac{q_i F_M}{T}. \end{aligned} \tag{4.69}$$

In order to determine the $\bar{h}$-functions, the bounce average operators previously introduced are employed. First, the solution in the passing region of phase space is considered. The operator of Eq.(4.66) averages out all the terms with partial derivatives in θ. This leads to (recall Eq.(4.63))

$$\left\langle \frac{\mathrm{d}h}{\mathrm{d}\Omega}\frac{\omega}{m\tilde{\psi}}\frac{Rqk_\parallel}{v_\parallel}+k_\parallel\right\rangle_\theta \left.\frac{\partial \bar{h}_P^{(1,0)}}{\partial\xi}\right|_\Omega = I\left\langle\left(\frac{\mathrm{d}h}{\mathrm{d}\Omega}\frac{\omega}{m\tilde{\psi}}\frac{Rqk_\parallel}{v_\parallel}+k_\parallel\right)\frac{v_\parallel}{\omega_c}\right\rangle_\theta \left.\frac{\partial}{\partial\xi}\right|_\Omega \left(\frac{\partial\phi}{\partial\chi}\right)\frac{q_iF_M}{T}+ I\left\langle\frac{m}{Rq}\frac{\partial}{\partial\chi}\left(\frac{v_\parallel}{\omega_c}\right)\right\rangle_\theta \frac{\partial\phi}{\partial\xi}\frac{q_iF_M}{T}. \tag{4.70}$$

As elucidated in chapter 3, the polarization current, in contrast to the bootstrap current, averages to zero on a perturbed magnetic flux surface. The corresponding average operator is defined as

$$\langle\ldots\rangle_\Omega = \frac{\oint\cdots\mathrm{d}\xi/\sqrt{\Omega+\cos\xi}}{\oint\mathrm{d}\xi/\sqrt{\Omega+\cos\xi}},$$

Ω being treated as a flux-surface label, thus independent on ξ. The constraint of vanishing flux-surface average is therefore applied to $\bar{h}$-functions, which are related to the polarization current. The integration of Eq.(4.70) is carried out under this condition, yielding

$$\bar{h}_P^{(1,0)} = -\frac{4I}{W_\chi^2}\frac{\omega q}{mc}\frac{\mathrm{d}h}{\mathrm{d}\Omega}\frac{q_iF_M}{T}\left\langle\left(\frac{\mathrm{d}h}{\mathrm{d}\Omega}\frac{\omega}{m\tilde{\psi}}\frac{Rq}{v_\parallel}+1\right)\frac{v_\parallel}{\omega_c}+\frac{q_s}{q_s'}\frac{\partial}{\partial\chi}\left(\frac{v_\parallel}{\omega_c}\right)\right\rangle_\theta \cdot \left[\left\langle\frac{\mathrm{d}h}{\mathrm{d}\Omega}\frac{\omega}{m\tilde{\psi}}\frac{Rq}{v_\parallel}+1\right\rangle_\theta\right]^{-1}\left[\chi-\langle\chi\rangle_\Omega\right]. \tag{4.71}$$

In order to isolate the polarization current contribution in Ref. [26], a further assumption, namely

$$\omega \gg k_\parallel v_\parallel \tag{4.72}$$

is made. Rigorously speaking, this condition cannot be justified within the scaling previously discussed. It can be shown that, for ω of the order of

the electron diamagnetic frequency, Eq.(4.72) corresponds to the condition $w \ll \rho_\theta$, so that the calculation applies to islands for which $\rho_b \ll w \ll \rho_\theta$. As expounded above, the physical meaning of $k_\parallel v_\parallel$ deals with the drift of the particles along the magnetic island due to the streaming on field lines which do not have in general the same helicity of the mode. Stating $\omega \gg k_\parallel v_\parallel$ corresponds to neglect this geometrical effect with respect to the rotation of the island itself. *The main consequence is that no resonance between particles and mode can occur in such limit, as no particle is able to follow the island rotation by means of the $k_\parallel v_\parallel$ mechanism.* In the next chapter, terms in $k_\parallel v_\parallel$ will be retained, and both their influence on the polarization current and the role of resonances will be discussed. Here, assuming the limit (4.72) and noticing that the average on θ acts only on the parallel velocity and on the cyclotron frequency, one obtains

$$\bar{h}_P^{(1,0)} = -\frac{4I}{W_\chi^2}\frac{\omega q}{mc}\frac{\mathrm{d}h}{\mathrm{d}\Omega}\frac{q_i F_M}{T}\left\langle\frac{1}{\omega_c}\right\rangle_\theta \cdot \left\langle\frac{1}{v_\parallel}\right\rangle_\theta^{-1}\left[\chi - \langle\chi\rangle_\Omega\right]. \tag{4.73}$$

The solution for $\bar{h}_T^{(1,0)}$ is derived in a completely analogous way, applying the bounce average operator of Eq.(4.67) to Eq.(4.69). Again, all the terms containing partial derivatives in θ disappear, as they depend on θ only trough $v_\parallel$ and B, which are both even functions of θ. The result is

$$\left\langle\frac{\mathrm{d}h}{\mathrm{d}\Omega}\frac{\omega}{m\tilde{\psi}}\frac{Rqk_\parallel}{\left|v_\parallel\right|}\right\rangle_\theta^T \left.\frac{\partial\bar{h}_T^{(1,0)}}{\partial\xi}\right|_\Omega =$$

$$I\left\langle k_\parallel\frac{\left|v_\parallel\right|}{\omega_c}\right\rangle_\theta \left.\frac{\partial}{\partial\xi}\right|_\Omega\left(\frac{\partial\phi}{\partial\chi}\right)\frac{q_i F_M}{T} + I\left\langle\frac{m}{Rq}\frac{\partial}{\partial\chi}\left(\frac{\left|v_\parallel\right|}{\omega_c}\right)\right\rangle_\theta \frac{\partial\phi}{\partial\xi}\frac{q_i F_M}{T}. \tag{4.74}$$

The important difference with the passing case is that terms odd in the parallel velocity in Eq.(4.69) now vanish because of the sum over σ ($\bar{h}_T^{(1,0)}$ is independent on σ, since it must be continuous at the bounce point). In the limit of $\omega \gg k_\parallel v_\parallel$, all terms in ω on the right-hand side of Eq.(4.74) are annihilated by the sum over σ, and consequently only negligible terms are

left over. Thus,

$$\bar{h}_T^{(1,0)} = 0. \tag{4.75}$$

This result has a strong physical implication, which will be discussed in detail in the next paragraph. The form of $\bar{h}_T^{(1,0)}$ without the assumption $\omega \gg k_\parallel v_\parallel$ will be derived in the next chapter.

4.4.2 The Perturbed Current

As pointed out in chapter 3, the polarization current is a perpendicular current caused by the time-varying electric field experienced by trapped ions. This current is in general not divergence-free. Therefore, because of the quasineutrality constraint (Eq.(1.3))

$$\nabla \cdot \mathbf{J} = \nabla_\parallel J_\parallel + \nabla_\perp \cdot \mathbf{J}_\perp = 0 \tag{4.76}$$

a closure parallel current $J_\parallel$ must develop. This parallel current is what ultimately affects island stability through Rutherford equation, see Eq.(3.27). In the tearing-mode jargon, the name "polarization current" often refers to this parallel current rather than to the perpendicular one. As this subsection is particularly tortuous from a mathematical point of view, a summary of the main physical features of interest is included at the end of the chapter.

The quasi-neutrality equation can be directly obtained by integrating the drift-kinetic equation over the velocity space for both ions and electrons, then multiplying each of them by the charge of the corresponding species and summing. The subsequent result reads

$$\frac{1}{Rq}\frac{\partial J_\parallel}{\partial \theta} + k_\parallel \left.\frac{\partial J_\parallel}{\partial \xi}\right|_\Omega + \sum_j q_j \int \mathrm{d}^3 v \mathbf{v}_{D,j} \cdot \nabla g_j -$$
$$\sum_j \frac{q_j^2}{m_j v} \int \frac{\mathrm{d}^3 v}{v} \mathbf{v}_{D,j} \cdot \nabla \phi \frac{\partial g}{\partial v} + \sum_j \frac{q_j^2}{T_j} \int \frac{\mathrm{d}^3 v}{v} \mathbf{v}_{D,j} \cdot \nabla \phi F_M = 0. \tag{4.77}$$

Terms related to the $\mathbf{E} \times \mathbf{B}$-drift cancel after sum over species. The quantity of interest for the purposes of the present work is the lowest order, θ-averaged

current. For this reason, terms in $\partial g/\partial v$ have been neglected, as they belong to higher orders (see Eq.(4.59)). Then, Eq.(4.77) is integrated over a period in θ. The first term on the left-hand side clearly vanishes, while terms containing F_M also are negligible, as

$$\oint \mathrm{d}\theta v_\parallel \frac{\partial}{\partial \theta}\left(\frac{v_\parallel}{\omega_{c,j}}\right) = 0, \tag{4.78}$$

and

$$\oint \mathrm{d}\theta v_\parallel \frac{\partial}{\partial \chi}\left(\frac{v_\parallel}{\omega_{c,j}}\right) = \mathcal{O}\left(\epsilon^2\right), \tag{4.79}$$

as can be proved writing $v_\parallel$ in pitch-angle coordinates. Thus, the quasi-neutrality condition simply amounts to

$$k_\parallel \left.\frac{\partial J_\parallel}{\partial \xi}\right|_\Omega = -\sum_j q_j \left\langle \int \mathrm{d}^3 v \mathbf{v}_{D,j}\cdot\nabla g_j \right\rangle_\theta \tag{4.80}$$

According to the physical description provided above, the perpendicular current, represented by the second term, is mostly carried by ions, and for this reason the sum over the species can be dropped. Moreover, only the lowest-order term of the drift velocity is retained (cf. Eq.(4.59)). This implies

$$k_\parallel \left.\frac{\partial J_\parallel}{\partial \xi}\right|_\Omega = -q_i \left\langle \int \mathrm{d}^3 v \frac{I v_\parallel}{Rq}\frac{\partial}{\partial\theta}\left(\frac{v_\parallel}{\omega_c}\right)\frac{\partial g}{\partial\chi}\right\rangle_\theta . \tag{4.81}$$

Following the scaling criteria previously discussed, it is possible to verify that

$$\frac{I v_\parallel}{Rq}\frac{\partial g}{\partial\chi} \approx \frac{\partial}{\partial\chi}\left(g\frac{I v_\parallel}{Rq}\right), \tag{4.82}$$

having neglected terms of higher-order in Δ. Integrating by parts the right-hand side of Eq.(4.81) with respect to θ, and in view of Eq.(4.82), one finds

$$\left\langle \int \mathrm{d}^3 v \frac{I v_\parallel}{Rq}\frac{\partial}{\partial\theta}\left(\frac{v_\parallel}{\omega_c}\right)\frac{\partial g}{\partial\chi}\right\rangle_\theta \approx -I\left\langle \int \mathrm{d}^3 v \frac{v_\parallel}{\omega_c}\frac{\partial}{\partial\chi}\left(\frac{v_\parallel}{Rq}\frac{\partial g}{\partial\theta}\right)\right\rangle_\theta , \tag{4.83}$$

having approximated

$$\frac{\partial}{\partial\theta}\left(g\frac{I v_\parallel}{Rq}\right) \approx \frac{I v_\parallel}{Rq}\frac{\partial g}{\partial\theta}, \tag{4.84}$$

neglecting higher-order terms in ϵ. As stated before, only the lowest-order non vanishing contribution is kept. Thus, one has to determine which is the right $g^{(m,n)}$ to be inserted in Eq.(4.83). Clearly, $g^{(0,0)}$ is not suitable, as it is zero. Moreover, $g^{(0,1)}$ and $g^{(1,0)}$ do not contribute either, as the first one is independent of θ while the θ-dependent part of the second one vanishes after velocity integration because of its oddness with respect to σ (see Eq.(4.15)). Therefore, the leading-order contribution comes from $g^{(1,1)}$. From $\mathcal{O}(\Delta\delta)$ equation it follows that

$$\frac{v_\parallel}{Rq}\frac{\partial g^{(1,1)}}{\partial\theta} = -\frac{\omega}{m\tilde{\psi}}\frac{\mathrm{d}h}{\mathrm{d}\Omega}Rqk_\parallel \left.\frac{\partial g^{(1,0)}}{\partial\xi}\right|_\Omega - k_\parallel v_\parallel \left.\frac{\partial g^{(1,0)}}{\partial\xi}\right|_\Omega + \ldots, \tag{4.85}$$

where Eq.(4.68) has been invoked and terms not contributing have not been shown. In the limit $\omega \gg k_\parallel v_\parallel$ the first term at the right-hand side clearly prevails on the second one. This last result is substituted into Eq.(4.83), yielding the following expression for the continuity equation:

$$k_\parallel \left.\frac{\partial J_\parallel}{\partial\xi}\right|_\Omega = -I\frac{Rq}{\omega_c}q_i\frac{\omega}{m\tilde{\psi}}\int \mathrm{d}^3v v_\parallel \frac{\partial}{\partial\chi}\left(\frac{\mathrm{d}h}{\mathrm{d}\Omega}\left\langle k_\parallel \left.\frac{\partial g^{(1,0)}}{\partial\xi}\right|_\Omega\right\rangle_\theta\right). \tag{4.86}$$

As only the lowest-order term in ϵ will be retained, the factor $v_\parallel/\omega_c$ has been taken out of the average operator.

Before proceeding with the calculation, some considerations about the physics lying behind it are necessary. As previously elucidated in chapter 3, the polarization current is a radial current which develops to provide the torque to balance the inertia term due to the time dependence of the toroidal precession ω_E, experienced by trapped particles. It has already been pointed out (see Eq.(4.64)) that the meaning of $g^{(1,0)}$ is to account for the perturbation of the velocity distribution due to the appearance of such toroidal precession. On the other hand, the operator in Eq.(4.68), which acts on $g^{(1,0)}$ in Eq.(4.85), represents exactly the θ-averaged total time derivative operator, see Eq.(4.68). *It is therefore clear that the argument of the integral in* Eq.(4.86) *is physically linked to the divergence of the total time derivative of*

the perturbation on the distribution function due to ω_E, i.e. it represents the perpendicular divergence of the polarization current as outlined in chapter 3. Recalling Eq.(4.63) and Eq.(4.73), and the identity Eq.(4.37), after some algebra, the expression

$$k_\parallel \left.\frac{\partial g^{(1,0)}}{\partial \xi}\right|_\Omega = \frac{4I}{W_\chi^2}\frac{\omega q}{mc}\frac{\mathrm{d}h}{\mathrm{d}\Omega}\frac{q_i F_M}{T}\frac{m\tilde{\psi}}{Rq}\left[\frac{v_\parallel}{\omega_c} - \left\langle\frac{1}{\omega_c}\right\rangle_\theta \cdot \left\langle\frac{1}{v_\parallel}\right\rangle_\theta^{-1}\right]\sin\xi \tag{4.87}$$

is derived. The derivative with respect to χ in Eq.(4.86) acts only on $h(\Omega)$. Recalling the definition of $k_\parallel$ (Eq.(4.30)), the quasineutrality condition can be rewritten substituting Eq.(4.87) into Eq.(4.86), yielding

$$\left.\frac{\partial J_\parallel}{\partial \xi}\right|_\Omega = q_i \frac{32I^2}{W_\chi^4}\frac{Rq}{\omega_c}\frac{\omega^2 q}{m^2 c}\frac{q_s}{q_s'}\frac{\mathrm{d}h}{\mathrm{d}\Omega}\frac{\mathrm{d}^2 h}{\mathrm{d}\Omega^2}$$
$$\int \mathrm{d}^3 v v_\parallel \frac{q_i F_M}{T}\left[\left\langle\frac{v_\parallel}{\omega_c}\right\rangle_\theta - \left\langle\frac{1}{\omega_c}\right\rangle_\theta \cdot \left\langle\frac{1}{v_\parallel}\right\rangle_\theta^{-1}\right]\sin\xi. \tag{4.88}$$

θ-averages in square brackets can be performed neglecting the θ-dependence of the cyclotron frequency, as only the lowest-order in ϵ is retained. On the contrary, the integration of the parallel velocity can be performed by means of pitch-angle variables, see Eq.(4.14). Again considering only the lowest-order terms after expanding the argument in ϵ, and introducing $\bar{\lambda} = \lambda B_0$, the first average reads

$$\left\langle v_\parallel\right\rangle_\theta = \frac{\sigma v_\parallel}{2\pi}\oint \mathrm{d}\theta\sqrt{1-\bar{\lambda}+\bar{\lambda}\epsilon\cos\theta} = \sigma v_\parallel\sqrt{1-\bar{\lambda}} + \mathcal{O}\left(\epsilon^2\right). \tag{4.89}$$

The second average turns out to be more complicated. Introducing

$$k = \frac{2\epsilon\bar{\lambda}}{1-\bar{\lambda}+\bar{\lambda}\epsilon} \tag{4.90}$$

and invoking the trigonometric identity

$$\cos\theta = 1 - 2\sin^2(\theta/2) \tag{4.91}$$

after some tedious but straightforward algebra one draws

$$\left\langle\frac{1}{v_\parallel}\right\rangle_\theta = \frac{1}{2\pi}\oint\frac{\mathrm{d}\theta}{\sigma v}\frac{1}{\sqrt{1-\bar{\lambda}+\bar{\lambda}\epsilon\cos\theta}} = \frac{2}{\pi}\frac{K[k]}{\sigma v\sqrt{1-\bar{\lambda}+\bar{\lambda}\epsilon}}, \tag{4.92}$$

where $K[k]$ is the complete elliptic integral of the first kind [35]

$$K[k] = \int_0^{\pi/2} \frac{\mathrm{d}\theta}{\sqrt{1 - k\sin^2\theta}}. \tag{4.93}$$

The following step consists in calculating the integral over velocity space in Eq.(4.88). Such operation is carried out employing pitch angle variables. Here, the expression of such integral operator is rewritten for convenience:

$$\int_{-\infty}^{\infty} \ldots \mathrm{d}^3 v = \pi B \sum_{\sigma=\pm 1} \int_0^{\infty} v^2 \mathrm{d}v \int_0^{\frac{1}{B}} \ldots \frac{\mathrm{d}\lambda}{\sqrt{1 - \lambda B}}.$$

The integration over v is straightforward. However, the integration over λ, which acts only on terms in square brackets in Eq.(4.88), owns a subtle but crucial peculiarity, which must be outlined before proceeding. The first term in square brackets Eq.(4.88) derives from the θ-dependent part of $g^{(1,0)}$, which is defined on the whole velocity space. *On the contrary, the second term in square brackets in* Eq.(4.88)*, which has been averaged according to* Eq.(4.92) *derives from* $\bar{h}_P^{(1,0)}$ *and it is therefore defined only in the passing region of the velocity space, where it must be integrated* . Recalling the definition of λ, it is clear that a passing particle is identified by $0 < \lambda < 1/B_M$, thus $0 < \bar{\lambda} < 1 - \epsilon$ (according to the large aspect-ratio approximation). Hence, focusing on the integration on λ, one achieves for the term defined on the whole velocity space (Eq.(4.89))

$$\int_0^1 \mathrm{d}\bar{\lambda}\sqrt{1 - \bar{\lambda}} = \frac{2}{3}, \tag{4.94}$$

while the term defined only in the passing region yields (Eq.(4.92))

$$\frac{\pi}{2}\int_0^{1-\epsilon} \mathrm{d}\bar{\lambda}\frac{\sqrt{1 - \bar{\lambda} + \bar{\lambda}\epsilon}}{K[k]}. \tag{4.95}$$

In the passing region of velocity space, k is small. It is therefore possible to add and subtract the first two terms of the expansion in k of the elliptic integral,

$$\frac{\pi/2}{K[k]} = 1 - \frac{k}{4} + \ldots, \tag{4.96}$$

yielding

$$\frac{\pi}{2}\int_0^{1-\epsilon}\mathrm{d}\bar{\lambda}\frac{\sqrt{1-\bar{\lambda}+\bar{\lambda}\epsilon}}{K\left[k\right]}=\int_0^{1-\epsilon}\mathrm{d}\bar{\lambda}\sqrt{1-\bar{\lambda}+\bar{\lambda}\epsilon+}$$
$$-\frac{1}{2}\int_0^{1-\epsilon}\mathrm{d}\bar{\lambda}\sqrt{1-\bar{\lambda}+\bar{\lambda}\epsilon}\frac{\epsilon\bar{\lambda}}{1-\bar{\lambda}+\bar{\lambda}\epsilon}+$$
$$\int_0^{1-\epsilon}\mathrm{d}\bar{\lambda}\sqrt{1-\bar{\lambda}+\bar{\lambda}\epsilon}\left(\frac{\pi/2}{K\left[k\right]}-1+\frac{1}{4}k\right). \tag{4.97}$$

Note that this operation does not introduce any approximation. The first two integrals amount to

$$\int_0^{1-\epsilon}\mathrm{d}\bar{\lambda}\sqrt{1-\bar{\lambda}+\bar{\lambda}\epsilon}=\frac{2}{3}\left(1+\epsilon-\left(2\epsilon\right)^{3/2}+\mathcal{O}\left(\epsilon^2\right)\right) \tag{4.98}$$

$$\frac{1}{2}\int_0^{1-\epsilon}\mathrm{d}\bar{\lambda}\sqrt{1-\bar{\lambda}+\bar{\lambda}\epsilon}\frac{\epsilon\bar{\lambda}}{1-\bar{\lambda}+\bar{\lambda}\epsilon}=\frac{2\epsilon}{3}-\frac{\left(2\epsilon\right)^{3/2}}{2}-\mathcal{O}\left(\epsilon^2\right). \tag{4.99}$$

The third integral can be transformed into an integral in $\mathrm{d}k$ (retaining only lowest-order terms in ϵ) and then evaluated numerically:

$$\int_0^{1-\epsilon}\mathrm{d}\bar{\lambda}\sqrt{1-\bar{\lambda}+\bar{\lambda}\epsilon}\left(\frac{\pi/2}{K\left[k\right]}-1+\frac{1}{4}k\right)\approx$$
$$\frac{\left(2\epsilon\right)^{3/2}}{4}\int_0^1\frac{\mathrm{d}k}{k^{5/2}}\left(\frac{2\pi}{K\left[k\right]}-4+k\right)\approx I_p\left(2\epsilon\right)^{3/2}, \tag{4.100}$$

$I_p=-0.219$ being the numerical value of the integral. Thus, recapitulating all the results, the square brackets of Eq.(4.88) integrated on $\bar{\lambda}$ yield (neglecting $\mathcal{O}\left(\epsilon^2\right)$)

$$\int\mathrm{d}\bar{\lambda}\left[\left\langle\frac{v_\parallel}{\omega_c}\right\rangle_\theta-\left\langle\frac{1}{\omega_c}\right\rangle_\theta\cdot\left\langle\frac{1}{v_\parallel}\right\rangle_\theta^{-1}\right]=$$
$$\frac{\sigma v}{\omega_c}\left[\frac{2}{3}-\frac{2}{3}\left(1+\epsilon-\left(2\epsilon\right)^{3/2}\right)+\frac{2\epsilon}{3}-\frac{\left(2\epsilon\right)^{3/2}}{2}-I_p\left(2\epsilon\right)^{3/2}\right]=$$
$$\frac{\sigma v}{\omega_c}\left(\frac{1}{6}-I_p\right)\left(2\epsilon\right)^{3/2} \tag{4.101}$$

It is evident that a cancellation at the zeroth-order in ϵ between the θ-dependent part of $g^{(1,0)}$ and $\bar{h}_P^{(1,0)}$ takes place, entailing a higher-order result.

This annihilation has a deep physical meaning. The polarization current is in fact carried only by trapped particles, as outlined in the previous chapter. This mathematically turns out in an annihilation of such current contribution in the passing region of the phase space. The remaning contribution is exactly the trapped particle one. The factor $\epsilon^{3/2}$ characterises the low collisional regime. High collisionality enhances this current [36], as trapped particles are able to transfer their motion to the passing ones, but such a case will not be analyzed here.

Eq.(4.88) can be straightforwardly integrated over v and over ξ, having as a condition the vanishing of the flux-surface average. The final expression is

$$J_{\parallel} = -26.3\epsilon^{3/2}\frac{q_i^2}{\omega_c T}n_0 v_{\mathrm{th}}^2 \frac{I^2}{W_\chi^4}\frac{Rq}{\omega_c}\frac{\omega^2 q}{m^2 c}\frac{q_s}{q_s'}\frac{\mathrm{d}h}{\mathrm{d}\Omega}\frac{\mathrm{d}^2 h}{\mathrm{d}\Omega^2}\left[\cos\xi - \langle\cos\xi\rangle_\Omega\right]. \quad (4.102)$$

This result can be substituted into Rutherford equation (see Eq.(3.27)), and the corresponding contribution to the island stability can be computed. Notice that the polarization current clearly exhibits a $\cos\xi$ component, and it is for this reason able to influence island stability. The calculation of the corresponding contribution is however not included in the present chapter, as it is not strictly linked to the present work. It is nevertheless worth to mention that the calculation presented in Wilson *et al.* [26], which derives a stabilizing effect, contains a mistake. The second derivative of $h(\Omega)$ causes in fact the appearence of a Dirac delta on the island separatrix (because of the Heaviside function, see Eq.(4.39)), neglected by the authors. This Dirac delta corresponds to a current "spike" on the separatrix, in turn able to turn the effect of the polarization current from stabilizing into destabilizing. This mistake was first pointed out by Waelbroeck and Fitzpatrick [37].

4.4.3 Summary

The kinetic calculation of the polarization current possesses many relevant physical features. Due to the complexity of the necessary mathematics, it

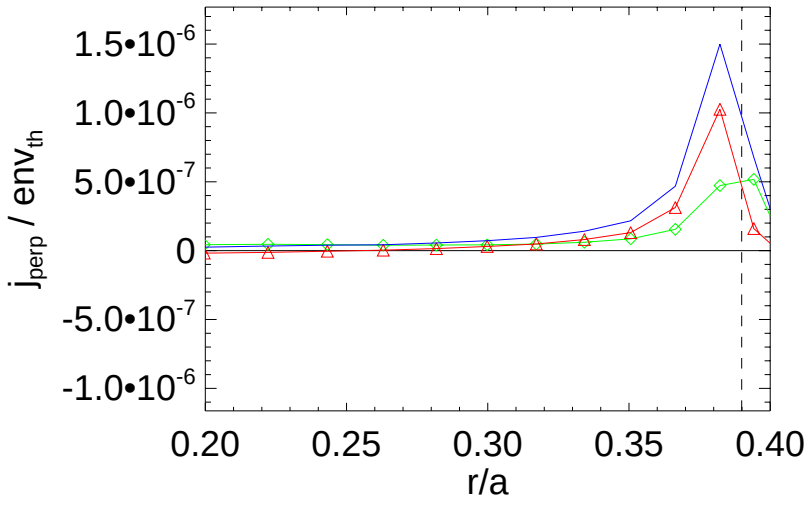

Figure 4.2: Perpendicular perturbed current as a function of the radius in presence of a rotating magnetic island ($\omega = 15000$ rad/s). Green diamonds represent the passing particle contribution, red triangles the trapped particles and the solid blue line corresponds to their sum. The vertical dashed line on the right identifies the inner separatrix of the island. This simulation has been performed with the code HAGIS.

may be worth to quickly summarise the most important aspects in view of the continuation of the present thesis.

- The drift-kinetic equation has been solved through a double parameter expansion of the perturbed distribution function g. The scaling of the island rotation frequency is not calculated self-consistently, but inferred from physical arguments.

- The toroidal precession due to the radial electric field, ω_E, enters the solution at the order $g^{(1,0)}$.

- The polarization current is shown analytically to be linked to the total time derivative of $g^{(1,0)}$. This is consistent with the physical picture of the polarization current, which links the current itself to the time derivative of the toroidal electric precession of trapped particles (see Eq.(2.44)).

- To isolate the polarization current contribution, the assumption $\omega \gg k_\parallel v_\parallel$ has been adopted. This assumption is inconsistent with the scaling criteria. It has the physical meaning of excluding the possibility of resonances between the particles and the mode, letting the island rotate faster than any particle in the $\nabla\xi$ direction. The consequences of these resonances represent the central issue of the following chapter.

- The polarization current is defined only in the trapped region of velocity space. This is mathematically reflected by the cancellation in the passing region of the phase space of $g^{(1,0)}$ after integration over the velocity space. The remainder pertains to $\mathcal{O}\left(\epsilon^{3/2}\right)$, as inferred from simple velocity space considerations [38, 39].

Fig.4.2 shows an HAGIS simulation of the polarization current (to be intended as perpendicular current). The trapped particle contribution, in the proximity of the island separatrix, clearly exceeds the passing particles one.

Chapter 5

Role of the Parallel Streaming of Passing Ions

In the previous chapter, following Ref.[26], in order to isolate the polarization current contribution, the assumption $\omega \gg k_{\|} v_{\|}$ was made, i.e. the parallel streaming of the ions along the island was supposed to be negligible as compared to the island drift frequency. As previously mentioned, this assumption cannot be justified within the scaling adopted for the perturbative solution of Eq.(4.41), see section 4.2.1. In the present chapter, terms in $k_{\|} v_{\|}$ will be on the contrary retained in the calculation. First, the formal derivation of the polarization current and the subsequent drive for the magnetic island is presented. Then, a physical picture of the process taking place when the island rotation is comparable with the parallel streaming of passing ions is discussed.

5.1 Solution of the Drift-Kinetic Equation

5.1.1 The Perturbed Distribution

For the purposes of this chapter, the same scaling criteria elucidated in chapter 4 are mantained. This implies that the frequency ω, whose scaling was

inferred from physical considerations, is supposed to be ordered as

$$\omega \sim k_\parallel v_\parallel \tag{5.1}$$

(see chapter 4 for a detailed discussion). Thus, such ordering allows the island rotation frequency and parallel streaming to compete. The expanded form of the drift-kinetic equation Eq.(4.41) is reported for convenience:

$$\begin{aligned} -\omega\frac{\partial g}{\partial \xi} + \frac{v_\parallel}{Rq}\frac{\partial g}{\partial \theta} + k_\parallel v_\parallel \left.\frac{\partial g}{\partial \xi}\right|_\Omega + m\frac{c}{B}\frac{I}{Rq}\frac{\partial \phi}{\partial \chi}\frac{\partial g}{\partial \xi} + \\ -m\frac{c}{B}\frac{I}{Rq}\frac{\partial \phi}{\partial \xi}\frac{\partial g}{\partial \chi} + \frac{Iv_\parallel}{Rq}\frac{\partial}{\partial \theta}\left(\frac{v_\parallel}{\omega_c}\right)\frac{\partial g}{\partial \chi} - m\frac{Iv_\parallel}{Rq}\frac{\partial}{\partial \chi}\left(\frac{v_\parallel}{\omega_c}\right)\frac{\partial g}{\partial \xi} \\ -\frac{q_i}{m_i v}\left[\frac{Iv_\parallel}{Rq}\frac{\partial}{\partial \theta}\left(\frac{v_\parallel}{\omega_c}\right)\frac{\partial \phi}{\partial \chi} - m\frac{Iv_\parallel}{Rq}\frac{\partial}{\partial \chi}\left(\frac{v_\parallel}{\omega_c}\right)\frac{\partial \phi}{\partial \xi}\right]\frac{\partial g}{\partial v} = \\ = -\frac{q_i F_M}{T}\left[\frac{Iv_\parallel}{Rq}\frac{\partial}{\partial \theta}\left(\frac{v_\parallel}{\omega_c}\right)\frac{\partial \phi}{\partial \chi} - m\frac{Iv_\parallel}{Rq}\frac{\partial}{\partial \chi}\left(\frac{v_\parallel}{\omega_c}\right)\frac{\partial \phi}{\partial \xi}\right], \end{aligned} \tag{5.2}$$

with the ordering

$$\Delta : 1 : \Delta : \Delta : \Delta : \delta : \Delta\delta : \Delta\delta : \Delta^2\delta = \delta : \Delta\delta. \tag{5.3}$$

Recall further that the solution for the perturbed distribution g is obtained by means of a double parameter expansion, such as

$$g = \sum_{m,n}^{\infty} g^{(m,n)}\delta^m \Delta^n, \tag{5.4}$$

where δ and Δ are small parameters introduced in Eq.(4.44) and Eq.(4.45). As both the equation and the ordering are the same as in the previous chapter, the solution path remains the same. This means

$$\bar{g}^{(0,0)} = 0, \tag{5.5}$$

$$g^{(1,0)} = -I\frac{v_\parallel}{\omega_c}\frac{\partial \phi}{\partial \chi}\frac{q_i F_M}{T} + \bar{h}_P^{(1,0)} + \bar{h}_T^{(1,0)}, \tag{5.6}$$

where $\bar{h}_P^{(1,0)}$ and $\bar{h}_T^{(1,0)}$ are defined in the passing and trapped region of phase space, respectively. The expression for $\bar{h}_P^{(1,0)}$, which now includes the parallel

streaming of the trapped ions, is (cf. Eq.(4.71) vs. Eq.(4.73))

$$\bar{h}_P^{(1,0)} = -\frac{4I}{W_\chi^2}\frac{\omega q}{mc}\frac{\mathrm{d}h}{\mathrm{d}\Omega}\frac{q_i F_M}{T}\left\langle\left(\frac{\mathrm{d}h}{\mathrm{d}\Omega}\frac{\omega}{m\tilde{\psi}}\frac{Rq}{v_\parallel}+1\right)\frac{v_\parallel}{\omega_c}+\frac{q_s}{q_s'}\frac{\partial}{\partial\chi}\left(\frac{v_\parallel}{\omega_c}\right)\right\rangle_\theta \cdot \left[\left\langle\frac{\mathrm{d}h}{\mathrm{d}\Omega}\frac{\omega}{m\tilde{\psi}}\frac{Rq}{v_\parallel}+1\right\rangle_\theta\right]^{-1}\left[\chi-\langle\chi\rangle_\Omega\right]. \quad (5.7)$$

The contribution in the trapped space, $\bar{h}_T^{(1,0)}$, is actually nonzero, if the limit $\omega \gg k_\parallel v_\parallel$ is rejected. However, it is uninfluential for the following considerations, and therefore it will be discussed at the end of this chapter.

The relevant peculiarity of $\bar{h}_P^{(1,0)}$, when terms in $k_\parallel v_\parallel$ are retained, is that it exhibits a denominator potentially leading to resonance phenomena in the velocity space. Following the path of derivation of $\bar{h}_P^{(1,0)}$ (see section 4.4.1, and in particular Eq.(4.70)), one can notice that the first term at the denominator comes from the total time derivative, proportional to ω (cf. Eq.(4.68)), while the second one is related to $k_\parallel v_\parallel$. Physically, the total time derivative accounts for the relative motion between the island and the plasma due to island rotation and $\mathbf{E}\times\mathbf{B}$-drifts [1]. On the other hand, the term in $k_\parallel v_\parallel$ accounts for the motion of the plasma with respect to the magnetic island due to the parallel streaming on surfaces which do not have in general the same helicity as the NTM. *The competition of these two terms can therefore lead to resonant interactions between the passing particles and the mode.* The influence of such resonances on the perturbed parallel current are analyzed in the following section.

[1] It can be shown that the total derivative operator (once θ-averaged), is related to a motion *along* the perturbed magnetic surfaces. In fact for every particle (see Eq.(4.68))

$$\frac{\mathrm{d}_0\Omega}{\mathrm{d}t} = -\omega\frac{\partial\Omega}{\partial\xi}+c\frac{\mathbf{B}\times\nabla\phi}{B^2}\cdot\nabla\Omega = 0, \quad (5.8)$$

as can be easily proved in view of Eq.(4.38).

5.1.2 The Perturbed Current

To evaluate the role of the terms in $k_\parallel v_\parallel$ to the perturbed parallel current, the technique outlined in the previous chapter is utilized. The starting point is again the quasineutrality equation $\nabla_\parallel J_\parallel = -\nabla_\perp \cdot \mathbf{J}_\perp$, where the right-hand side of the quasineutrality equation is expressed by (see Eq.(4.83))

$$\left\langle \int \mathrm{d}^3 v \frac{I v_\parallel}{Rq} \frac{\partial}{\partial \theta} \left(\frac{v_\parallel}{\omega_c} \right) \frac{\partial g}{\partial \chi} \right\rangle_\theta \approx -I \left\langle \int \mathrm{d}^3 v \frac{v_\parallel}{\omega_c} \frac{\partial}{\partial \chi} \left(\frac{v_\parallel}{Rq} \frac{\partial g}{\partial \theta} \right) \right\rangle_\theta . \tag{5.9}$$

Like in the analysis of chapter 4, the lowest-order term which yields a nonvanishing contribution is $g^{(1,1)}$. Such term can be directly obtained by $\mathcal{O}(\Delta\delta)$ equation, namely (Eq.(4.85))

$$\frac{v_\parallel}{Rq} \frac{\partial g^{(1,1)}}{\partial \theta} = -\frac{\omega}{m\tilde{\psi}} \frac{\mathrm{d}h}{\mathrm{d}\Omega} Rqk_\parallel \left. \frac{\partial g^{(1,0)}}{\partial \xi} \right|_\Omega - k_\parallel v_\parallel \left. \frac{\partial g^{(1,0)}}{\partial \xi} \right|_\Omega + \ldots , \tag{5.10}$$

where again terms not contributing have not been shown. Of course, for the analysis presented in this chapter, the second term on the right-hand side of Eq.(5.10) must be retained. Therefore, Eq.(4.86), which has been derived in the limit $\omega > k_\parallel v_\parallel$, now takes the form

$$k_\parallel \left. \frac{\partial J_\parallel}{\partial \xi} \right|_\Omega = -\frac{q_i I}{\omega_c} \frac{\omega}{m\tilde{\psi}} \int \mathrm{d}^3 v v_\parallel \frac{\partial}{\partial \chi} \left\langle \left[\frac{\mathrm{d}h}{\mathrm{d}\Omega} \frac{\omega}{m\tilde{\psi}} Rqk_\parallel + k_\parallel v_\parallel \right] \left. \frac{\partial g^{(1,0)}}{\partial \xi} \right|_\Omega \right\rangle_\theta . \tag{5.11}$$

The appropriate expression for $g^{(1,0)}$ (Eq.(5.6)) and $\bar{h}_P^{(1,0)}$ (Eq.(5.7)) are now substituted in Eq.(5.11), yielding

$$\begin{aligned} \left. \frac{\partial J_\parallel}{\partial \xi} \right|_\Omega = -\frac{q_i I}{\omega_c} \frac{\partial}{\partial \chi} \int \mathrm{d}^3 v v_\parallel \Lambda F_M \Big\langle \left(\bar{u} + v_\parallel \right) \cdot \Big[\left(\frac{v_\parallel}{\omega_c} \right) + \\ - \left\langle \left(\frac{\bar{u}}{v_\parallel} + 1 \right) \frac{v_\parallel}{\omega_c} + \frac{q_s}{q_s'} \frac{\partial}{\partial \chi} \left(\frac{v_\parallel}{\omega_c} \right) \right\rangle_\theta \cdot \left\langle \frac{\bar{u}}{v_\parallel} + 1 \right\rangle_\theta^{-1} \Big] \Big\rangle_\theta \end{aligned} \tag{5.12}$$

having introduced

$$\Lambda = \frac{4I}{W_\chi^2} \frac{\omega q}{mc} \frac{\mathrm{d}h}{\mathrm{d}\Omega} \frac{q_i}{T} \left. \frac{\partial \chi}{\partial \xi} \right|_\Omega$$

and

$$\bar{u} = \frac{\mathrm{d}h}{\mathrm{d}\Omega}\frac{\omega}{m\tilde{\psi}}Rq.$$

Equation (5.12) exhibits an important feature: the resonant denominator that appears in $\bar{h}_P^{(1,0)}$ (Eq.(5.7)) is almost cancelled by a similar numerator which arises from including the parallel streaming in the advection (Eq.(5.10)). In order to carry out Eq.(5.12), the factor

$$\left\langle \bar{u} + v_\parallel \right\rangle_\theta \left\langle \frac{\bar{u}}{v_\parallel} + 1 \right\rangle_\theta^{-1} \tag{5.13}$$

is for the moment considered. In the previous chapter, it has been shown (Eq.(4.92)) that

$$\left\langle \frac{1}{v_\parallel} \right\rangle_\theta = \frac{1}{2\pi}\oint \frac{\mathrm{d}\theta}{\sigma v}\frac{1}{\sqrt{1-\bar{\lambda}+\bar{\lambda}\epsilon\cos\theta}} = \frac{2}{\pi}\frac{K\left[k\right]}{\sigma v\sqrt{1-\bar{\lambda}+\bar{\lambda}\epsilon}}, \tag{5.14}$$

where $K\left[k\right]$ is the complete elliptic integral of the first kind. Following a completely analogous calculation, it can be easily derived that

$$\left\langle v_\parallel \right\rangle_\theta = \frac{\sigma v}{2\pi}\oint \mathrm{d}\theta\sqrt{1-\bar{\lambda}+\bar{\lambda}\epsilon\cos\theta} = \frac{2}{\pi}\sigma v\sqrt{1-\bar{\lambda}+\bar{\lambda}\epsilon}E\left[k\right], \tag{5.15}$$

$E\left[k\right]$ being the complete elliptic integral of the second kind, namely

$$E\left[k\right] = \int_0^{\pi/2}\mathrm{d}\theta\sqrt{1-k\sin^2\theta}. \tag{5.16}$$

The variable k has already been introduced in the previous chapter as

$$k = \frac{2\epsilon\bar{\lambda}}{1-\bar{\lambda}+\bar{\lambda}\epsilon}. \tag{5.17}$$

Recall that $\bar{\lambda} = \lambda B_0$, λ being the pitch-angle variable introduced in chapter 4 (see Eq.(4.15)). The variable k can be supposed to remain below the value of 1 for passing particles. Considering a region of phase space sufficiently far away from the resonance $\left\langle \bar{u} + v_\parallel \right\rangle_\theta = 0$, the factor in Eq.(5.13) can be

therefore expanded as

$$\left\langle \bar{u}+v_{\parallel}\right\rangle_{\theta}\left\langle \frac{\bar{u}}{v_{\parallel}}+1\right\rangle_{\theta}^{-1}=\frac{\bar{u}+\frac{2}{\pi}v_{\parallel,0}E\left[k\right]}{\frac{2}{\pi}\frac{\bar{u}}{v_{\parallel,0}}K\left[k\right]+1}\sim$$
$$v_{\parallel,0}\left(1-\frac{k}{4}\right)-k^{2}\frac{v_{\parallel,0}\left(3v_{\parallel,0}+5\bar{u}\right)}{64\left(v_{\parallel,0}+\bar{u}\right)}+\mathcal{O}\left(k^{3}\right), \tag{5.18}$$

having introduced $v_{\parallel,0}=\sigma v\sqrt{1-\lambda+\lambda\epsilon\cos\theta}$. The variable k, in the passing region of phase space is clearly $\mathcal{O}\left(\epsilon\right)$ (see Eq.(5.17)). *It is therefore manifest that the contribution of the resonant denominator enters in the calculations only at* $\mathcal{O}\left(\epsilon^{2}\right)$. This point is discussed in section 5.2 below.

In view of these last results, Eq.(5.12) can be cast in the form

$$\left.\frac{\partial J_{\parallel}}{\partial\xi}\right|_{\Omega}=-\frac{q_{i}I}{\omega_{c}}\frac{\partial}{\partial\chi}\int\mathrm{d}^{3}v v_{\parallel}\Lambda F_{M}\left[\left\langle \left(\bar{u}+v_{\parallel}\right)\cdot\frac{v_{\parallel}}{\omega_{c}}\right\rangle_{\theta}+\right.$$
$$\left.-\left(v_{\parallel,0}-v_{\parallel,0}\frac{k}{4}\right)\left\langle \left(\frac{\bar{u}}{v_{\parallel}}+1\right)\frac{v_{\parallel}}{\omega_{c}}+\frac{q_{s}}{q_{s}'}\frac{\partial}{\partial\chi}\left(\frac{v_{\parallel}}{\omega_{c}}\right)\right\rangle_{\theta}\right]. \tag{5.19}$$

All the terms odd in the sign of the parallel velocity σ vanish after integration over the velocity space, see Eq.(4.15), and can therefore be disregarded. This yields

$$\left.\frac{\partial J_{\parallel}}{\partial\xi}\right|_{\Omega}=-\frac{q_{i}I}{\omega_{c}}\frac{\partial}{\partial\chi}\int\mathrm{d}^{3}v v_{\parallel}\Lambda F_{M}\left[\bar{u}\left\langle \frac{v_{\parallel}}{\omega_{c}}\right\rangle_{\theta}-\left(v_{\parallel,0}-v_{\parallel,0}\frac{k}{4}\right)\left\langle \frac{\bar{u}}{\omega_{c}}\right\rangle_{\theta}\right]. \tag{5.20}$$

The integration over the velocity space can now be carried out along the same line as in the previous chapter. Recalling in particular that

$$\int_{0}^{1-\epsilon}\mathrm{d}\bar{\lambda}\sqrt{1-\bar{\lambda}+\bar{\lambda}\epsilon}=\frac{2}{3}\left(1+\epsilon-\left(2\epsilon\right)^{3/2}+\mathcal{O}\left(\epsilon^{2}\right)\right) \tag{5.21}$$

and

$$\frac{1}{2}\int_{0}^{1-\epsilon}\mathrm{d}\bar{\lambda}\sqrt{1-\bar{\lambda}+\bar{\lambda}\epsilon}\frac{\epsilon\bar{\lambda}}{1-\bar{\lambda}+\bar{\lambda}\epsilon}=\frac{2\epsilon}{3}-\frac{\left(2\epsilon\right)^{3/2}}{2}-\mathcal{O}\left(\epsilon^{2}\right), \tag{5.22}$$

the final expression for the parallel current amounts to

$$J_{\parallel} = -11.4\epsilon^{3/2}\frac{q_i^2}{\omega_c T}n_0 v_{\rm th}^2 \frac{I^2}{W_\chi^4}\frac{Rq}{\omega_c}\frac{\omega^2 q}{m^2 c}\frac{q_s}{q_s'}\frac{{\rm d}h}{{\rm d}\Omega}\frac{{\rm d}^2 h}{{\rm d}\Omega^2}\left[\cos\xi - \langle\cos\xi\rangle_\Omega\right]. \qquad (5.23)$$

Comparing Eq.(5.23) *with the polarization current derived in* Eq.(4.102), *it is clear that the only influence of the parallel streaming on the* $\cos\xi$*-component of the parallel current simply reduces to a change in the numerical coefficient in front of the current itself.* According to the analytical calculations exposed, the difference between Eq.(5.23) and Eq.(4.102) consists, roughly, in a factor of 2. Actually, such difference might have been overestimated, see Fig.5.1, by virtue of the approximations adopted in the calculation (terms $\mathcal{O}\left(\epsilon^{3/2}\right)$ are retained, while terms $\mathcal{O}\left(\epsilon^2\right)$ are discarded). The important fact to stress is that no relevant physical mechanism connected to the parallel streaming of passing ions influences significantly the island stability.

It is worth to stress the fact that the expansion in k is mathematically correct only sufficiently far away from the resonance, as clearly a resonant term can not be expanded in Taylor series. The role of resonant particles is discussed shortly afterwards.

5.2 Considerations on the Results

5.2.1 The Contribution of Parallel Streaming

The limited influence of the parallel streaming on the perturbed parallel current, and as a consequence on the NTM stability, has a twofold reason.

First, sufficiently far away from the resonance (i.e. where the expansion in k is meaningful), all the terms linked to $k_\parallel v_\parallel$ (i.e. the new terms appearing in Eq.(5.19) in comparison with Eq.(4.88)) are anyhow annihilated up to $\mathcal{O}\left(\epsilon^2\right)$ by the integration on the velocity space, by virtue of their oddness in σ. Simulations performed with the HAGIS code (Fig.5.1) support this analytical result. The perpendicular current linked to co-passing particles ($\sigma = 1$) is shown to be approximatively cancelled by the counter-passing one

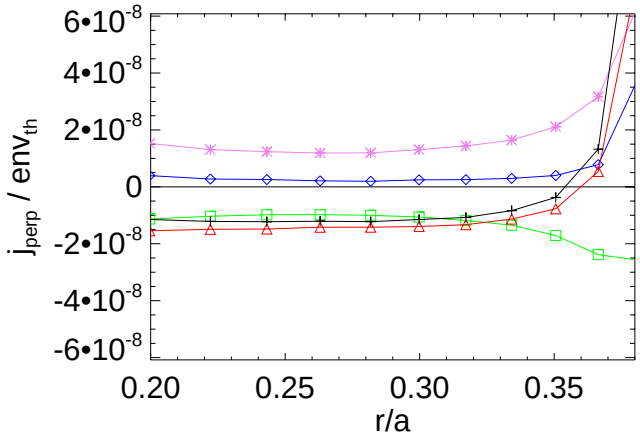

Figure 5.1: Radial profile of the perpendicular current (the inner island separatrix is located at $r/a = 0.38$) for $\omega = -4000$ rad/s. Magenta stars represent the contribution of the passing particles with $v_{\|} > 0$, green squares passing particles with $v_{\|} < 0$, blue diamonds the total current due to passing particles, red triangles the trapped particles and the crossed black line the total perpendicular current. The sudden rise of the current close to the island separatrix is due to the onset of the standard polarization current. The trapped-particle contribution to the current at some distance from the island separatrix is discussed in the next chapter. In this chapter and in the following, all numerical simulations have been performed with the code HAGIS, see chapter 4.

($\sigma = -1$), see again Fig.5.1. The trapped particle contribution, linked to the "standard" polarization current, remains thus the prevalent component of the total current.

Moreover, particles whose motion is most affected by the presence of the island (i.e. particles streaming almost "in phase" with the island itself) are the ones which provide the smallest contribution to the θ-averaged perturbed current. In fact, particles which have a reduced θ-averaged relative motion with respect to the island are more influenced by the mode itself, and there-

fore the perturbation on the distribution is peaked in such region of the velocity space. On the other hand, the perpendicular current is induced by the *advection* of particles along the perturbed magnetic surfaces, in complete analogy with the fluid description of polarization current given in chapter 3 (the perpendicular current arises as a consequence of the time-varying plasma flow along the island). This advection is of course reduced if the particle tends to remain "locked" with the mode. This physical statement is reflected by the almost exact cancellation of the resonant denominator in $\bar{h}_P^{(1,0)}$ by the similar numerator arising from the inclusion of the parallel streaming in the advection terms, see Eq.(5.12). Numerical simulations (see Fig.5.2) clearly show that the perturbed distribution function (a) exhibits a resonant behaviour for a given sign of $v_\parallel$. Note in addition that such resonance occurs at higher energies if the ratio $v_\parallel/v$ is reduced (as $v_\parallel$ must remain the same). On the contrary, the subsequent perpendicular current (b) turns out to be odd in σ, having in addition lost any resonant feature. Such result is in complete agreement with the analytical calculation. Incidentally, it will be shown in the next chapter that trapped particles are able to provide a perpendicular current contribution even in the proximity of a resonance, by virtue of their nonvanishing θ-averaged flux through the perturbed magnetic surfaces caused by the magnetic drifts.

5.2.2 The Role of Resonating Particles

As previously stated, the analytical treatment presented fails for particles very close to the resonance, as of course no Taylor expansion is meaningful if the function diverges. Anyway, numerical simulations show that the effect of the resonant particles on the perturbed current is nevertheless small, as just discussed. This allows to conclude that *the contribution of the resonant particles to the perturbed current can be safely supposed to be negligible, even though the mathematical derivation is not strictly valid in such limit.*

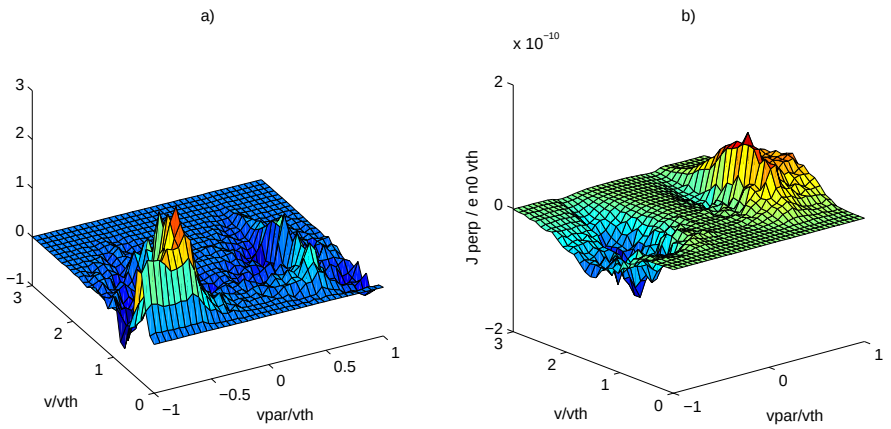

Figure 5.2: Perturbed distribution (a) and perpendicular current (b) in velocity space for $\omega = -4000$ rad/s, calculated a $r/a \approx 0.32$ (i.e outside the magnetic island towards the magnetic axis of the tokamak, see Fig.5.1).

To properly evaluate the contribution of the resonance, a Landau-like approach, similarly to Ref.[29, 30, 40, 41, 42], is necessary. However, in these papers it is shown that such Landau resonances contribute only to the "out-of-phase" part of the perturbed current, i.e. the $\sin\xi$ harmonic. The $\sin\xi$-component of $J_{\|}$ is in fact connected to the island rotation, as discussed in chapter 3, and thus it will not be included in this thesis, where the rotation frequency is not calculated self-consistently but it is rather introduced as a free parameter.

5.3 The Perturbed Distribution in the Trapped Space

At the end of this chapter, the calculation of the perturbed distribution in the perturbed region of phase space $\bar{h}_T^{(1,0)}$ is derived. The equation $\mathcal{O}(\Delta\delta)$ (see Eq.(4.69)) is bounce-averaged in the trapped region of the phase space

(Eq.(4.67)), yielding

$$\left.\frac{\partial \bar{h}_T^{(1,0)}}{\partial \xi}\right|_\Omega = I\left\langle k_\parallel \frac{\left|v_\parallel\right|}{\omega_c}\left.\frac{\partial}{\partial \xi}\right|_\Omega\left(\frac{\partial \phi}{\partial \chi}\right) + m\frac{\partial}{\partial \chi}\left(\frac{\left|v_\parallel\right|}{\omega_c}\right)\frac{\partial \phi}{\partial \xi}\right\rangle_\theta^T \times \left(\left\langle \frac{\mathrm{d}h}{\mathrm{d}\Omega}\frac{\omega}{m\tilde{\psi}}\frac{Rqk_\parallel}{\left|v_\parallel\right|}\right\rangle_\theta^T\right)^{-1}\frac{q_i F_M}{T}. \tag{5.24}$$

This equation can be simplified, noticing that

$$\left(\left\langle \frac{1}{v_\parallel}\right\rangle_\theta^T\right)^{-1}\left\langle \nabla v_\parallel\right\rangle_\theta^T = \left\langle v_\parallel \nabla v_\parallel\right\rangle_\theta^T + \mathcal{O}\left(\epsilon^2\right). \tag{5.25}$$

Eq.(5.25) and the identity

$$k_\parallel \left.\frac{\partial \chi}{\partial \xi}\right|_\Omega = \frac{m}{q}\frac{\partial A_\parallel}{\partial \xi} = \frac{m}{q}\frac{\tilde{\psi}}{R}\sin\xi \tag{5.26}$$

allow to write Eq. (5.24) in the more perspicuous form

$$\bar{h}_T^{(1,0)} = -\frac{q_i F_M}{T}\left\langle \omega_D + \omega_{\hat{s}}\right\rangle_\theta^T \frac{\left[\chi - \langle\chi\rangle_\Omega\right]}{c}. \tag{5.27}$$

Here, ω_D and $\omega_{\hat{s}}$ are the θ-averaged toroidal precession frequencies of trapped particles introduced in chapter 2 (Eq.(2.43) and Eq.(2.47), respectively), i.e.

$$\omega_D = \frac{q}{Rr\omega_c}\left[\frac{\mu B}{m_i} + v_\parallel^2\right]\cos\theta \tag{5.28}$$

and

$$\omega_{\hat{s}} = \frac{q\hat{s}v_\parallel^2}{r^2\omega_c}. \tag{5.29}$$

The correlation of $\omega_{\hat{s}}$ and ω_D with the first and the second term on the right-hand side of Eq.(5.24), respectively, will be discussed in detail in the next chapter. As both ω_D and $\omega_{\hat{s}}$ are related to the equilibrium magnetic field, from here on the magnetic toroidal precession frequency ω_{tp} is introduced:

$$\omega_{\mathrm{tp}} = \omega_D + \omega_{\hat{s}}. \tag{5.30}$$

Note that, within this ordering, $\bar{h}_T^{(1,0)}$ does not depend on any quantity related to the island, apart from the average radial position $\langle\chi\rangle_\Omega$. The trapped particle distribution introduces therefore the magnetic toroidal precession in the solution. This will be the central topic of the following chapter. There, it is shown that the expression for $\bar{h}_T^{(1,0)}$ found above (Eq.(5.27)) represents the limit for $\omega \gg \omega_{\rm tp}$ of the solution calculated allowing for possible resonances between island rotation and trapped particle precession.

Chapter 6

Modification of the Polarization Current due to the Toroidal Precession of Trapped Ions

In chapter 4, it has been shown that, in absence of equilibrium pressure gradients, the current perpendicular to a rotating magnetic island should exhibit a quadratic dependence on the rotation frequency ω (see Eq.(4.102)). However, simulations performed with HAGIS (see Ref.[34] and Fig.6.1) clearly indicate that such description fails when ω attains sufficiently low values, in the sense that will be specified below. In particular, four changes of sign occur, and such circumstance is crucial in order to determining the stabilizing or destabilizing effect of the current on the evolution of the neoclassical tearing mode. The purpose of this chapter is to address such departure from the parabolic scaling, and to provide both a physical picture of the underlying phenomena and a quantitative evaluation of their contribution to the stability of the magnetic island.

6.1 Solution of the Drift-Kinetic Equation

6.1.1 Scaling of the Island Frequency

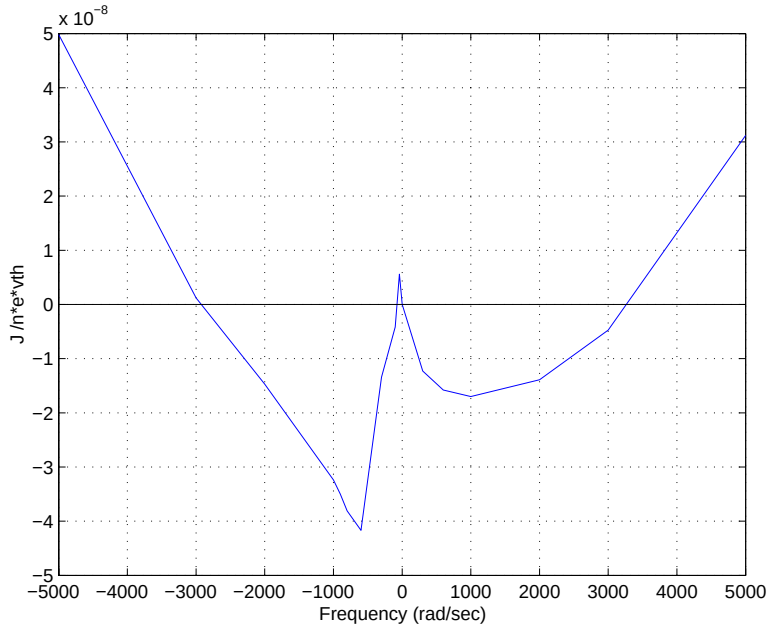

Figure 6.1: Averaged perpendicular current[1] on the inner side of the magnetic island as a function of the island rotation frequency ω. The parabolic dependence clearly breaks for slowly rotating modes. Such figure has been published in Ref.[34].

Numerical simulations show that, in the range of frequencies where the parabolic dependence of the current does not hold, the perturbed current is mainly carried by trapped particles, see Fig.6.2. Therefore, one may suppose that the dominant current contribution in such range is linked to the interaction of the island with some characteristic timescales of the trapped particle motion, in particular the toroidal precession of the banana orbits ω_D (see chapter 2)

[1]Since the perpendicular polarization current averages to zero on the perturbed flux surface, see Fig.3.7, here the average is defined as $\left(J_\perp^{up} - J_\perp^{low}\right)/2$, where subscripts *up* and *low* indicate the upper- ($\xi > 0$) and lower- ($\xi < 0$) half of the island, respectively.

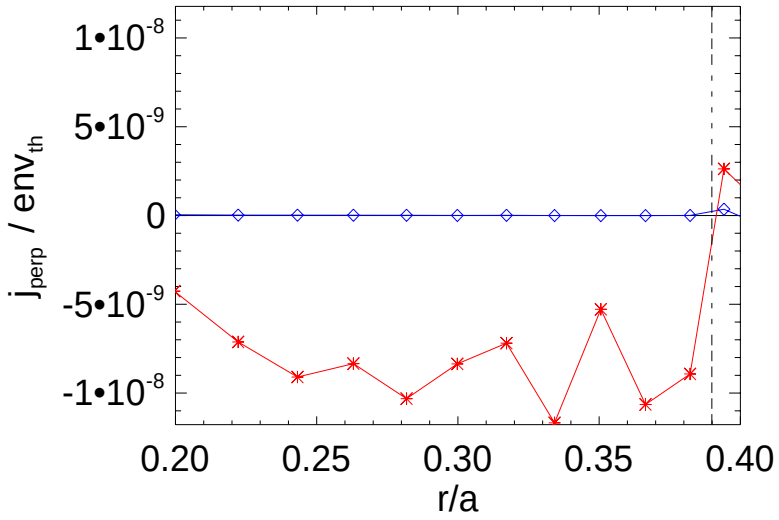

Figure 6.2: Perpendicular current as a function of the radius for $\omega = -300$ rad/s. Red stars correspond to the trapped particle contribution, while blue diamonds to the passing one. The vertical dashed line indicates the inner island separatrix.

$$\omega_D = \frac{q}{Rr\omega_c}\left[\frac{\mu B}{m_i} + v_\parallel^2\right]\cos\theta. \tag{6.1}$$

The term of the drift-kinetic equation Eq.(4.41) which is related to ω_D is the one linked to the the poloidal component of the magnetic drift, i.e.

$$m\frac{Iv_\parallel}{Rq}\frac{\partial}{\partial\chi}\left(\frac{v_\parallel}{\omega_c}\right)\frac{\partial g}{\partial\xi}. \tag{6.2}$$

In fact, as the spatial derivatives in the drift-kinetic equation have to be calculated at constant kinetic energy, see chapter 4, it can be shown that

$$\nabla v_\parallel = -\frac{1}{m_i v_\parallel}\mu\nabla B.$$

Using such relation, recalling that the parallel velocity and the cyclotron frequency depend on space only through the magnitude of the magnetic field, one can write

$$\frac{\partial}{\partial\chi}\left(\frac{v_\parallel}{\omega_c}\right) = -\frac{1}{\omega_c}\left[\frac{\mu}{m_i v_\parallel} + \frac{v_\parallel}{B}\right]\frac{\partial B}{\partial\chi}.$$

As the large aspect-ratio approximation holds

$$\frac{\partial B}{\partial \chi} = -\frac{q}{rR}\cos\theta,$$

therefore

$$\frac{\partial}{\partial \chi}\left(\frac{v_\parallel}{\omega_c}\right) = \frac{q}{rR\omega_c}\left[\frac{\mu}{m v_\parallel} + \frac{v_\parallel}{B}\right]\cos\theta.$$

Thus, the term reported in Eq.(6.2) may be understood as

$$m\frac{I v_\parallel}{Rq}\frac{\partial}{\partial \chi}\left(\frac{v_\parallel}{\omega_c}\right)\frac{\partial g}{\partial \xi} = \frac{m}{q}\frac{q}{rR\omega_c}\left[\frac{\mu B}{m_i} + v_\parallel^2\right]\frac{\partial g}{\partial \xi}\cos\theta = \frac{m}{q}\omega_D\frac{\partial g}{\partial \xi}. \tag{6.3}$$

In the remainder of the chapter, the symbol ω_D will refer to the θ-average (in the trapped region of phase space) of the toroidal precession frequency, as introduced in Eq.(5.28). In order to investigate the interaction of the island rotation with the trapped particle precession, a suitable choice for the scaling is therefore

$$\omega \sim \omega_D, \tag{6.4}$$

which leads to

$$\omega\frac{Rq}{v_\parallel} \sim \Delta\delta. \tag{6.5}$$

This implies that the scaling $\omega \sim k_\parallel v_\parallel$ adopted in chapter 4, 5 has to be abandoned. The following manipulations of the drift-kinetic equation, reported again for convenience

$$\begin{aligned}
&-\omega\frac{\partial g}{\partial \xi} + \frac{v_\parallel}{Rq}\frac{\partial g}{\partial \theta} + k_\parallel v_\parallel \left.\frac{\partial g}{\partial \xi}\right|_\Omega + m\frac{c}{B}\frac{I}{Rq}\frac{\partial \phi}{\partial \chi}\frac{\partial g}{\partial \xi} + \\
&-m\frac{c}{B}\frac{I}{Rq}\frac{\partial \phi}{\partial \xi}\frac{\partial g}{\partial \chi} + \frac{I v_\parallel}{Rq}\frac{\partial}{\partial \theta}\left(\frac{v_\parallel}{\omega_c}\right)\frac{\partial g}{\partial \chi} - m\frac{I v_\parallel}{Rq}\frac{\partial}{\partial \chi}\left(\frac{v_\parallel}{\omega_c}\right)\frac{\partial g}{\partial \xi} \\
&-\frac{q_i}{m_i v}\left[\frac{I v_\parallel}{Rq}\frac{\partial}{\partial \theta}\left(\frac{v_\parallel}{\omega_c}\right)\frac{\partial \phi}{\partial \chi} - m\frac{I v_\parallel}{Rq}\frac{\partial}{\partial \chi}\left(\frac{v_\parallel}{\omega_c}\right)\frac{\partial \phi}{\partial \xi}\right]\frac{\partial g}{\partial v} = \\
&= -\frac{q_i F_M}{T}\left[\frac{I v_\parallel}{Rq}\frac{\partial}{\partial \theta}\left(\frac{v_\parallel}{\omega_c}\right)\frac{\partial \phi}{\partial \chi} - m\frac{I v_\parallel}{Rq}\frac{\partial}{\partial \chi}\left(\frac{v_\parallel}{\omega_c}\right)\frac{\partial \phi}{\partial \xi}\right]
\end{aligned} \tag{6.6}$$

will be therefore carried out according to the scaling

$$\Delta\delta : 1 : \Delta : \Delta\delta : \Delta\delta : \delta : \Delta\delta : \Delta\delta^2 : \Delta^2\delta^2 = \delta^2 : \Delta\delta^2. \tag{6.7}$$

Note that the change of scaling for the frequency reflects on all terms containing the scalar potential, since it is linear in ω (see Eq.(4.38)).

6.1.2 The Perturbed Distribution

The solution of the drift-kinetic equation follows the path discussed in details in chapter 4 and 5. As no term at the lowest-order has been added (rather, some terms have been moved to higher orders), it is again meaningful to suppose that

$$g^{(0,0)} = 0, \tag{6.8}$$

in analogy with the calculation performed in the previous chapter. The $\mathcal{O}(\delta)$ equation, on the contrary, amounts to

$$\frac{v_\parallel}{Rq}\frac{\partial}{\partial\theta}g^{(1,0)} = 0, \tag{6.9}$$

which leads to

$$g^{(1,0)} = \bar{h}_P^{(1,0)} + \bar{h}_T^{(1,0)}. \tag{6.10}$$

Again, the $\bar{h}^{(1,0)}$ has been split, so as to separate the passing and the trapped contribution. It is worth to stress the fact that the θ-dependent part of $g^{(1,0)}$ vanishes, as a consequence of the new scaling criteria. The $\mathcal{O}(\Delta)$ equation is again the same as in the previous chapter

$$\frac{v_\parallel}{Rq}\frac{\partial}{\partial\theta}g^{(0,1)} = 0. \tag{6.11}$$

Again, for the purposes of the present calculation, it is sufficient to conclude that $g^{(0,1)} = \bar{g}^{(0,1)}$ is θ-independent.

In order to provide an expression for $\bar{h}^{(1,0)}$, it is first mandatory to solve $\mathcal{O}(\delta^2)$ equation, namely

$$\frac{v_\parallel}{Rq}\frac{\partial}{\partial\theta}g^{(2,0)} + \frac{Iv_\parallel}{Rq}\frac{\partial}{\partial\theta}\left(\frac{v_\parallel}{\omega_c}\right)\frac{\partial}{\partial\chi}\bar{g}^{(1,0)} = -\frac{Iv_\parallel}{Rq}\frac{\partial}{\partial\theta}\left(\frac{v_\parallel}{\omega_c}\right)\frac{\partial\phi}{\partial\chi}\frac{q_i F_M}{T} \tag{6.12}$$

which can be integrated over θ, with the result

$$g^{(2,0)} = -I\frac{v_\parallel}{\omega_c}\frac{\partial}{\partial\chi}\left[\frac{q_i\phi}{T}F_M + \bar{g}^{(1,0)}\right] + \bar{h}_P^{(2,0)} + \bar{h}_T^{(2,0)} \tag{6.13}$$

where again the trapped and passing contributions in defining $\bar{h}^{(2,0)}$ have been split. The $\mathcal{O}\left(\Delta\delta^2\right)$ equation, which must be invoked to calculate $\bar{h}^{(1,0)}$, reads

$$
\begin{aligned}
-\omega\frac{\partial}{\partial\xi}\bar{g}^{(1,0)}+\frac{v_\parallel}{Rq}\frac{\partial}{\partial\theta}g^{(2,1)}+k_\parallel v_\parallel\left.\frac{\partial}{\partial\xi}\bar{g}^{(2,0)}\right|_\Omega+\\
c\frac{\mathbf{B}\times\nabla\phi}{B^2}\cdot\nabla\bar{g}^{(1,0)}+\frac{Iv_\parallel}{Rq}\frac{\partial}{\partial\theta}\left(\frac{v_\parallel}{\omega_c}\right)\frac{\partial}{\partial\chi}\bar{g}^{(1,1)}+\\
-m\frac{Iv_\parallel}{Rq}\frac{\partial}{\partial\chi}\left(\frac{v_\parallel}{\omega_c}\right)\frac{\partial}{\partial\xi}\bar{g}^{(1,0)}=m\frac{Iv_\parallel}{Rq}\frac{\partial}{\partial\chi}\left(\frac{v_\parallel}{\omega_c}\right)\frac{\partial\phi}{\partial\xi}\frac{q_iF_M}{T}.
\end{aligned}
\tag{6.14}
$$

The solution in the trapped region of phase space is presented first. Eq.(6.14) is therefore θ-averaged therein (see Eq.(4.67)). Recalling Eq. (6.10) and Eq. (6.13), this yields

$$
\begin{aligned}
-\omega\left\langle\frac{Rq}{\left|v_\parallel\right|}\right\rangle_\theta^T\frac{\partial}{\partial\xi}\bar{h}_T^{(1,0)}-I\left\langle Rqk_\parallel\frac{\partial}{\partial\xi}\left(\frac{\left|v_\parallel\right|}{\omega_c}\frac{\partial}{\partial\chi}\bar{h}_T^{(1,0)}\right)\right|_\Omega\Bigg\rangle_\theta^T+\\
+c\left\langle\frac{Rq}{\left|v_\parallel\right|}\frac{\mathbf{B}\times\nabla\phi}{B^2}\right\rangle_\theta^T\cdot\nabla\bar{h}_T^{(1,0)}-mI\left\langle\frac{\partial}{\partial\chi}\frac{\left|v_\parallel\right|}{\omega_c}\right\rangle_\theta^T\frac{\partial}{\partial\xi}\bar{h}_T^{(1,0)}=\\
mI\left\langle\frac{\partial}{\partial\chi}\frac{\left|v_\parallel\right|}{\omega_c}\right\rangle_\theta^T\frac{\partial\phi}{\partial\xi}\frac{q_iF_M}{T}+I\left\langle Rqk_\parallel\frac{\partial}{\partial\xi}\left[\frac{\left|v_\parallel\right|}{\omega_c}\frac{\partial}{\partial\chi}\left(\frac{q_i\phi}{T}F_M\right)\right]\right|_\Omega\Bigg\rangle_\theta^T.
\end{aligned}
\tag{6.15}
$$

The circumstance

$$
\left\langle\frac{\partial}{\partial\theta}\left(\frac{\left|v_\parallel\right|}{\omega_c}\right)\frac{\partial g^{(1,1)}}{\partial\chi}\right\rangle_\theta^T=0
$$

is employed, since $g^{(1,1)}$ can be supposed to be an even function in θ (for the symmetry of the problem). It has been moreover assumed that $\bar{h}_T^{(2,0)}$ is independent on σ, which is consistent with the bounce point continuity condition.

An analytic solution of Eq. (6.15) is extremely difficult. Nevertheless, it can be simplified by means of physical considerations. First, Eq.(6.15) is

multiplied by the factor

$$\left(\left\langle \frac{Rq}{\left| v_\parallel \right|} \right\rangle_\theta^T \right)^{-1},$$

then the approximation (see Eq.(5.25))

$$\left(\left\langle \frac{1}{\left| v_\parallel \right|} \right\rangle_\theta^T \right)^{-1} \left\langle \left| v_\parallel \right| \right\rangle_\theta^T \approx \left\langle v_\parallel^2 \right\rangle_\theta^T$$

is invoked. Subsequently, noting that

$$I \frac{v_\parallel}{\omega_c} k_\parallel v_\parallel \left. \frac{\partial}{\partial \xi} \right|_\Omega \left(\frac{\partial \phi}{\partial \chi} \right) = -I \frac{v_\parallel}{\omega_c} k_\parallel v_\parallel \frac{4}{W_\chi^2} \frac{\omega q}{mc} \frac{dh}{d\Omega} \left. \frac{\partial \chi}{\partial \xi} \right|_\Omega , \tag{6.16}$$

and recalling

$$k_\parallel \left. \frac{\partial \chi}{\partial \xi} \right|_\Omega = \frac{m}{q} \frac{\partial A_\parallel}{\partial \xi} = \frac{m}{q} \frac{\tilde{\psi}}{R} \sin \xi \tag{6.17}$$

with

$$\tilde{\psi} = \frac{W_\chi^2}{4} \frac{q_s'}{q_s} \tag{6.18}$$

one can conclude that

$$\left\langle I \frac{v_\parallel}{\omega_c} k_\parallel v_\parallel \left. \frac{\partial}{\partial \xi} \right|_\Omega \frac{\partial \phi}{\partial \chi} \right\rangle_\theta^T = \frac{m}{q} \left\langle \frac{q \hat{s} v_\parallel^2}{r^2 \omega_c} \right\rangle_\theta^T \frac{\partial \phi}{\partial \xi} = \frac{m}{q} \omega_{\hat{s}} \frac{\partial \phi}{\partial \xi}, \tag{6.19}$$

where $\omega_{\hat{s}}$ is the toroidal precession frequency due to magnetic shear, Eq.(5.29). In analogy with ω_D, the symbol $\omega_{\hat{s}}$ will be hereafter referred to the θ-averaged value. Recollecting also the relationship between the poloidal component of the magnetic drifts and the toroidal precession frequency ω_D (see Eq.(6.3)), and focusing on the dynamics along the island (the radial component of the $\mathbf{E} \times \mathbf{B}$ drift, which goes to zero faster with χ than the other terms, will be shown later to be important only to unlock resonating particles), it is possible to write Eq. (6.15) in the more perspicuous form:

$$\left[-\omega - \frac{m}{q} \omega_E - \frac{m}{q} \omega_{\mathrm{tp}} \right] \frac{\partial \bar{h}_T^{(1,0)}}{\partial \xi} = \frac{m}{q} \omega_{\mathrm{tp}} \frac{q_i F_M}{T} \frac{\partial \phi}{\partial \xi}. \tag{6.20}$$

The relation between the poloidal component of the $\mathbf{E} \times \mathbf{B}$-drift and the toroidal precession ω_E (see Eq.(2.44)) can be easily proved following the same derivation path as for Eq.(6.3). The frequency $\omega_{\rm tp} = \omega_D + \omega_{\hat{s}}$ has been introduced as in chapter 5, see Eq.(5.30). Recall that it refers to a θ-averaged value.

Eq. (6.20) can be integrated with the condition $\bar{h}_T^{(1,0)} \to 0$ for $\chi \to \infty$. For the sake of simplicity, the dependence of ω_E on ξ is neglected, so that the only quantity depending on ξ is the electrostatic potential. This assumption is justified by the fact that ω_E is typically smaller than $\omega_{\rm tp}$ in the frequency range under investigation. The final result is

$$\bar{h}_T^{(1,0)} = -\frac{m}{q} \frac{\omega_{\rm tp}}{\omega + \frac{m}{q}\omega_E + \frac{m}{q}\omega_{\rm tp}} \frac{q_i \phi}{T} F_M. \tag{6.21}$$

Note that in this case the χ part of the potential plays the role of an integration constant. In analogy with chapter 4 (in particular see Eq.(4.71)), the perturbed distribution exhibits a resonant denominator, which involves both the island rotation and the relevant timescales of the particle dynamics. A detailed physical discussion will be presented in section 6.3.

Eq. (6.14) is now solved it in the passing region of phase space. The fundamental difference with respect to the trapped particles is that, for passing ones,

$$\left\langle \frac{\partial}{\partial \chi} \left(\frac{v_\parallel}{\omega_c} \right) \right\rangle_\theta = \mathcal{O}\left(\epsilon^2\right),$$

so the term on the right-hand side of Eq. (6.14) is negligible. Such equation becomes then

$$-\omega \frac{\partial}{\partial \xi} \bar{h}_P^{(1,0)} - \left\langle Rqk_\parallel \frac{\partial}{\partial \xi} g^{(2,0)} \right|_\Omega \Bigg\rangle_\theta + c \frac{\mathbf{B} \times \nabla \phi}{B^2} \cdot \nabla \bar{h}_P^{(1,0)} = 0. \tag{6.22}$$

It is consistent to choose

$$\bar{h}_P^{(1,0)} = 0,$$

since such solution is in agreement with the fact that, in this frequency range, the contribution of the passing particles to the perpendicular current is negligible, see Fig.6.2. This leads to

$$\left\langle Rqk_{\parallel} \frac{\partial}{\partial \xi} g^{(2,0)} \right|_{\Omega} \Big\rangle_{\theta} = 0 \tag{6.23}$$

which in view of Eq. (6.13) implies

$$\bar{h}_P^{(2,0)} = \left\langle I \frac{v_{\parallel}}{\omega_c} \frac{\partial}{\partial \chi} \frac{q_i \phi}{T} F_M \right\rangle_{\theta}. \tag{6.24}$$

Inserting Eq. (6.24) into Eq. (6.13), it is manifest that such a result is linked to the cancellation of the polarization current in the passing region of the phase space [26] discussed in chapter 4, which characterises the low-collisionality regime discussed in this thesis. Within the ordering employed in this chapter, such contribution still exists, but it pertains to a higher order because of the ordering adopted here for the island propagation frequency, which implies that all the purely electric effects (see Eq. (4.38)) become less important.

6.1.3 The Perturbed Perpendicular Current

In this subsection, an estimate of the perpendicular current generated by the perturbed distribution $\bar{h}_T^{(1,0)}$ is presented. Although what ultimately matters for the stability of the magnetic island is the closure parallel current, the perpendicular contribution is important in the frame of the present work in order to allow a comparison between the numerical simulations and the analytical derivation.

The perpendicular current can be effectively estimated as

$$\mathbf{J}_{\perp} \sim q_i \delta f \mathbf{v}_{\perp}, \tag{6.25}$$

where δf is the perturbation on the distribution, $\mathbf{v}_\perp$ is the velocity perpendicular to the perturbed magnetic surfaces, and again the contribution of electrons has been neglected. The velocity $\mathbf{v}_\perp$ is related to the total derivative of the Ω coordinate with respect to time, i.e. $\mathrm{d}\Omega/\mathrm{d}t$. Noticing that $\nabla_\parallel \Omega = 0$, one can write

$$\frac{\mathrm{d}\Omega}{\mathrm{d}t} = \frac{\partial \Omega}{\partial t} + \mathbf{v} \cdot \nabla \Omega = \frac{\partial \Omega}{\partial t} + (\mathbf{v}_{\mathbf{E}\times\mathbf{B}} + \mathbf{v}_{\mathbf{D}}) \cdot \nabla \Omega. \tag{6.26}$$

Considering Eq. (4.38), and recalling that

$$\frac{\partial}{\partial t} = -\omega \frac{\partial}{\partial \xi},$$

it follows that

$$\frac{\partial \Omega}{\partial t} + \mathbf{v}_{\mathbf{E}\times\mathbf{B}} \cdot \nabla \Omega = 0.$$

This fact has already been mentioned in the previous chapter. Since only the θ-averaged perturbed current is considered, Eq.(6.26) can be recast as

$$\frac{\mathrm{d}\Omega}{\mathrm{d}t} = -\frac{m}{q}\omega_D \sin\xi. \tag{6.27}$$

In fact, the radial component of the magnetic drift θ-averages to zero even in the trapped region of phase space. *Hence, the toroidal precession in this frequency regime is the main mechanism which allows a particle to cross magnetic surfaces. This is a fundamental difference with passing particles as for the latter this contribution averages to* $\mathcal{O}(\epsilon^2)$, *and it is therefore negligible.*

In view of Eq. (6.27), the expression for the θ-averaged current crossing the perturbed magnetic surface in presence of a slowly rotating NTM as a function of v reads:

$$J_\perp(v) = q_i \left\langle g^{(1,0)} \frac{\mathrm{d}\Omega}{\mathrm{d}t} \frac{1}{|\nabla\Omega|} \right\rangle_\theta = \frac{m^2}{q^2} \frac{q_i^2 \phi}{T} \frac{\omega_D \omega_{\mathrm{tp}}}{\omega + \frac{m}{q}\omega_{\mathrm{tp}} + \frac{m}{q}\omega_E} \frac{1}{|\nabla\Omega|} F_M \sin\xi, \tag{6.28}$$

having estimated with $\mathrm{d}\Omega/\mathrm{d}t \cdot 1/|\nabla\Omega|$ the velocity component perpendicular to the perturbed magnetic surface. This expression for the perpendicular current at low rotation frequencies is confirmed by numerical simulations, as discussed in detail in section 6.3.

6.1.4 The Perturbed Parallel Current

As previously remarked, in order to evaluate explicitly the effect of the current found in the previous subsections (Eq.(6.28)) on the NTM stabilization, the closure parallel current has to be determined. In principle, this result can be easily attained, once the perpendicular current is known, by means of the quasi neutrality constraint (Eq.(1.3)). Nevertheless, such calculation cannot be brought to end with the expression of perpendicular current in Eq.(6.28), since the resonant denominator in $\bar{h}_T^{(1,0)}$ (see Eq. (6.21)) leads to a divergence of the integral over velocity space.

In order to smooth the resonance, a model collision operator is introduced in the drift-kinetic equation (this approach is discussed in section 6.3.2). As for the present treatment the details of the collision processes are unimportant, a simple Krook collision operator [43] ($\partial f/\partial t|_{coll} = -\nu\,(f - F_M)$, where $(f - F_M) = \bar{h}_T^{(1,0)}$ and $\nu = \nu_0 v_{\rm th}^3/v^3$) is chosen. Eq. (6.20) reads therefore

$$\left[-\omega - \frac{m}{q}\omega_{\rm tp} - \frac{m}{q}\omega_E\right]\frac{\partial \bar{h}_T^{(1,0)}}{\partial \xi} = \frac{m}{q}\omega_{\rm tp}\frac{q_i F_M}{T}\frac{\partial \phi}{\partial \xi} - \nu \bar{h}_T^{(1,0)}, \tag{6.29}$$

Again, the ξ dependence of ω_E is neglected for the sake of simplicity. Denoting

$$\bar{\omega} = \omega + \frac{m}{q}\omega_{\rm tp} + \frac{m}{q}\omega_E \qquad \bar{F} = \frac{m}{q}\omega_{\rm tp}\frac{q_i F_M}{T}$$

and expanding the island potential into its Fourier components

$$\phi = \sum_{k=0}^{\infty} \hat{\phi}_k\,(\chi)\cos\,(k\xi)$$

a solution to Eq. (6.29) is found in the form

$$\bar{h}_T^{(1,0)} = -\bar{\omega}\bar{F}\sum_{k=0}^{\infty}\frac{k^2\hat{\phi}_k\,(\chi)}{\bar{\omega}^2k^2+\nu^2}e^{\nu/\bar{\omega}\cdot\xi} - e^{\nu/\bar{\omega}\cdot\xi}\frac{\bar{F}}{\bar{\omega}}\int_0^{\xi}{\rm d}\xi' e^{-\nu/\bar{\omega}\cdot\xi'}\frac{\partial\phi}{\partial\xi'}, \tag{6.30}$$

using as a boundary condition the fact that the solution must be finite for $\bar{\omega} \to 0$.

At this point, the quasi-neutrality condition $\nabla \cdot \mathbf{J} = 0$, can be invoked. The equation is the same as the one used for the θ-averaged polarization current (see Eq.(4.80)), namely

$$k_\parallel \left.\frac{\partial J_\parallel}{\partial \xi}\right|_\Omega = -q_i \left\langle \int \mathrm{d}^3 v \mathbf{v}_D \cdot \nabla g \right\rangle_\theta , \tag{6.31}$$

where again only the ion contribution to the perpendicular current has been considered. The average over θ is easily computed, as the lowest-order perturbed distribution is independent on θ. Thus

$$k_\parallel \left.\frac{\partial J_\parallel}{\partial \xi}\right|_\Omega = m q_i \left\langle \int \mathrm{d}^3 v \frac{I v_\parallel}{Rq} \frac{\partial}{\partial \chi} \left(\frac{v_\parallel}{\omega_c}\right) \frac{\partial \bar{h}_T^{(1,0)}}{\partial \xi} \right\rangle_\theta \approx n q_i \int \mathrm{d}^3 v \; \omega_D \frac{\partial \bar{h}_T^{(1,0)}}{\partial \xi}, \tag{6.32}$$

where the estimate $m/q \approx n$ has been performed. The approximations leading to the appearance of ω_D in the last step have been discussed previously. Note that the radial component of the magnetic drift θ-averages to zero even in the trapped region of the phase space. Exploiting Eq. (6.30), one obtains after some algebra

$$\frac{\partial \bar{h}_T^{(1,0)}}{\partial \xi} = \bar{F} \sum_{k=0}^{\infty} k^2 \hat{\phi}_k \frac{\bar{\omega} k \sin(k\xi) - \nu \cos(k\xi)}{\bar{\omega}^2 k^2 + \nu^2}. \tag{6.33}$$

The cosine terms in Eq. (6.33) are neglected, because they are related to out-of-phase current contributions which are not involved in the island stabilization [14], and thus they are not considered in the present analysis. With such approximation

$$\frac{\partial \bar{h}_T^{(1,0)}}{\partial \xi} = \bar{F} \sum_{k=0}^{\infty} \hat{\phi}_k \frac{\bar{\omega} k \sin(k\xi)}{\bar{\omega}^2 + \nu^2/k^2} = -\frac{\bar{\omega} \bar{F}}{\bar{\omega}^2 + \nu_{\mathrm{eff}}^2} \frac{\partial \phi}{\partial \xi}, \tag{6.34}$$

where the effective collision frequency ν_{eff} is implicitely defined by this equation.

Going back to Eq. (6.32), with the help of the pitch-angle variables (v, λ), see Eq.(4.15), and writing for simplicity

$$\omega_{\mathrm{tp}} \sim \omega_D \sim \left\langle \frac{q v^2}{2 r R \omega_c} \right\rangle_\theta^T \tag{6.35}$$

(which relies on the fact that in the trapped region of phase space $v \approx v_\perp \gg v_\parallel$, cf. Eq.(2.43) and Eq.(2.47)), one obtains

$$J_\parallel = -n_0 \frac{4}{\sqrt{\pi} k_\parallel} \sqrt{\epsilon} n^2 \frac{q_i^2}{T} \left(\omega_{\rm tp}^0\right)^2 \frac{q}{mc} \frac{{\rm d}h}{{\rm d}\Omega} K_1(\omega) \left[\cos(\xi) - \langle \cos(\xi) \rangle_\Omega\right], \quad (6.36)$$

where

$$K_1(\omega) = \int_0^\infty {\rm d}y y^{12} \frac{\omega e^{-y^2} \left(\omega + n\omega_E + n\omega_{\rm tp}^0 y^2\right)}{\left(\omega + n\omega_E + n\omega_{\rm tp}^0 y^2\right)^2 y^6 + \left(\nu_{\rm eff}^0\right)^2},$$

having defined $y = v/v_{\rm th}$ and $\omega_{\rm tp} = \omega_{\rm tp}^0 y^2$, $\nu_{\rm eff} = \nu_{\rm eff}^0/y^3$. The parameter $K_1(\omega)$ can be computed if all the plasma parameters are known, and it is the only factor in Eq.(6.36) which depends on the island rotation frequency ω. The integration has been performed within the condition that this parallel current vanishes when flux-surface averaged, as already supposed for the polarization current (see Eq.(4.102)). From here on, this perturbed current will be named *precessional current*, and it will be indicated it as $J_\parallel^{\rm Pr}$.

6.2 Effects on the Island Stabilization

The contribution of the precessional current on the stability of the neoclassical tearing mode is evaluated by means of the Ampére's law in the form discussed in chapter 3 for a large-aspect ratio tokamak (Eq.(3.17)), namely

$$\sum_\pm \int_{-1}^\infty {\rm d}\Omega \oint {\rm d}\xi \frac{J_\parallel^{\rm Pr} \cos(\xi)}{\sqrt{\Omega + \cos(\xi)}} = \frac{c}{8\sqrt{2}} \Delta'_{\rm Pr} \frac{wB}{Rq}, \quad (6.37)$$

where $\Delta'_{\rm Pr}$ represents the analogue of Δ' due to the precessional current. Here, the sum is defined over the $\chi > \chi_s$ and $\chi < \chi_s$ regions (recall that $h(\Omega)$ is defined to be odd in $(\chi - \chi_s)$, see Eq.(4.39)). This yields, after tedious but straightforward algebra

$$\Delta'_{\rm Pr} = \frac{32 n_0}{\sqrt{2\pi} wB} \sqrt{\epsilon} n^2 \frac{q_i^2}{T} \left(\omega_{\rm tp}^0\right)^2 \frac{q}{m^2 c^2} \frac{q_s}{q'_s} R^2 q^2 K_1(\omega) K_2, \quad (6.38)$$

where K_2 is a numerical constant defined as

$$K_2 = \int_1^\infty \frac{\mathrm{d}\Omega}{\sqrt{\Omega}} \oint \mathrm{d}\xi \frac{\cos^2(\xi) - \cos(\xi) \langle \cos(\xi) \rangle_\Omega}{\Omega + \cos(\xi)}$$

The numerical evaluation provides $K_2 \simeq -6.65$. The sign of Δ'_{Pr} depends therefore only on the sign of $K_1(\omega)$. Recall that positive values of Δ' correspond to destabilizing effects (Eq.(3.17)). *Thus, the contribution of the precessional current is stabilizing if* $\omega > 0$ *and, if* $\omega < 0$*, for* $|\omega|$ *sufficiently larger than* ω_{tp}.

6.2.1 Comparison with the Polarization Current

In order to understand under which circumstances the "standard" polarization current prevails on the precessional current, a comparison between such contributions is performed. For the parallel current which closes the polarization current, the $\omega \gg k_\parallel v_\parallel$ case is anyway considered, since the contribution of $k_\parallel v_\parallel$ terms is negligible, as shown in the previous chapter. As the two currents are defined in the trapped space, $\bar{h}_P$ functions are not considered. Using the identity Eq. (6.17), the polarization current, indicated with the superscript Pol for convenience, reads

$$k_\parallel \left. \frac{\partial J_\parallel^{\mathrm{Pol}}}{\partial \xi} \right|_\Omega = -\frac{q_i I^2}{\omega_c^2} \frac{\omega^2 q}{mc} \frac{dh}{d\Omega} \frac{8}{W_\chi^2} \int \mathrm{d}^3 v v_\parallel^2 \frac{\partial}{\partial \chi} \left(\frac{dh}{d\Omega} \right) \frac{q_i F_M}{T} \sin \xi, \tag{6.39}$$

while (see Eq.(6.21) and Eq.(6.32))

$$\begin{aligned} k_\parallel \left. \frac{\partial J_\parallel^{\mathrm{Pr}}}{\partial \xi} \right|_\Omega \approx n q_i \int \mathrm{d}^3 v \, \omega_D \frac{\partial \bar{h}_T^{(1,0)}}{\partial \xi} \approx \\ -n q_i \int \mathrm{d}^3 v \frac{m}{q} \frac{\omega_{\mathrm{tp}}}{\omega + \frac{m}{q}\omega_E + \frac{m}{q}\omega_{\mathrm{tp}}} \frac{q_i}{T} F_M \frac{\partial \phi}{\partial \xi}. \end{aligned} \tag{6.40}$$

The comparison between $J_\parallel^{\mathrm{Pr}}$ and $J_\parallel^{\mathrm{Pol}}$ can be carried out by equating the integrands of Eq.(6.39) and Eq.(6.40). Therefore, the two contribution are of the same order if

$$\frac{I}{\omega_c^2} \omega \frac{1}{W_\chi^2} \frac{\partial}{\partial \chi} \frac{dh}{d\Omega} \sim \frac{m}{Rq} \frac{\partial}{\partial \chi} \left(\frac{v_\parallel}{\omega_c} \right) \frac{n\omega_{\mathrm{tp}}}{\omega + n\omega_{\mathrm{tp}}}, \tag{6.41}$$

where ω_E in Eq.(6.32) has been discarded for the sake of simplicity. Since the evaluation is performed in the island region, i.e. supposing $(\chi - \chi_s) \sim W_\chi$, the derivative in χ of $\mathrm{d}h/\mathrm{d}\Omega$ is $\mathcal{O}(1)$. According to the estimate

$$\frac{\partial}{\partial \chi}\left(\frac{v_\parallel}{\omega_c}\right) \approx \frac{Rq\omega_{\mathrm{tp}}}{Iv_\parallel}, \tag{6.42}$$

Eq. (6.41) becomes

$$\frac{I^2}{\omega_c^2}\omega\frac{v_\parallel^2}{W_\chi^2} \sim \frac{n^2\omega_{\mathrm{tp}}^2}{\omega}, \tag{6.43}$$

having assumed $\omega > \omega_{\mathrm{tp}}$, which represents a reasonable assumption in the frequency range where $J_\parallel^{\mathrm{Pol}}$ and $J_\parallel^{\mathrm{Pr}}$ coexist. The estimate $v_\parallel \sim \sqrt{\epsilon}v_{\mathrm{th}}$ is introduced, as both contribution are defined in the trapped region of phase space, see chapter 2. Recalling that the ion banana width ρ_b can be calculated as $\rho_b = \sqrt{\epsilon}\rho_\theta$, it is possible to conclude that the polarization current is comparable with the precessional current if

$$\frac{n\omega_{\mathrm{tp}}}{\omega} \sim \frac{\rho_b}{w}. \tag{6.44}$$

The ratio on the right-hand side of Eq. (6.44) is assumed to be small in the present calculation, cf. Eq. (4.44), so that the assumption that the ratio on the left-hand side of Eq.(6.44) is of the same order of magnitude is absolutely realistic, and therefore the precessional current is expected to compete with the polarization current in determining the stability of the magnetic island.

6.3 Discussion of the Results

6.3.1 The Interplay of Toroidal Precessions

In this section, all the relevant aspects of the physics which emerges from the calculations presented above are discussed, in order to provide a clear picture of the underlying phenomena. Numerical simulations performed with the HAGIS code are displayed to support the analytic results.

It can be seen from Eq.(6.21) that for positive frequencies no particle can be resonant with the NTM (recall that $\omega_{\rm tp}$ is always positive in the present notation). Thus, in that case the perpendicular current Eq.(6.28) is a smooth function of v. On the other hand, if the frequency is negative, the perturbed current exhibits a resonant behaviour around the region of phase space where $\omega \approx n\omega_{\rm tp}$ (remember also that $\omega_{\rm tp}$ is proportional to v^2), and changes sign around this critical value of velocity, as depicted in Fig.6.3. The physical

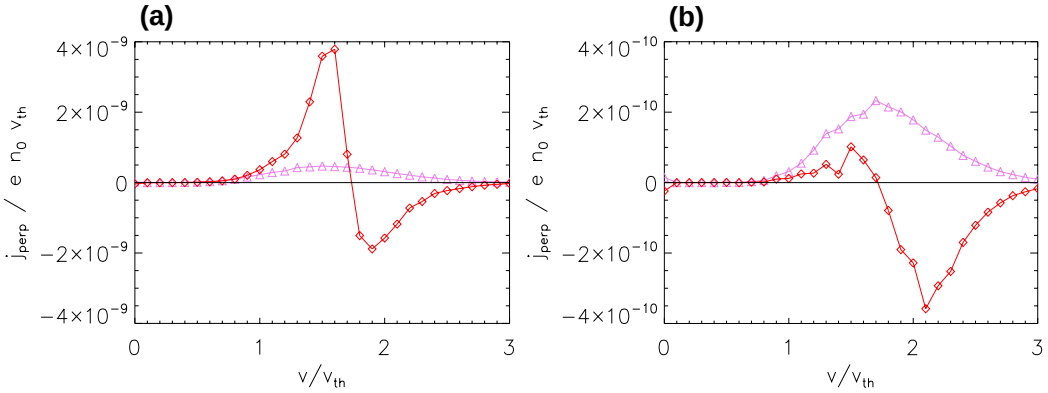

Figure 6.3: Perpendicular current as a function of velocity, calculated at $r/a \approx 0.34$ (i.e. outside the magnetic island towards the magnetic axis) for $\omega = 300$ rad/s (triangles) and for $\omega = -300$ rad/s (diamonds) in the collisionless regime (a) and in a standard banana collisional regime (b) for the "upper"-half of the island (i.e. $\xi > 0$) . Note the different scale on the y-axis.

explanation is the following : for positive frequencies, the magnetic island is moving towards $-\nabla\zeta$-direction, while both electric and magnetic toroidal drifts point in the $\nabla\zeta$-direction. Supposing to build a frame of reference which moves in the toroidal direction together with the island (from here on: IFR, island frame of reference), all trapped particles would appear to travel in the $\nabla\zeta$-direction. The toroidal component of the electric field E_ζ varies sinusoidally along the island, see Eq. (4.38). So in regions where it points in the $\nabla\zeta$-direction, all particles tend to increase their kinetic energy and finally their magnetic precession frequency, while they slow down in the opposite case. This means that between O-X points and between X-O points,

all trapped particles either accelerate or decelerate, depending on the sign of E_ζ (they accelerate for $E_\zeta > 0$ and decelerate for $E_\zeta < 0$, respectively). Where they decelerate, they tend to accumulate, so that the local density increases. On the contrary, they tend to disperse as they accelerate, so that the local density decreases.

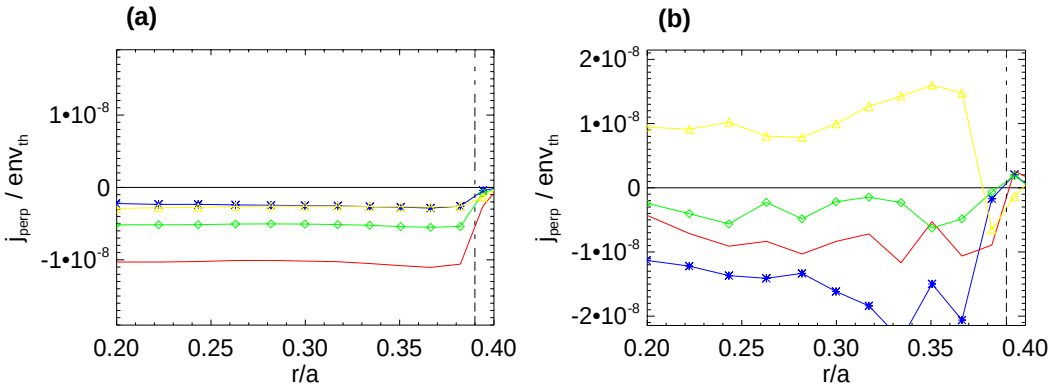

Figure 6.4: Current on the X-point helical cell (triangles), on the O-point cell (stars), on the intermediate cell (diamonds) and their sum (solid) for a) $\omega = 300\ rad/s$ and b) $\omega = -300\ rad/s$.

This picture is different if $\omega < 0$. In this case the island is propagating in the same direction as the particles ($\nabla\zeta$-direction), so *in the IFR* there are particles moving in the $\nabla\zeta$ direction (if $|\omega| < \omega_{\rm tp}$, high-energy particles) and in the $-\nabla\zeta$ direction (if $|\omega| > \omega_{\rm tp}$, low-energy particles). Therefore, when for example E_ζ points in the $-\nabla\zeta$-direction, again all particles decrease their magnetic precession frequency. The behaviour of more energetic particles is the same as the one described before. But slower particles, if decelerated in the laboratory frame, *actually increase their relative speed with respect to the island, so the effect is an acceleration in the* IFR. In other words, where slower particles accumulate, faster particle disperse and viceversa, and this explains why the perturbation changes sing around $\omega_{\rm tp} \sim |\omega|$.

Another mechanism complicates the picture given above in the case $\omega < 0$.

The electric toroidal precession ω_E acts in this case in the opposite direction with respect to the magnetic drifts. So, moving from O-point (where the radial electric field is maximum, in absolute value) to X-point (where the radial electric field is the lowest in absolute value) *the number of particles which overtake the island or are overtaken by it in* IFR *can change* (cf. Eq. (6.21)). The variation of ω_E with ξ is such that the integral of $J_\perp$ over velocity space can change its sign depending on where with respect to the island the integration is carried out. This especially happens if $|\omega| \sim \omega_{\rm tp}\,(v_{\rm th})$, because in that region of phase space lies a large number of particles, so even a small shift of the resonant point means turning a large number of faster particles into slower or *vice versa* (cf. Fig.6.3a). This physical picture is confirmed by comparing Fig.6.4a and Fig.6.4b. In this case, it is possible to identify the change of sign of the current going from O-point to X-point, as indeed $|\omega| \approx \omega_{\rm tp}\,(v_{\rm th})$. It is important to stress that resonance conditions are highly local, so after a while a resonant particle will be able to unlock from the island, for example through the radial component of the $\mathbf{E} \times \mathbf{B}$ drift, or through collisions, as discussed below. The changes of sign in the perturbed distribution function determine the stabilizing or destabilizing effect of these currents. The precessional current is found to be stabilizing for $\omega > 0$ and, if $\omega < 0$, for $|\omega|$ sufficiently larger than $\omega_{\rm tp}$. It is known that polarization current is globally *destabilizing*, if equilibrium pressure gradient effects are neglected, because of the "current spike" at the island separatrix [37], without which it would be stabilizing. The precessional current described here acts therefore against the polarization current. *The result that precessional effects can compete with the neoclassical polarization and that trapped-particle resonances have a major impact on this effect demonstrates that a kinetic approach is mandatory in view of a exhaustive theory of NTMs in toroidal plasmas* [44].

There are some strong analogies between the behaviour of the trapped and passing particles as their motion along the island starts to be comparable

with the rotation of the island itself (i.e. the case $\omega \sim \omega_D$ and $\omega \sim k_\parallel v_\parallel$, respectively).

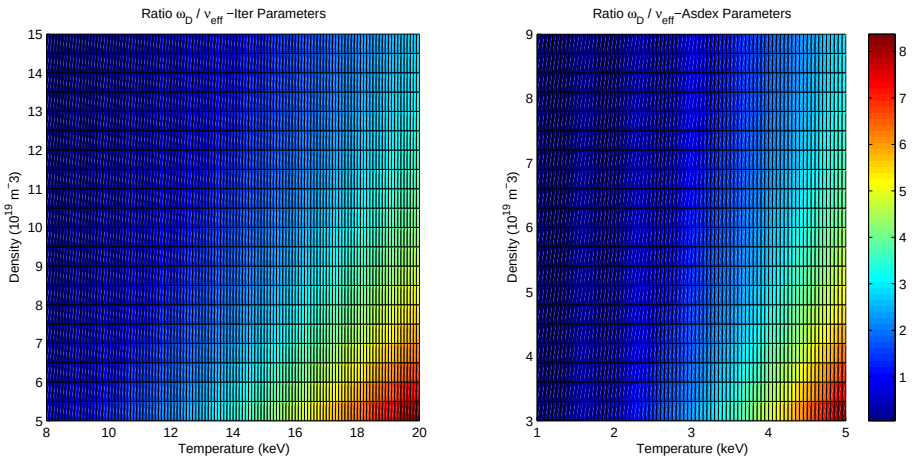

Figure 6.5: Ratio between ω_D (calculated for $v = v_{\rm th}$) and the collisional detrapping frequency ν/ϵ for a wide range of ion density and temperature, for ITER machine parameters ($T_e = 10$ keV, $R = 620$ cm, $B = 5.3$ T, $\epsilon = 0.33$) and ASDEX Upgrade machine parameters ($T_e = 2$ keV, $R = 165$ cm, $B = 2.5$ T, $\epsilon = 0.33$). The collisional frequency has been evaluated following Ref.[1].

In both cases, the lowest-order perturbed distribution function exhibits a resonant denominator (Eq. (4.71) and (6.21)), which underlines the fact that the interaction between the particles and the mode (and the subsequent modification of the distribution function) is stronger if the particle and the island have a small relative motion. Indeed, this result is not surprising for most wave-particle interactions. Nevertheless, significant differences occur while focusing on the corresponding perturbed current. Trapped particles have a net θ-averaged velocity perpendicular to the perturbed magnetic surfaces just because of their equilibrium drifts (see Eq. (6.27)), so that every perturbation on the distribution immediately leads to a perturbed current, namely

$$\delta J_\perp \propto q_i \left\langle \delta f \mathbf{v}_D \cdot \nabla \Omega \right\rangle_\theta .$$

This is not the case for passing particles, as their θ-averaged equilibrium drift across the perturbed flux-surface is much smaller. For resonating particles, in particular, the advection is such that it nearly cancels the contribution of the perturbed distribution function to the current, as shown in the previous chapter.

6.3.2 The Role of Collisions

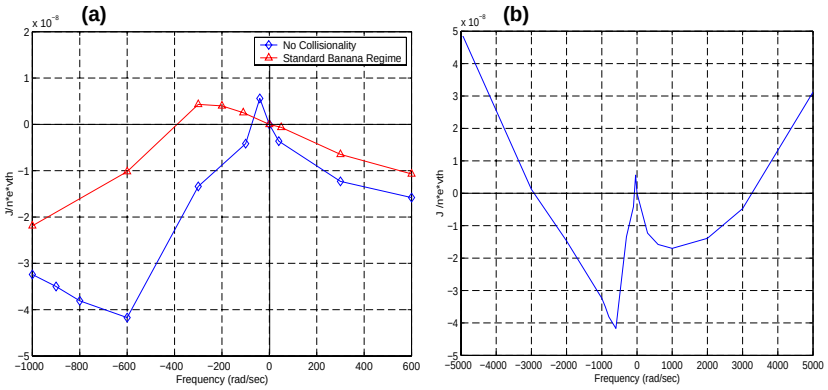

Figure 6.6: a) Comparison between the perpendicular current integrated in the velocity space versus island propagation frequency in non collisional regime (diamonds) and in standard banana regime (triangles).b) Perpendicular current integrated in the velocity space versus island propagation frequency in the non-collisional regime showing the transition to the standard polarization current (proportional to ω^2) at high frequencies.

For the trapped-particle resonance under consideration, the physical effect that resolves the singularity in Eq.(6.28) is represented by collisions, even for the low-collisionality regime discussed in this paper. For a realistic tokamak scenario, the frequency on which trapped particles can be scattered into the passing domain is comparable or higher than the toroidal precession of thermal ions. Fig.6.5 illustrates the ratio between the toroidal precession frequency and the collisional detrapping frequency (which corresponds to ν/ϵ [16]) for a wide range of experimental parameters for the tokamaks ITER

[45] and ASDEX Upgrade [46], corroborating the previous statement. Such occurrence clearly reflects on the perturbed currents. Fig.6.3b is obtained in the standard banana regime (i.e. the collisional detrapping is slower than the bounce frequency, so that the banana orbits can exist for a reasonably long time [16]), while in Fig.6.3a the collision frequency is reduced by five orders of magnitude (this may be named a "collisionless" regime). It is manifest from the comparison of the two pictures that collisions drastically reduce the peaks of $J_\perp(v)$ around the resonance, this effect being more pronounced for slower particles, as can be expected. As a consequence of this last fact, in particular, the sign of the total perpendicular current density (i. e. of the integral of $J_\perp(v)$ over v) can change depending on the collision frequency, as shown in Fig.6.6a. The sign of the perpendicular current is of course crucial for the determination of the stabilizing or destabilizing nature of the perturbed parallel current.

6.3.3 The Deviation from Parabolic Dependence

Referring to Fig.6.1, which corresponds to Fig.6.6b , all the changes of sign of $J_\perp$ as a function of ω, going from right to left, can be discussed. For positive island frequencies, a change of sign is experienced when the precessional current starts to exceed the standard polarization current. The sign reversal at ω=0 is due to the fact that the electric potential goes through zero and changes sign across that value (cf. Eq. (4.38) and Eq. (6.21)). As a matter of fact, for extremely small negative values of ω, the situation more or less corresponds to the one which occurs for small positive values of ω, as almost all particles are faster than the island. So the sign reversal is due to a sign reversal in the electric field. As ω grows, the fraction of slower particles gets larger, and this leads to the third change of sign. Collisions contribute to determining the position of this third reversal, since they determine how the singularity in Eq. (6.28) is resolved. Finally, for large negative values of ω the polarization current prevails again.

Chapter 7

Gyrokinetic Investigation of Magnetic Islands

The natural evolution of the description presented in the previous chapters consists in an enhancement of the self-consistency of the model, in order to achieve an increasing generality in the representation of the island dynamics. In this final chapter, the problem of the inclusion of a magnetic island in a gyrokinetic flux-tube spectral code is tackled. The model discussed below has been implemented in the code GKW [47], a gyrokinetic code developed by A. G. Peeters and co-workers to the University of Warwick, United Kingdom. First results obtained by means of GKW simulations including a magnetic island are reported.

7.1 The Gyrokinetic Equation

The gyrokinetic equation is a simplified form of the kinetic equation. In analogy with the drift-kinetic equation, derived in chapter 4, the gyrokinetic equation is averaged on the gyromotion of particles, and it is therefore defined on a 5-dimensional phase space. The peculiarity of the gyrokinetic equation consists in retaining the effects of the variation of the fields on the Larmor-radius scale. Roughly speaking, according to the drift-kinetic

approach, particles are described as charged "points", whose position corresponds to that of their guiding centre, where the fields affecting their motion are evaluated. On the contrary, the gyrokinetic approach describes particles as charged "rings", whose motion is determined by means of the "average" fields on the ring itself.

There is a number of methods [48, 49, 50, 51] to derive the gyrokinetic set of equations (i.e. the gyrokinetic equation plus the equations for the fields, needed in order to achieve a self-consistent description of the phenomena), most of which mainly based on the work of Littlejohn [7, 52, 53]. The code GKW contains such system in the form presented in Ref.[54, 55, 56], which also relies on the Hamiltonian techniques described in Littlejohn's work. The derivation of the self-consistent gyrokinetic field theory is rather complicated. Here, only the most relevant aspects are outlined. The interested reader is referred to the papers quoted above for details (see also the excellent review by Brizard and Hahm [57]). Starting point of the derivation is the variational principle [58]:

$$\delta I \doteq \delta \int_{t_1}^{t_2} L \mathrm{d}t = 0, \tag{7.1}$$

where I represents the action integral and L the total Lagrangian,

$$L \doteq L_p + L_f \tag{7.2}$$

in turn composed by a particle component L_p (defined by means of the single-particle Lagrangian L_{sp})

$$\begin{aligned} L_p = \int \mathrm{d}^3\mathbf{x}_0 \int \mathrm{d}^3\mathbf{v}_0 f\left(\mathbf{x}_0, \mathbf{v}_0, t_0\right) \times \\ L_{sp}\left[\mathbf{x}_{sp}\left(\mathbf{x}_0, \mathbf{v}_0, t_0; t\right), \mathbf{v}_{sp}\left(\mathbf{x}_0, \mathbf{v}_0, t_0; t\right), \dot{\mathbf{x}}_{sp}\left(\mathbf{x}_0, \mathbf{v}_0, t_0; t\right)\right] \end{aligned} \tag{7.3}$$

with

$$\begin{aligned} L_{sp}\left(\mathbf{x}_{sp}, \mathbf{v}_{sp}, \dot{\mathbf{x}}_{sp}\right) = \left(m_{sp}\mathbf{v}_{sp} + \frac{q_{sp}}{c}\mathbf{A}\left(\mathbf{x}_{sp}, t\right)\right) \cdot \dot{\mathbf{x}}_{sp} + \\ - \left(\frac{1}{2} m_{sp} \left|\mathbf{v}_{sp}\right|^2 + q_{sp}\phi\left(\mathbf{x}_{sp}, t\right)\right) \doteq \mathbf{p}_{sp} \cdot \dot{\mathbf{x}}_{sp} - H_{sp}, \end{aligned} \tag{7.4}$$

plus a field component L_f

$$L_f = \frac{1}{8\pi}\int \mathrm{d}\mathbf{x}\left(\left|\nabla\phi\left(\mathbf{x},t\right)\right|^2 - \left|\nabla\times\mathbf{A}\left(\mathbf{x},t\right)\right|^2 + \frac{2}{c}\lambda\left(\mathbf{x},t\right)\nabla\cdot\mathbf{A}\left(\mathbf{x},t\right)\right). \tag{7.5}$$

Here, the subscript 0 denotes the initial conditions of the system, H_{sp} indicates the Hamiltonian and $\lambda\left(\mathbf{x},t\right)$ indicates the Lagrange multiplier. Note that this form of the Lagrangian for the fields is different from the one found in standard text books (see for example [59]). In fact, the term in $\partial\mathbf{A}/\partial t$, which is connected to the displacement current, has been neglected, as typically done for most of the problems concerning plasma confinement. This is due to the fact that the relevant physics mainly occurs on slower timescales than the ones related to such term, or in other words waves travelling at the speed of light are not accounted for.

As discussed in chapter 2, in presence of a strong magnetic field, the motion of a charged particle is not isotropic: it gyrates around the field lines whereas it is free to move along them. The scale of the gyration, for typical tokamak parameters, is much shorter than the scale of variation of the magnetic field. This allows to perform a series expansion, introducing the small parameter δ

$$\delta = \frac{\rho_L}{L_B}, \tag{7.6}$$

in complete analogy with the calculation exposed in chapter 2 (cf. Eq.(2.11)). The most systematic approach for carrying out a coordinate transformation which conveniently separates the gyration motion from the drifts to all orders in δ involves the Lie transform technique [60]. Such transformations offer many advantages. In particular

- They allow an expansion of the Euler-Lagrange equations in the small parameter $\delta = \rho_L/L_B$ *leaving unaltered the Hamiltonian conservation properties*. In other words, Lie transforms allow to build a set of dynamical equations which has an exact Hamiltonian structure, retaining

therefore all the desirable conservation properties of the Euler-Lagrange system, but at the same time accurate up to the desired order in δ.

- The expansion can be straightforwardly extended to any order in δ.

The coordinates obtained by means of this operation are referred to as *guiding-centre coordinates* $\left(\mathbf{X}, v_{\parallel}, \mu, \gamma\right)$, where $\mathbf{X}$ identifies the guiding-centre position, $v_{\parallel}$ the parallel velocity, μ the magnetic moment and γ the gyrophase. Such coordinates have already been introduced in chapter 2 (where the total energy U was used as phase-space coordinate instead of $v_{\parallel}$, but clearly these choices are completely equivalent). The resulting single-particle Lagrangian in the new coordinate system is given by

$$L_{sp} = \delta^{-1}\frac{q_{sp}}{c}\mathbf{A}^*_{sp}\left(\mathbf{X}_{sp}, v_{\parallel,sp}, \mu_{sp}\right)\cdot\dot{\mathbf{X}} + \delta\frac{m_{sp}c}{q_{sp}}\mu\dot{\gamma} - H_{sp,0}\left(\mathbf{X}_{sp}, v_{\parallel,sp}, \mu_{sp}\right) \quad (7.7)$$

with

$$\mathbf{A}^*_{sp}\left(\mathbf{X}_{sp}, v_{\parallel,sp}, \mu_{sp}\right) = \mathbf{A}_0\left(\mathbf{X}_{sp}\right) + \delta\frac{m_{sp}c}{q_{sp}}v_{\parallel,sp}\mathbf{b}\left(\mathbf{X}_{sp}\right) + \quad (7.8)$$

$$-\delta^2\frac{m_{sp}c^2}{q^2_{sp}}\mu_{sp}\mathbf{W}\left(\bar{\mathbf{X}}_{sp}\right) \quad (7.9)$$

and

$$\mathbf{W}\left(\mathbf{X}_{sp}\right) = \nabla\mathbf{e}_1\left(\mathbf{X}_{sp}\right)\cdot\mathbf{e}_2\left(\mathbf{X}_{sp}\right) + \frac{1}{2}\mathbf{b}\left(\mathbf{X}_{sp}\right)\mathbf{b}\left(\mathbf{X}_{sp}\right)\cdot\nabla\times\mathbf{b}\left(\mathbf{X}_{sp}\right), \quad (7.10)$$

where $\mathbf{e}_1, \mathbf{e}_2$ form an orthonormal triplet with $\mathbf{b}$, and $H_{sp,0}\left(\mathbf{X}_{sp}, v_{\parallel,sp}, \mu_{sp}\right)$ represents the lowest-order Hamiltonian, namely

$$H_{sp,0}\left(\mathbf{X}_{sp}, v_{\parallel,sp}, \mu_{sp}\right) = \frac{1}{2}m_{sp}v^2_{\parallel,sp} + \mu_{sp}B_0\left(\mathbf{X}_{sp}\right). \quad (7.11)$$

It is important to note that the Lagrangian above still includes gyromotion, through the magnetic moment μ_{sp} . But since L_{sp} does not contain any γ-dependence, μ_{sp} is a constant of motion (recall that, according to the Lagrangian approach, γ and $\dot{\gamma}$ are treated as completely independent variables,

although they are linked from a physical point of view). The Euler-Lagrange equations derived from this guiding-centre Lagrangian would lead to the drift-kinetic equation.

As previously stated, the peculiarity of the gyrokinetic equation consists in the possibility of retaining field variations on the Larmor-radius scale. This means that it is necessary to include in the derivation modes with $k_\perp \rho_L \sim 1$, which are typically treated as perturbations of the equilibrium system. If such perturbations occur, the guiding-centre coordinates are no longer advantageous, in the sense that the gyromotion is no longer decoupled from the guiding center drifts, since the perturbed fields destroy the independence of the Lagrangian on the gyrophase. For this reason, again by means of the Lie transforms, is it possible to construct a new set of coordinates, quasi-identical to the guiding-centre coordinates, where even in presence of perturbations the gyration decouples from the drifts, and in addition where the Hamiltonian nature of the equations of motion is still preserved. Such coordinates are called *gyrocentre coordinates* (indicated with a bar, $\bar{\mathbf{X}}, \bar{v}_\parallel, \bar{\mu}$). The final form of the (collisionless) gyrokinetic set of equations is written in terms of such gyrocentre coordinates. It consists in a kinetic equation

$$\left(\frac{\partial}{\partial t} + \frac{\mathrm{d}\bar{\mathbf{X}}}{\mathrm{d}t}\frac{\partial}{\partial \bar{\mathbf{X}}} + \frac{\mathrm{d}\bar{v}_\parallel}{\mathrm{d}t}\frac{\partial}{\partial \bar{v}_\parallel} + \frac{\mathrm{d}\bar{\mu}}{\mathrm{d}t}\frac{\partial}{\partial \bar{\mu}}\right) f\left(\bar{\mathbf{X}}, \bar{v}_\parallel, \bar{\mu}\right) = 0 \tag{7.12}$$

with

$$\frac{\mathrm{d}\bar{\mathbf{X}}}{\mathrm{d}t} = \frac{1}{B^*_\parallel}\left[\left(\bar{v}_\parallel + \frac{1}{m_{sp}}\frac{\partial H_2}{\partial \bar{v}_\parallel}\right)\mathbf{B}^* + \frac{c}{q_{sp}}\mathbf{b}\times\left(\bar{\mu}\nabla B_0 + \nabla H_2\right)\right] \tag{7.13}$$

$$\frac{\mathrm{d}\bar{v}_\parallel}{\mathrm{d}t} = -\frac{\mathbf{B}^*}{m_{sp}B^*_\parallel}\cdot\left[\bar{\mu}\nabla B_0 + \nabla H_2\right] \tag{7.14}$$

$$\frac{\mathrm{d}\bar{\mu}}{\mathrm{d}t} = 0, \tag{7.15}$$

where H_2 identifies the gyro-averaged perturbed Hamiltonian, which contains the electrostatic potential plus the perturbed magnetic potential, namely

$$H_2 = \frac{q_{sp}^2}{2m_{sp}c^2}\left\langle\left|\mathbf{A}_1\left(\bar{\mathbf{X}} + \delta\bar{\rho}_L, t\right)\right|^2\right\rangle_\gamma - \frac{q_{sp}}{2}\left\langle\{S, \hat{\psi}\}\right\rangle_\gamma \tag{7.16}$$

where $\langle \ldots \rangle_\gamma$ indicates the gyro-average, $\{\ldots\}$ denote Poisson brackets, S indicates a gauge function defined for example in Ref.[56] whose explicit form is not of importance here, and

$$\hat{\psi}\left(\bar{\mathbf{X}}, \bar{v}_\parallel, \bar{\mu}\right) = \phi\left(\bar{\mathbf{X}} + \delta\bar{\rho}_L, t\right) - \bar{\mathbf{v}}_0 \cdot \mathbf{A}_1\left(\bar{\mathbf{X}} + \delta\bar{\rho}_L, t\right) + \\ - \left\langle \phi\left(\bar{\mathbf{X}} + \delta\bar{\rho}_L, t\right) - \bar{\mathbf{v}}_0 \cdot \mathbf{A}_1\left(\bar{\mathbf{X}} + \delta\bar{\rho}_L, t\right)\right\rangle_\gamma \tag{7.17}$$

while

$$\mathbf{B}^* = \nabla \times \mathbf{A}^* \tag{7.18}$$

$$B^*_\parallel = \mathbf{b} \cdot \mathbf{B}^*. \tag{7.19}$$

Note that all the drifts which have been pointed out in chapter 2 are still present in this form of the gyrokinetic equation. For example, the term in $\bar{v}_\parallel \mathbf{B}^*$ in Eq.(7.13) accounts both for the parallel streaming on the unperturbed field lines and for the curvature drift (recall Eq.(2.30) and Eq.(7.18)), while the other term in the first bracket is linked to the radial component of the parallel velocity which arises in presence of a perturbed vector potential (accounted for in the Hamiltonian). The second bracket in the same equation is linked to the grad-B drift (Eq.(2.21)) through $\bar{\mu}\nabla B_0$, and to the $\mathbf{E} \times \mathbf{B}$-drift via the perturbed Hamiltonian (equilibrium electrostatic potentials can be included in the gyrokinetic formalism, if needed [61]). Finally, it is easy to identify the mirror force (Eq.(2.24)) in Eq.(7.14).

The gyrokinetic set of equations is closed by the two equation for the fields, namely the Poisson's law and the Ampère's law. They come from the field Lagrangian, and they are written in the form

$$\Delta\nabla^2\phi\left(\mathbf{x}, t\right) = -4\pi \sum_{sp} q_{sp} \int \mathrm{d}^6\mathbf{Z} J\left(\mathbf{Z}\right) \delta\left[\bar{\mathbf{X}} + \rho_L - \mathbf{x}\right] \cdot \\ \left(f\left(\mathbf{Z}, t\right) + \Delta\{S, f\}\right) \tag{7.20}$$

and

$$\Delta\nabla^2\mathbf{A}\left(\mathbf{x}, \mathbf{t}\right) = -\frac{4\pi}{c}\left(\mathbf{j}\left(x, t\right) - \mathbf{j}_0\left(\mathbf{x}, t\right)\right) \tag{7.21}$$

where Δ indicates the finite difference between the initial value and the value at time t, while

$$\mathbf{j}_0(\mathbf{x},t) = -\frac{4\pi}{c}\nabla^2\mathbf{A}_0 \tag{7.22}$$

(having neglected, as mentioned, the displacement current) and

$$\mathbf{j}(x,t) = \sum_{sp} q_{sp} \int \mathrm{d}^6\mathbf{Z} J(\mathbf{Z})\, \delta\left[\bar{\mathbf{X}} + \rho_L - \mathbf{x}\right] \cdot \left(\left[\mathbf{v}_0(\mathbf{Z}) - \Delta\mathbf{A}_1\left(\bar{\mathbf{X}} + \rho_L, t\right)\right] f(\mathbf{Z},t) + \Delta\mathbf{v}_0(\mathbf{Z})\{S,f\}\right) \tag{7.23}$$

with $\delta(x)$ denoting the Dirac delta function, $J(\mathbf{Z}) = B_\parallel^*(\mathbf{Z})/m_{sp}$, and $\mathbf{Z} = \left(\bar{\mathbf{X}}, \bar{\mu}, \bar{v}_\parallel\right)$ is the phase space coordinates vector. *Note that the gyroaveraged fields are calculated as a function of the actual space coordinate* $\mathbf{x}$, *while the distribution function depends on the gyrocentre coordinate* $\bar{\mathbf{X}}$. In the equation for the distribution function, only the gyroaveraged fields are involved, but the closure field equations yield the correct space dependence. The difference between the local fields and the gyroaveraged fields at a given position is of crucial importance, as it causes the appearance of *polarization* effects on the Larmor-radius scale, which are of course not treatable with a drift-kinetic approach (where the field is supposed not to vary on the Larmor-radius scale and thus the local and the gyroaveraged value coincide).

7.2 GKW Coordinates and Local Limit

As previously stated, the code GKW solves the gyrokinetic set of equations in the δf-limit in a flux-tube geometry. While the δf-limit has been widely discussed in the previous chapters, the purpose of the present section is to elucidate the relevant aspects of the flux-tube geometry, as its peculiarities are fundamental for a proper implementation of a magnetic island.

The code GKW adopts the so called *Hamada coordinates* [4]. They are flux-surface coordinates, and therefore they are defined in such a way that the contravariant components of the equilibrium magnetic field with respect

to both the poloidal and the toroidal angle are flux-surface quantities (see chapter 2). These coordinates consist in an unperturbed poloidal flux χ, a poloidal angle s (which is supposed to vary between $-1/2$ and $1/2$, being 0 on the outer midplane) and in a helical angle φ defined as

$$\varphi = qs - \hat{\zeta}, \tag{7.24}$$

where $\hat{\zeta}$ corresponds to the toroidal angle ζ as defined in chapter 1, normalized by a factor 2π. This coordinate is slightly different from the helical angle ξ defined in chapter 2, as the latter labels the magnetic field line only on a given magnetic surface (the rational one), while the former is constant on the magnetic field line for every given magnetic surface, by virtue of the explicit dependence on q. The coordinate φ is therefore more convenient in order to efficiently separate the parallel from the perpendicular dynamics, but on the other side the "natural" choice in order to describe magnetic islands is its periodicity coordinate ξ. In the next section, such problem will be addressed.

Gyrokinetic codes are typically adopted to investigate turbulence, which represents a phenomenon occurring on relatively small space scales and which moreover admits a convenient representation in terms of Fourier modes in the plane perpendicular to the magnetic field line (i.e. the (χ, φ)-plane in the present case). In view of these peculiarities a common approach is represented by the *flux-tube* approximation [62, 63]. In this approach, a magnetic field line is followed an integer number of poloidal turns around the torus. A curved and sheared box around this central field line is then taken as simulation domain, and the equilibrium quantities are Taylor-expanded to first order in the perpendicular coordinates around the central field line. The values and first derivatives, together with the metric coefficients that describe the shaping of the box, are then considered to be constant over the perpendicular extent of the computational domain, i.e. only parallel variations are taken into account. Clearly, such radial approximation is justified if the radial extent of the box is small compared to the machine size. As the temperature

and the density profiles at the equilibrium are constant on the flux-surfaces, their parallel dependence can be therefore neglected. Thus, they are completely determined, in this approximation, by two scalars, namely their value on the central field line and their radial gradient.

Since in the flux-tube approximation the simulation domain does not cover the full extent of the plasma vessel, its boundaries do not correspond to material boundaries. It is therefore very important to define suitable boundary conditions that keep the effects of this artificial reduction as small as possible. In order to write radial gradients in a simple form, and in order to separate properly what happens *across* the flux surface from what happens *on* it, the two directions on which the flux-tube section lies are conveniently identified by $\nabla\chi$ and $\nabla\varphi$, while of course the flux tube follows the coordinate s. In the radial and in the binormal direction (which is often called *poloidal*, while the s-direction is referred to as *parallel*), periodic boundary conditions hold for every (perturbed) quantity G computed by the code:

$$G(\chi, \varphi, s) = G(\chi + \Delta\chi, \varphi + \Delta\varphi, s) \tag{7.25}$$

where $\Delta\chi, \Delta\varphi$ define the size of the box. These boundary conditions are consistent with the local approximation introduced above and they automatically ensure that heat and particles, which leave the simulation domain due to the various drifts arising, are replenished at the opposite side of the simulation domain. Moreover, such assumption prevents the accumulation of heat or particles at certain radial positions, so that the average radial gradients are not changed in the simulation. Note that the size of the computational box has to be big enough to accomodate all structures created in the simulation. More specifically, the box lengths have to be bigger than the correlation length of the turbulent fields in the corresponding direction, otherwise the boundary condition can lead to unphysical effects.

In GKW, the solution of the gyrokinetic set of equations is carried out directly in the Fourier space in the two directions perpendicular to the mag-

netic field, profiting from the periodicity constraint (such codes are referred to as "spectral"). On the contrary, the parallel coordinate parametrizes the field line. Roughly speaking, on every point of the magnetic field line (i.e. on every point of the parallel grid), the code builds a box, where the solution is computed spectrally. The parallel dynamics which connects all the boxes on the grid is on the contrary accounted for with an explicit numerical scheme.

7.3 Implementation of a Magnetic Island in a Flux-Tube

A code like GKW, which solves in a self-consistent way for the fields, can be used as a numerical tool in order to study the self-consistent problem of the island evolution, rotation and stability. However, before approaching the problem of the island dynamics in the presence of microturbulence, it is appropriate to address simplified problems. Here, a non-evolving magnetic island, with imposed rotation frequency, is considered. This greatly simplifies the problem, giving nevertheless the possibility to investigate relevant aspects of the NTM physics, as for example the self-consistent calculation of the island potential.

As discussed in the previous chapters, magnetic islands are generated by means of a perturbed parallel component of the magnetic vector potential, which develops on rational surfaces and which has the same helicity of the magnetic field lines therein. If a magnetic island of fixed width is considered, it is possible to write

$$A_{\parallel} = C \cos \xi, \tag{7.26}$$

or equivalently (for a spectral code)

$$A_{\parallel} = C \exp \left[i\xi \right], \tag{7.27}$$

where C is a constant which determines the amplitude of the mode and ξ

can be written in the GKW coordinates as

$$\xi = m\theta - n\zeta - \omega t = 2\pi \left(ms - n\hat{\zeta} - \frac{\omega}{2\pi} t \right). \tag{7.28}$$

The final goal is to write the vector potential in a form which satisfies the requirements to be implemented in a flux-tube code. In particular, as it is desirable to treat the tearing mode as a perturbation, and not to include it in the background equilibrium, it is necessary for it to fulfil the periodic boundary conditions. Writing Eq.(7.27) in terms of χ, φ, s, it yields

$$A_{\parallel} = C \exp \left[2\pi i \left(n \left(\varphi + \left(\frac{m}{n} - q \right) s \right) - \frac{\omega}{2\pi} t \right) \right] \tag{7.29}$$

A convenient way to build the flux-tube in presence of a magnetic island is to center it on a magnetic field line on the rational surface. Therefore, the quantity q, as an equilibrium quantity, can be Taylor-expanded in the radial direction, introducing $\hat{\chi} = \chi - \chi_s$ (the subscript s denoting again quantities defined on the rational surface):

$$q\left(\hat{\chi}\right) \approx \frac{m}{n} + \frac{\partial q}{\partial \hat{\chi}} \hat{\chi} \tag{7.30}$$

as, of course, $q\left(\hat{\chi} = 0\right) = m/n$. Thus, Eq.(7.29) may be re-written as

$$A_{\parallel} = C \exp \left[2\pi i \left(n \left(\varphi - \frac{\partial q}{\partial \hat{\chi}} \hat{\chi} s \right) - \frac{\omega}{2\pi} t \right) \right], \tag{7.31}$$

or equivalently, introducing

$$k_{\varphi} = 2\pi n, \tag{7.32}$$

$$k_{\hat{\chi}} = \frac{\partial q}{\partial \hat{\chi}} k_{\varphi}, \tag{7.33}$$

one can write

$$A_{\parallel} = C \exp \left[i \left(k_{\varphi} \varphi - s k_{\hat{\chi}} \hat{\chi} - \omega t \right) \right]. \tag{7.34}$$

The most natural choice for the width of the flux-tube in the radial direction is

$$\Delta\hat{\chi} = \left[-\frac{\pi}{k_{\hat{\chi}}}, \frac{\pi}{k_{\hat{\chi}}} \right]. \tag{7.35}$$

The central point is that the mode, written as in Eq.(7.34) is *not* periodic on the chosen box for any given position on the parallel grid, because of the dependence on s which appears in front of the $k_{\hat{\chi}}$ term. This problem does not depend on the choice on the box width, but it is rather intrinsic, because the island has a constant helicity over its radial extent, while within such radial extent the helicity of magnetic field lines may significantly change.

In order to outflank the problem, the idea is to consider *only* the projections of the mode *on* the radial Fourier harmonics defined on the computational box. This approximation, which in fact consists in forcing a non-periodic object to be periodic on a given domain, may sound too violent, but as will be shown shortly afterwards, its consequences on the fidelity of the representation are not dramatic. The Fourier coefficients of the projection of the mode on the p-th harmonics are calculated as follow. Writing

$$A_{\parallel} = C \exp\left[i\left(k_{\varphi}\varphi - \omega t\right)\right] A\left(\hat{\chi}, s\right). \tag{7.36}$$

with

$$A\left(\hat{\chi}, s\right) = \exp\left[-isk_{\hat{\chi}}\hat{\chi}\right] \tag{7.37}$$

the coefficients of the harmonics are derived as

$$A_p = \frac{k_{\hat{\chi}}}{2\pi} \int_{\Delta\hat{\chi}} \mathrm{d}\hat{\chi} A \exp\left[-ipk_{\hat{\chi}}\hat{\chi}\right]. \tag{7.38}$$

The factor $k_{\hat{\chi}}/2\pi$ in front of the integral is of course a normalization factor which corresponds to the inverse of the length of periodicity. Substituting Eq.(7.37) in Eq.(7.38), one finds

$$A_p = \frac{\sin\left(\pi\left(s+p\right)\right)}{\pi\left(s+p\right)} \tag{7.39}$$

and thus the form to which the approximated vector potential amounts is

$$A_{\parallel} = C \exp\left[i\left(k_{\varphi}\varphi - \omega t\right)\right] \sum_{p} \frac{\sin\left(\pi\left(s+p\right)\right)}{\pi\left(s+p\right)} \exp\left[ipk_{\hat{\chi}}\hat{\chi}\right]. \tag{7.40}$$

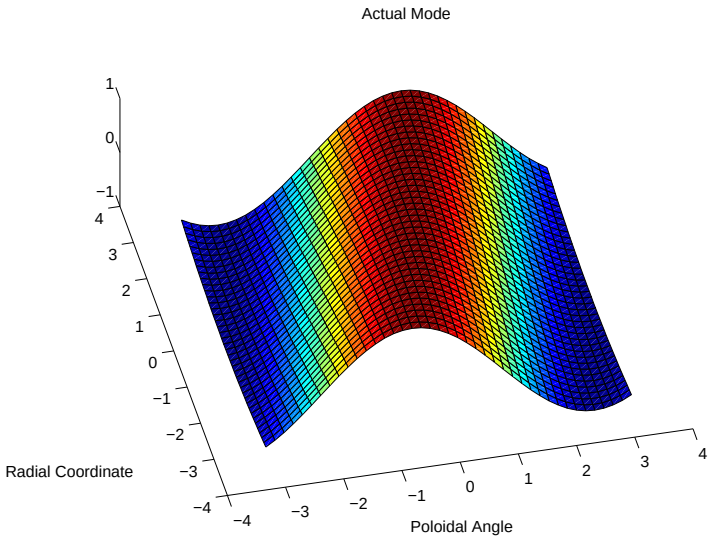

Figure 7.1: Visualization of the vector potential in a (χ, φ)-plane. The mode is clearly not periodic on the box. This series of figures refers to $s = 0.2$.

This form satisfies the flux-tube boundary conditions. In fact, it is clearly periodic on both the radial and the poloidal direction on the given box. Moreover, only the coefficients of the harmonics depend on s, and this is compatible with a separate solution of the problem on every point of the parallel grid.

However, the solution suggested in Eq.(7.40) is still not suitable for implementation. Actually, the periodicity constraint applied to a non-periodic mode allows abrupt discontinuities to take place at the edge of the computational box. This can be clearly seen by comparing Fig.7.1, which shows the "true", non periodic shape of the vector potential, with Fig.7.2, where the vector potential (7.40) is visualized. In order to avoid such "jump", an artificial smoothing of the high-p modes has been added, in the form

$$\exp\left[-\frac{(s+p)^2}{L_{\rm sm}^2}\right], \tag{7.41}$$

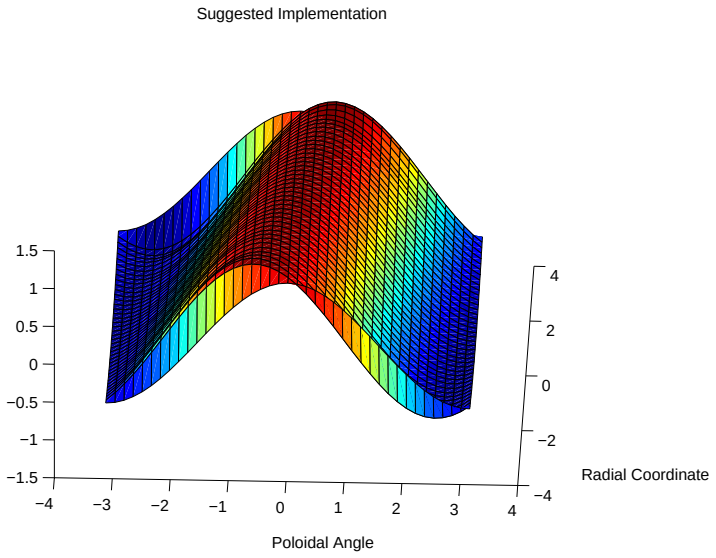

Figure 7.2: Visualization of the vector potential (7.40) in a (χ, φ)-plane. The mode is now periodic, but a sudden and undesirable "jump" at the edge of the box is clearly visible. This "jump" consist in an abrupt kinking of the mode in the proximity of the boundary of the flux-tube.

where $L_{\rm sm}$ is a parameter which must be optimized (too high values would yield an unefficient smoothing, while on the contrary too small values would cause an exaggerated modification of the mode). A reasonable value has been found to be $L_{\rm sm} = 2$. The resulting perturbed vector potential is depicted in Fig.7.3. It looks sufficiently similar to the "true" one, but it clearly exhibits a slight kink of the structure, which allows the mode to fulfil the periodicity constraint. Fig.7.4 and Fig.7.5 represent the magnetic island resulting from the real mode and from the approximated one (in presence of Gaussian smoothing), respectively. The comparison is quite encouraging. The approximation is more evident at the edge of the box, where the X-points are located. In the middle of the box, on the contrary, the resemblance is extremely satisfactory.

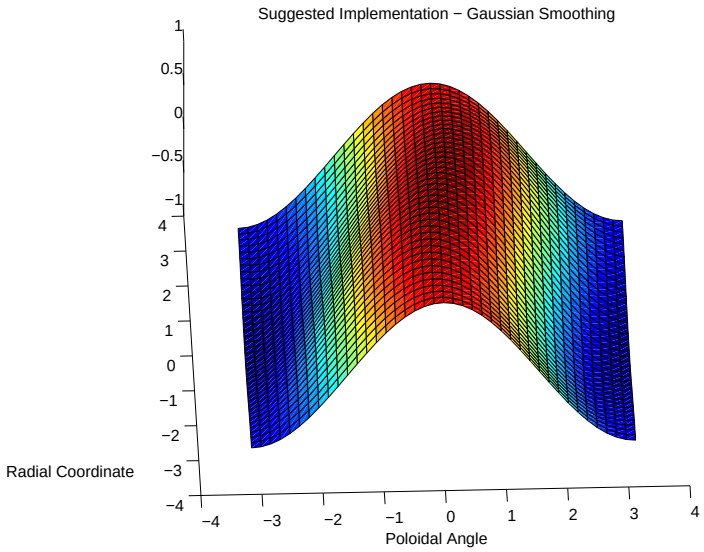

Figure 7.3: Visualization of the vector potential in a (χ, φ)-plane in presence of a Gaussian smoothing. The deformation of the shape, although still visible, is significantly reduced.

7.4 First Results

In this section, some of the first results obtained with GKW are illustrated. Of course, to this preliminary stage, it is necessary to benchmark the code letting it simulate some well-known physical phenomena, rather than starting with the investigation of new physical aspects. The purpose of this section is to address such benchmarks.

7.4.1 Nonlinear Flattening of the Pressure Profile

As previously stated, although the code might be suitable for self-consistent simulations, somewhat easier problems are tackled at first. The presence of a magnetic island in a tokamak plasma, as elucidated in chapter 2, leads to a local flattening of the pressure profile in the plasma by virtue of the presence of a radial component in the plasma parallel velocity. The station-

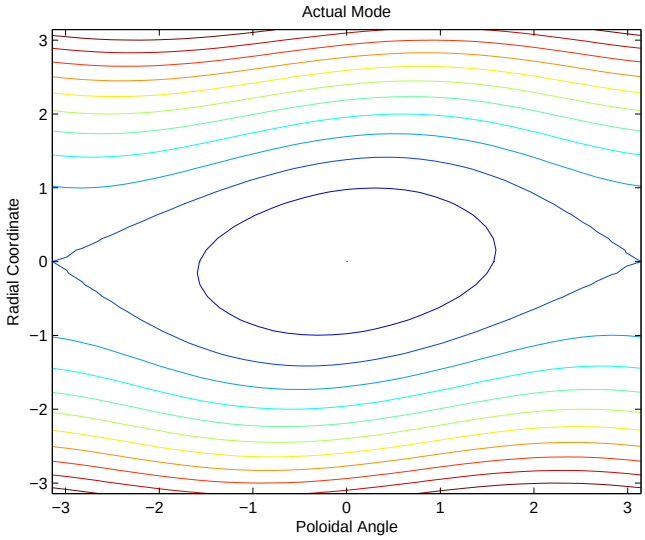

Figure 7.4: Magnetic island generated by the real mode. Recall that the name "Poloidal Angle" refers to the coordinate φ, in this case multiplied times 2π.

ary drift-kinetic equation, supposing for simplicity a non-rotating island and neglecting the corresponding electrostatic potential, reads

$$v_{\parallel}\nabla_{\parallel}f + \mathbf{v}_D \cdot \nabla f = 0. \tag{7.42}$$

The parallel gradient is composed by an equilibrium part $\nabla_{\parallel,\mathrm{Eq}}$ plus a new component arising from the perturbed radial component of the magnetic field $\tilde{\nabla}_{\parallel}$. Writing $f = F_0 + g$, where F_0 is supposed to be the solution of the unperturbed case, Eq.(7.42) amounts to

$$v_{\parallel}\left(\nabla_{\parallel,\mathrm{Eq}} + \tilde{\nabla}_{\parallel}\right) g = -v_{\parallel}\tilde{\nabla}_{\parallel}F_0, \tag{7.43}$$

having neglected the magnetic drifts applied on the perturbed distribution g. Eq.(7.43) governs the flattening of the density profile inside the island, and a similar argument can be applied for the temperature profile. It is clear that the term $\tilde{\nabla}_{\parallel}g$ plays a major role in the dynamics of the flattening. Such

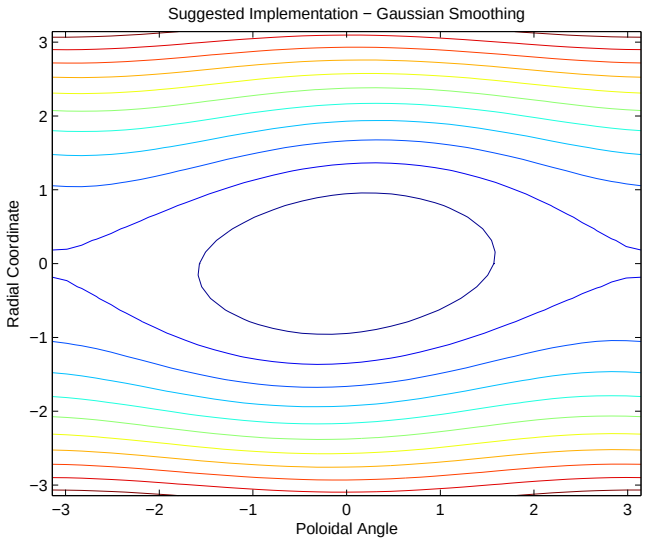

Figure 7.5: Magnetic island generated by the approximated mode, in presence of a gaussian smoothing. This represents a reasonable adaptation in the frame of satisfying the flux-tube periodicity constraints.

term exhibits the peculiarity of being *nonlinear*, as it depends both on the perturbed distribution and on the perturbed vector potential through $\tilde{\nabla}_{\|}$ (which would in fact be zero as no island were present).

Fig.7.6 shows the total temperature profile for both ions and electrons as calculated from GKW simulations. It is obtained by summing the equilibrium background profile, which is given as an input, and the perturbed distribution, which is calculated solving the gyrokinetic set of equations. The Ampère equation has been turned off, in order to neglect the self-consistent evolution of the magnetic island. The rotation frequency has been set to zero. It is worth to note that, as an input, GKW requires the island width. The corresponding amplitude of the perturbed vector potential is straightforwardly determined by means of Eq.(3.10) and Eq.(3.11).

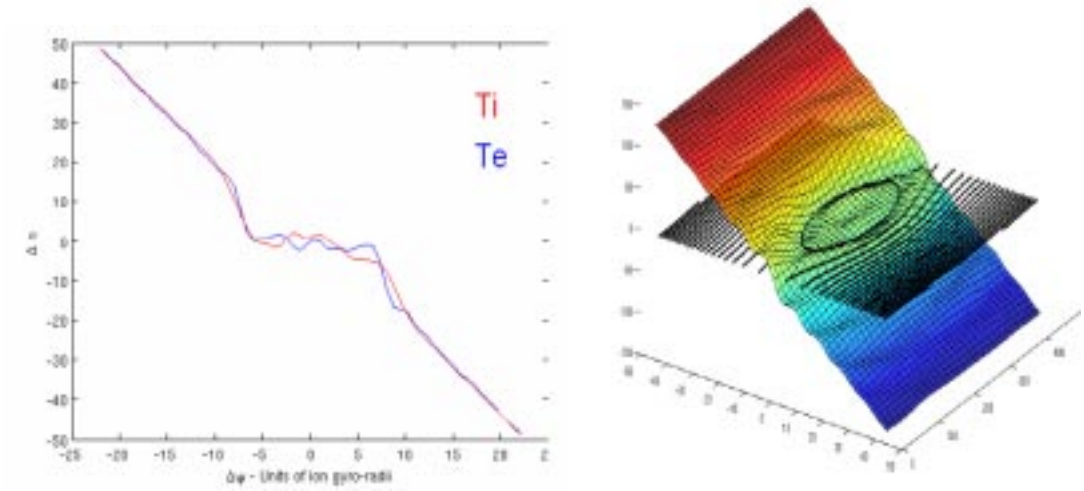

Figure 7.6: Nonlinear flattening for ion and electron temperature profile calculated for a static island with the code GKW. The island is centered in 0, and its half-width is around 8 gyroradii. This simulation has been performed in a circular tokamak geometry with $\epsilon = 0.19$. The contribution of trapped particles has been switched off. The figure on the right represents a 3-dimensional visualization of the ion temperature profile.

7.4.2 The Electrostatic Potential

A further benchmark which has been performed with the code GKW concerns the profiles of the electrostatic potential associated with the magnetic island. In chapter 4, an analytical expression for the electrostatic potential has been derived with the assumption that electrons are sufficiently fast to short out any parallel electric field (see Eq.(4.38)). The corresponding expression is reported here for convenience:

$$\phi = \frac{\omega q}{mc} \left[\chi - \chi_s - h\left(\Omega\right) \right]. \tag{7.44}$$

The code GKW allows to calculate numerically the electrostatic potential starting from the ion and electron response to the mode, by means of the self-consistent Poisson equation. Although the analytical expression of Eq.(7.44)

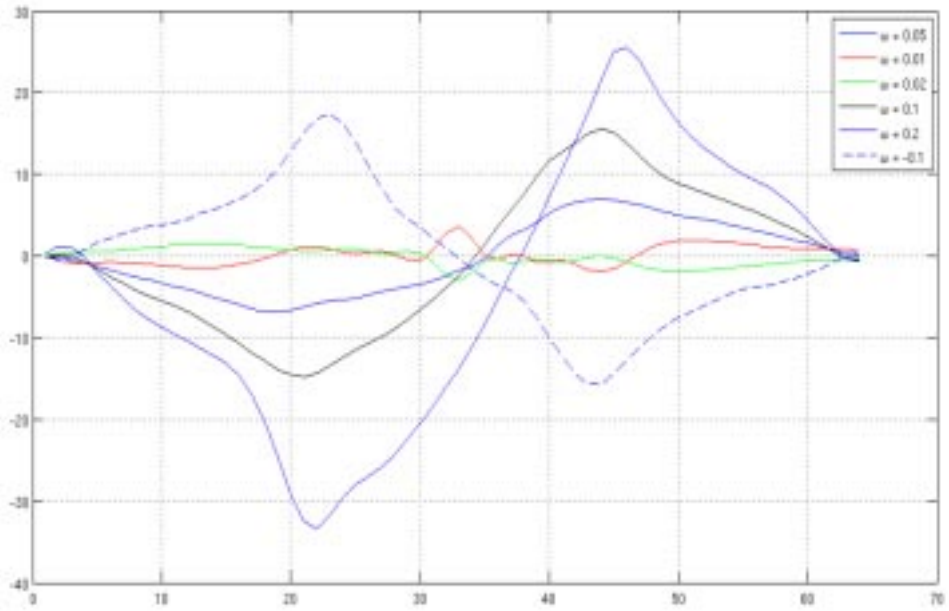

Figure 7.7: Radial profiles of the self-consistent electrostatic potential calculated through the O-point of a magnetic island for various values of the island rotation frequency. The O-point is around the point 35 in the radial coordinate, while the island is approximatively from 25 to 45 (units normalized to the ion thermal gyroradius). The frequency ω is normalized in $v_{\rm th}/R$ units, while the potential is expressed in terms of $q_i\phi/T\rho_*$, where $\rho_* = \rho_L/R$.

is approximated, an almost linear scaling of the potential with the island rotation frequency is reasonable to be expected even for the numerical simulations. Indeed, this is the outcome of GKW simulations. Fig.7.7 shows the parametric dependence of the radial potential profile on the island rotation frequency, and the expected linear correlation is clearly visible. Moreover, the functional dependence of ϕ on the radial coordinate is reproduced by the code, although small discrepancies can bee seen (cf. Fig.4.1).

It is important to underline that in order to obtain a reliable self-consistent calculation of the island potential, it is necessary to perform a full kinetic

calculation for *both* ions *and* electrons. This is a drawback from the computational point of view, because electron dynamics is characterized by very fast timescales, which need a much shorter timestep to be properly investigated. This of course requires a longer time for simulations. Gyrokinetic codes have typically the possibility to neglect the dynamics of electrons, which by virtue of their celerity may be supposed to respond adiabatically to disturbances (the so called *adiabatic electrons* approximation). The point is that, in presence of a magnetic island, although the reaction of the electrons to the perturbations is still fast enough compared to other characteristic timescales, within the adiabatic approximation they would not see the deformation of the magnetic surfaces, or in other words they will remain adiabatic on the unperturbed magnetic surfaces rather than on the perturbed one, where their fast parallel dynamics should physically take place. This computational problem forces one to adopt a kinetic treatment for both species in order to determine a proper potential profiles.

7.5 Outlook

The code GKW exhibits a huge potential as a tool for the numerical study of magnetic islands. For the next future, investigations along the following lines are planned:

- The first point to be studied is the evaluation of the effects of finite Larmor radius on the potential profile [64]. Such effects, as can be intuitively inferred, are in particular relevant for small islands. In addition, all the results discussed in chapter 5 and 6, with particular attention on the effect of the resonant particles, may be efficiently investigated. It is worth to mention that there already exist gyrokinetic studies of the polarization current in slab geometry [29, 65, 66].

- Along the same direction, it has been supposed that the flattening of the pressure profile inside the island is not complete for sufficiently

small island [21]. This has of course noteworthy consequences on the seed island stability, recall the neoclassical drive. A gyrokinetic code possesses all the physics necessary to describe such incomplete flattening.

- There exists, obviously, the huge topic of interaction between island and turbulence, which is partially connected to the previous point. Both the problem of how the presence of the island influences the turbulent transport [67], and the dual problem of how turbulence can affect island stability [68] are extremely wide topics which are relatively unexplored [69, 70].

- A very interesting point, finally, will be the study of the self-consistent island rotation. Once that the Ampère's law is turned on, the mode is let free to evolve and therefore to rotate. It will thus be possible to evaluate the role of the mechanisms discussed in literature on the island rotation frequency. In fact, the variety of the phenomena which determine the island rotation (or, equivalently, which are linked to a $\sin\xi$ component of the perturbed parallel current) is huge. One can mention, for example, the effect of the electron pressure gradient pointed out by means of fluid calculations [31], but also dissipative phenomena such like electron- and ion-Landau damping [29, 30] or collisional friction between trapped and passing particles [26] have been shown to play a major role. Possibly, other effects still have to be identified.

Chapter 8

Summary and Outlook

The neoclassical tearing mode (short NTM) is an instability which, under appropriate conditions, develops in tokamak plasmas, allowing the appearance of structures called *magnetic islands*, which in turn lead to an enhanced particle and energy radial transport. As its occurrence significantly deteriorates the performances of a tokamak machine, the investigation of the dynamics of this mode takes on great importance in view of achieving a satisfactory plasma confinement. The stability of a neoclassical tearing mode, which is a magnetic perturbation, is determined through the Ampère's law by the balance of the currents induced by the presence of the mode itself. In the present work, a particular attention is given to the current caused by the rotation of the island with respect to the surrounding plasma.

The main contribution linked to the island rotation is represented by the so called *polarization current* [26], which in absence of equilibrium pressure gradients has been derived to scale as ω^2, where ω is the island rotation frequency. It has been shown, however, that such a parabolic dependence on the frequency holds only for $\omega \gg k_\parallel v_\parallel$ (where $k_\parallel$ has been defined in Eq.(4.30)), breaking otherwise (see Fig.8.1).

The main goal of the present work is to address such departure from the parabolic scaling. The calculation of the perturbed current is carried out both

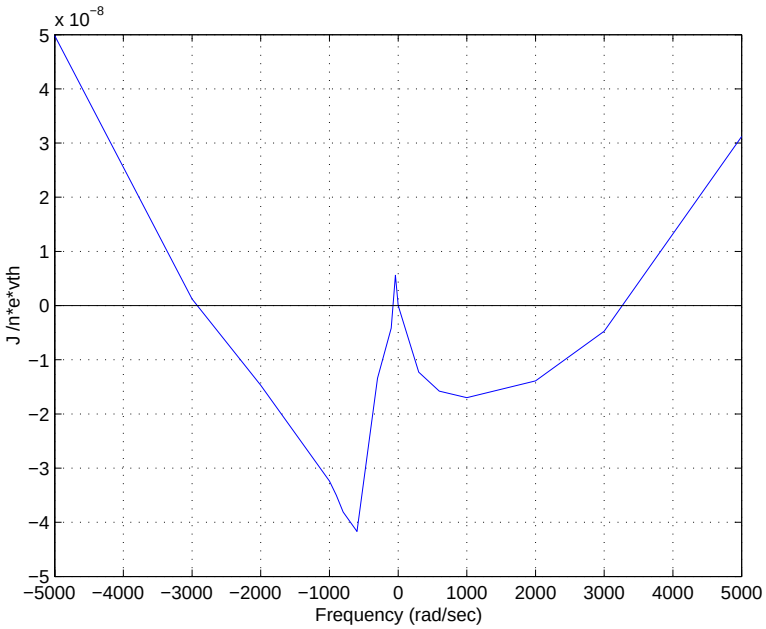

Figure 8.1: Averaged perpendicular current on the inner side of the magnetic island as a function of the island rotation frequency ω. The parabolic dependence clearly breaks for slowly rotating modes. Such figure has been published in Ref.[34].

analytically and numerically, adopting a drift-kinetic approach, and treating the island rotation frequency as a free parameter. It is found that, for island frequencies close to or lower than $k_\parallel v_\parallel$, a relevant effect originates from the interplay between the island rotation and some characteristic timescales of the particle motion, possibly leading to resonant interactions. In particular, a new current contribution, due to the modification of the toroidal precession frequency of trapped particles by virtue of the island electrostatic potential, has been pointed out. This current, named *precessional current*, is what ultimately causes the deviation from the parabolic dependence on the frequency previously outlined, competing therefore with the polarization current in a wide range of experimentally relevant frequencies. The effect of the precessional current on the NTM stability is also discussed.

In the last chapter, the implementation of a magnetic island in the flux-tube spectral gyrokinetic code GKW [47] is presented, together with the results of the first simulations. This represents the first step in the frame of a long-term cooperation with the University of Warwick, United Kingdom. In particular, this code will allow to analyse the effects of finite Larmor radius on important aspects of the island dynamics, e.g. self-consistent determination of the island potential, mutual influence between island and turbulence, *et cetera*. The final goal is to provide an extremely powerful tool in order to achieve a complete description of the magnetic island evolution.

Bibliography

[1] J. Wesson, *Tokamaks*, (Clarendon Press, Oxford, 1987)

[2] L. A. Artsimovitch, Nucl. Fusion **12** 215 (1972)

[3] R. O. Dendy, *Plasma Dynamics* (Clarendon Press, Oxford, 1990)

[4] S. Hamada, Nucl. Fusion **2** 23 (1962)

[5] A. H. Boozer, Phys. Fluids **26**, 5 (1983)

[6] R. D. Hazeltine and J. D. Meiss, *Plasma Confinement* (Addison-Wesley, New York, 1992)

[7] R. G. Littlejohn, J. Math. Phys **23**, 742 (1982)

[8] R. Cary and R. G. Littlejohn, Ann. Phys. (NY) **151**, 1 (1983)

[9] A. G. Peeters, PhD Thesis, *Technische Universiteit Eindhoven*, unpublished (1994)

[10] R. B. White and M. S. Chance, Phys. Fluids **27** 2455 (1984)

[11] F. L. Hinton and J. A. Robertson, Phys. Fluids **27** 1243 (1984)

[12] J. P. Freidberg, *Ideal Magnetohydrodynamics*, (Plenum Press, New York, 1987)

[13] H. P. Furth, J. Killeen and M. N. Rosenbluth, Phys. Fluids **6** 459 (1963)

[14] P. H. Rutherford, Phys. Fluids **16** 1903 (1973)

[15] R. Carrera, R. D. Hazeltine and M. Kotschenreuther, Phys. Fluids **29** 899 (1986)

[16] F. L. Hinton and R. D. Hazeltine, Rev. Mod. Physics **48** 239 (1976)

[17] A. G. Peeters, Plasma Phys. Control. Fusion **42** B231 (2000)

[18] R. J. Bickerton, J. W. Connor and J. B. Taylor, Nat. Phys. Sci. **229** 110 (1971)

[19] Z. Chang *et al.*,Phys. Rev. Letters **74** 4663 (1995)

[20] O. Sauter *et al.*, Phys. Plasmas **4**1654 (1997)

[21] R. Fitzpatrick, Phys. Plasmas **2** 825 (1995)

[22] E. Poli *et al*, Phys. Rev. Letters **88** 075001 (2002)

[23] A. I. Smolyakov, Sov. J. of Plasma Phys. **15** 667 (1989)

[24] H. R. Wilson *et al.*, Plasma Phys. Control. Fusion **38** A149 (1996)

[25] M. Brambilla, *Kinetic Theory of Plasma Waves* (Clarendon Press, Oxford, 1996)

[26] H. R. Wilson *et al.*, Phys. Plasmas **3** 248 (1996)

[27] A. I. Smolyakov *et al.*, Phys. Plasmas **2** 1581 (1995)

[28] A. I. Morozov and L. S. Solov'ev, Review Plasma Physics **2** Consultants Bureau (1966)

[29] J. W. Connor and H. R. Wilson, Phys. Plasmas **2** 4575 (1995)

[30] V. S. Marchenko, Nucl. Fusion **39** 1541 (1999)

[31] B. D. Scott, A. B. Hassam and J. F. Drake, Phys. Fluids **28**(1) 275 (1985)

[32] S. D. Pinches *et al.*, Comput. Phys. Commun. **111** 133 (1998)

[33] A. Bergmann, A. G. Peeters, S. D. Pinches, Phys. Plasmas **8** 5192 (2001)

[34] E. Poli *et al*, Nucl. Fusion **45** 384 (2005)

[35] M. Abramowitz and I. A. Stegun (edited by), *Handbook of Mathematical Functions* (Dover, 1970)

[36] A. I. Smolyakov, Sov. J. Plasma Phys. **15** 667 (1989)

[37] F. L. Walbroeck and R. Fitzpatrick, Phys. Rev. Lett. **78** 1703 (1997)

[38] M. N. Rosenbluth, D. W. Ross and D. P. Kostomarov, Nucl. Fusion **12** 3 (1972)

[39] A. B. Mikhailovskii and V. S. Tsypin, Sov. J. Plasma Phys. **9** 91 (1983)

[40] H. L. Berk and B. N. Breizman, Phys. Fluids B **2** 2226 (1990)

[41] H. L. Berk and B. N. Breizman, Phys. Fluids B **2** 2235 (1990)

[42] H. L. Berk and B. N. Breizman, Phys. Fluids B **2** 2246 (1990)

[43] P. L. Bhatnagar, E. P. Gross, M. Krook, Phys. Rev. **94** 511 (1954)

[44] M. Siccinio and E. Poli, Plasma Phys. Control. Fusion **51** 075005 (2009)

[45] R. Aymar, P. Barabaschi and Y. Shimomura, Plasma Phys. Control. Fusion **44** 519 (2002)

[46] A. Herrmann and O. Gruber, Fusion Science and Technology **44** 569 (2003)

[47] A. G. Peeters *et al*, accepted by Comput. Phys. Commun.

[48] T. M. Antonsen, Jr. and B. Lane, Phys. Fluids **23** 1205 (1980)

[49] A. Brizard, J. Plasma Physics **41** 541 (1989)

[50] A. Brizard, Phys. Plasmas **1** 2480 (1994)

[51] E. A. Frieman and L. Chen, Phys. Fluids **25(3)** 502 (1982)

[52] R. G. Littlejohn, Phys. Fluids **24** 1730 (1981)

[53] R. G. Littlejohn, J. Plasma Physics **29** 111 (1983)

[54] T. S. Hahm, Phys. Fluids **31(9)** 2670 (1988)

[55] A. Brizard, Phys. Plasmas **7** 4816 (2000)

[56] H. Sugama, Phys. Plasmas **7** 466 (2000)

[57] A. J. Brizard and T. S. Hahm, Rev. Mod. Phys. **79** 421 (2007)

[58] H. Goldstein, C. Poole and J. Safko, *Classical Mechanics* (Pearson Education, 2002)

[59] L. D. Landau and E. M. Lifshitz *The Classical Theory of Fields* (Pergamon Oxford, 1975)

[60] R. Abraham, J. E. Marsden and T. Ratiu, *Manifolds, Tensor Analysis and Applications* (Springer Verlag, 1988)

[61] T. S. Hahm, Phys. Plasmas **1** 2940 (1994)

[62] S. Cowley, R. Kulsrud and R. Sudan, Phys. Fluids B **3** 2767 (1991)

[63] M. Beer, S. Cowley and G. Hammet, Phys. Plasmas **2** 2687 (1995)

[64] A. Bergmann, E. Poli and A. G. Peeters, Phys. Plasmas **16** 092507 (2009)

[65] F. Waelbroeck, J. W. Connor and H. R. Wilson, Phys. Rev. Letters **87** 215003-1 (2001)

[66] M. James and H. R. Wilson, Plasma Phys. Control. Fusion **48** 1647 (2006)

[67] E. Poli, A. Bottino and A. G. Peeters, Nucl. Fusion **49** 075010 (2009)

[68] A. Smolyakov *et al.*, Journal of the Physical Society of Japan **76** 113501 (2007)

[69] A. Ishizawa *et al.*, Phys. Plasmas **14** 040702 (2007)

[70] F. Militello *et al.*, Phys. Plasmas **15** 050701 (2008)